Investigation on High Performance Surface Acoustic Wave Devices Using ScAlN Thin Films

January 2017

by

Gongbin Tang

Graduate School of Engineering

Chiba University

Investigation on High Performance Surface Acoustic Wave Devices Using ScAlN Thin Films

(ScAlN 薄膜を用いた高性能弾性表面波素子に関する研究)

2017 年 1 月

唐供賓

人工システム科学専攻

電気電子系コース

Affiliation:

Graduate School of Engineering

Department of Electrical and Electronic Engineering

Chiba University

1-33 Yayoi-cho, Inage-ku, Chiba-shi 263-8522 Japan

Supervisor:

Prof. Ken-ya Hashimoto, Dep. Elec. and Electronic Engineering, Graduate School of Engineering, Chiba University

Examiners:

Prof. Ken-ya Hashimoto, Dep. Elec. and Electronic Engineering, Graduate School of Engineering, Chiba University

Prof. Kazuhiro Kudo, Dep. Elec. and Electronic Engineering, Graduate School of Engineering, Chiba University

Prof. Toshiaki Takano, Dep. Elec. and Electronic Engineering, Graduate School of Engineering, Chiba University

Prof. Chang-Jun Ahn, Dep. Elec. and Electronic Engineering, Graduate School of Engineering, Chiba University

DECLARATION

I hereby declare that this submission is my own work and that, to the best of my knowledge and belief, it contains no material which to a substantial extent has been accepted for the award of any other degree or diploma of the university or other institute of higher learning, except where due acknowledgement has been made in the text.

Gongbin Tang, Chiba, January 2017

ACKNOWLEDGEMENT

ABSTRACT

To design high performance surface acoustic wave (SAW) filters working in the SHF band, it is quite beneficial to employ the ScAlN film based layered structures.

First, the deposition of ScAlN thin films by conventional RF magnetron sputtering using large size Sc-Al alloy targets with large Sc content is discussed. Two 4-inch Sc–Al alloy targets with different Sc content were prepared by the sintering method instead of the conventional dissolution method, and deposited film qualities and uniformity were evaluated. In both cases, uniform ScAlN thin films were obtained throughout the 3-inch wafer. However, measured Sc content was significantly lower than that of the target. Influence of the N_2 content in the sputtering gas was also investigated, and the result indicated that nitridation of the target surface is at least one of the major reasons causing the reduction of the Sc content in the deposited films. Variation of deposited film qualities was observed with the accumulated sputtering time.

Then drastic enhancement of effective coupling factor K_e^2 by mass loading in layered SAW device structures, such as the ScAlN film/Si substrate, is described. This phenomenon occurs when the piezoelectric layer possesses high acoustic wave velocities. The mass loading decreases the SAW velocity, and causes SAW energy confinement close to the top surface where the interdigital transducer is placed. It is shown that this phenomenon is obvious even when an amorphous SiO_2 film is deposited on the top surface for temperature compensation. This K_e^2 enhancement was also found in various combinations of electrode, piezoelectric layer and/or substrate materials.

Existence of this phenomenon was verified experimentally using the ScAlN film/Si substrate structure.

Besides, the validity of material constants reported for the use in SAW device simulations. Based on the full set of material constants calculated by the first principle, bulk acoustic wave velocities are calculated for $Sc_xAl_{1-x}N$ and compared with published experimental results. The effects of $Sc_xAl_{1-x}N$ film material constants with different Sc contents on acoustic characteristics are calculated and the influences of shear components on SAW characteristics are recognized. The effects of $Sc_xAl_{1-x}N$ film material constants with different Sc contents on acoustic characteristics are calculated. Series of SAW devices are fabricated on the structure with various Cu and ScAlN thicknesses h_{Cu} and h_{ScAlN}, respectively, and measured variations of V and K_e^2 with these parameters are compared with the calculation. Good agreements indicate a reliable set of $Sc_xAl_{1-x}N$ material constants for SAW device simulations.

LIST OF CONTENTS

1 Introduction

1.1 Background

Surface acoustic wave (SAW) usually refers to elastic waves mainly propagating on the solid surface. It was first predicated theoretically by Lord Rayleigh in 1885 [1.1], when free boundary surfaces on semi-infinite isotropic elastic bodies. Later, SAW was observed experimentally in earthquakes. Since then, SAWs have been extensively investigated. For vibrations suited in the sagittal plane, a higher order Rayleigh mode, named Sezawa mode, was analyzed on an isotropic plate over an isotropic half space [1.2], and vibrations in the horizontal direction, such as Love mode [1.3], were also analyzed.

SAW devices are widely used for signal processing purpose after the invention of interdigital transducers (IDT) [1.4]. Amongst all, the most famous ones are SAW resonator filters, which are usually fabricated on piezoelectric substrates [1.5]. These filters can be fabricated to be very small size due to the fact that SAW velocities are about the 10^5 times slower than electromagnetic (EM) waves.

Nowadays, due to the high benefit-to-cost ratio, SAW devices are widely used in modern communication systems, especially for applications in receiver front ends of duplexers and as receiver filters under 2 GHz. As is well known, the specifications of existing frequency bands, such as bandwidth and spacing, vary according region to region. On the other hand, low frequency and middle frequency regions (around and below 2 GHz) are quite crowded, and it's believed the situation will become worse in

the future regarding the increasing demand in bandwidths. Thus, it is necessary to expand the operation frequency and improve the filter characteristics, such as insertion loss and bandwidth [1.6].

Traditional piezoelectric material (e.g., rotated y cut LiTaO$_3$ or LiNbO$_3$) based SAW devices, nearly all have employed the fundamental SAW modes, no matter Rayleigh mode or other (quasi) horizontally polarized modes, like surface transverse wave (STW) [1.7]. Thus, for a given fabrication ability, the operation frequency of those devices are intrinsically limited by their slow phase velocities. To expand the operation frequency, usually, there are three methods, where one method is fabricating finer electrodes, the second one is employing substrate with high acoustic velocity, and the third one is choosing the higher order SAW modes. As for the first method, due to the increased ohmic loss, fabrication of finer electrode SAW devices are not so ideal compared to the second and/or third schemes.

Thus, the key points for expanding the operation frequency range lie in the proper choice of the piezoelectric film and/or a higher order SAW mode on layered SAW device structures, where the typical structure is shown in Fig. 1.1. Figure 1.1 (a) stands for the traditional SAW device structure, while Fig. 1.1 (b) stands for the layered SAW device structure [1.8]. Recently, c-axis oriented wurtzite aluminum nitride (AlN) film, due to the low dielectric and acoustic losses, high acoustic wave velocity, thermal stability, and compatibility with conventional silicon manufacture process, has become more and more popular in SAW devices [1.9]. In Ref. [1.10], Fujii, *et al.* demonstrated that high quality factor (Q) SAW resonators operating in the 5 GHz range can be

realized by using the AIN film/single crystalline diamond (SCD) substrate structure. However, due to relative small effective electromechanical coupling factor (K_e^2), AIN film/SCD substrate structure is not appropriate for wideband filter and duplexer applications. Thus, many researchers proposed to improve the piezoelectric property of AlN by doping with other materials (e.g., Ga, In, Sc, Y, Cr, Ti, Ta, etc.), according to the possibility of piezoelectricity enhancement indicated by the first principle calculation [1.11~1.14].
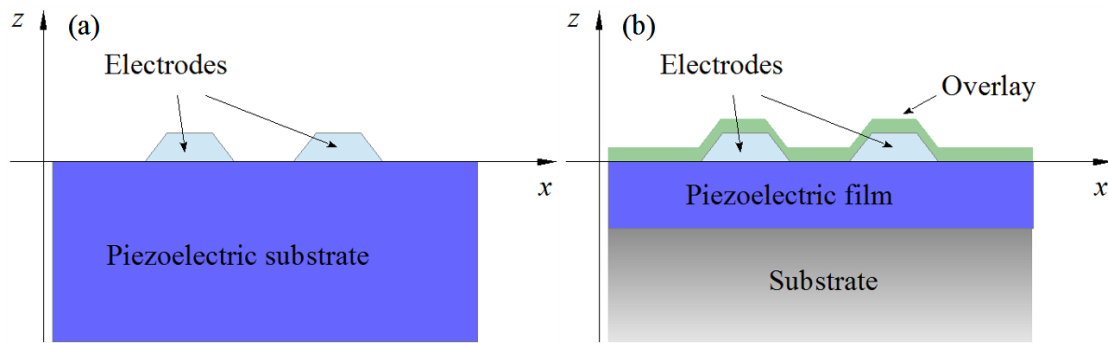
Figure 1.1 Typical SAW device structure and relevant parameters.

Recently, Sc doped AlN (ScAlN), especially when Sc content is about 43%, is paid much attention due to their anomaly strong piezoelectricity (about 5 times larger pure AlN) [1.15~1.16]. Refs. [1.17~1.18] showed that large SAW velocity V, large K_e^2, and small SAW propagation loss are simultaneously obtainable on ScAIN film/SCD substrate structure (V=7200m/s, K_e^2=6.1%, Q_r=520) and ScAIN film/6H-SiC substrate structure (V=6500m/s, K_e^2=4.5%, Q_r=340). These results enable the application of high Q and wideband SAW filters to above 2 GHz frequency bands.

Actually, ScAlN film is not only attractive for SAW devices, but also important for thin film based bulk acoustic wave (BAW) devices. As is well known, BAW devices,

no matter film bulk acoustic wave resonator (FBAR) type, shown in Fig. 1.2 (a), or solidly mounted resonator (SMR) type, shown in Fig. 1.2 (b), mainly employ thickness extensional modes of the piezoelectric layer [1.19~1.21].

Usually, AlN film is preferred as the piezoelectric layer due to its compatibility with CMOS process [1.22], low intrinsic material losses and high deposition rates. Yet again due to the limited K_e^2, performances for BAW devices can't be enhanced drastically during the past decade. Thus, ScAlN film at first was mainly used in BAW devices. Ref. [1.23] showed that giant electromechanical coupling factor k_{33}^2 and k_{15}^2 can reach about 15% and 10% for c-axis normal ScAlN film, respectively. Later, Ref. [1.24] showed K_e^2 for the fabricated ScAlN based FBAR devices are 6.89%, 9.50% and 12.07% when Sc content is 3%, 9% and 15%, respectively. Though the unloaded Q (730, 690 and 410, respectively) is not so high compared with that of pure AlN (790), the ScAlN based FBAR devices are still of great potential.
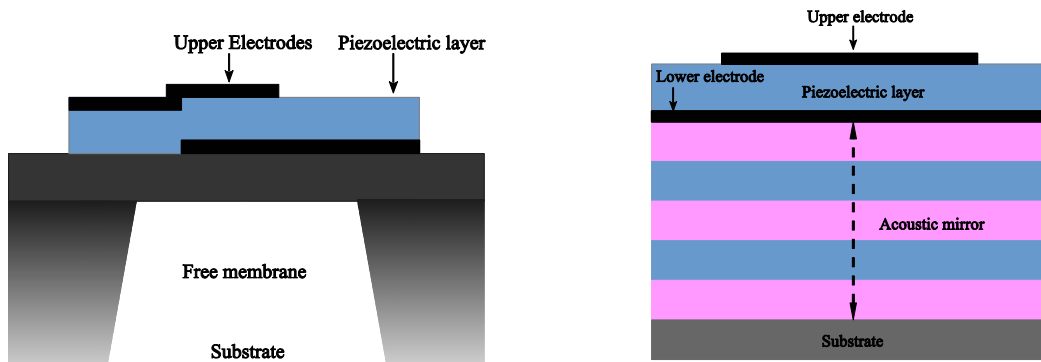
Figure 1.2 BAW device structures, (a) FBAR, (b) SMR.

Thus, the deposition of high quality ScAlN film is the first step to develop high performance SAW devices. Until now, majority of ScAlN films was deposited by co-sputtering using either two targets (Al and Sc) or a pure Al target on which multiple Sc

pellets are placed or inlaid [1.23]. However, on one hand, co-sputtering is not suitable for mass production because of difficulty in controlling film uniformity within a wafer. Several groups have successfully deposited ScAlN films using the conventional radio frequency (RF) magnetron sputtering with single ScAl alloy target [1.23, 1.25~1.27]. On the other hand, since reported Sc content of the targets is relatively low, the electromechanical coupling factor k_e^2 of the deposited films was not enhanced dramatically [1.26].

Yanagitani *et al*. and Akiyama *et al*. independently reported deposition of ScAlN films using a three-inch alloy target with large Sc content [1.23, 1.27]. They could successfully deposit high quality films with large k_e^2. When Sc content is large, hard and brittle intermetallic compounds are often produced in Sc–Al alloy, and large size targets were hard to realize owing to difficulty in its mechanical processing. Meanwhile, when deposition conditions for $Sc_xAl_{1-x}N$ films are unfavorable, phase transitions will show up when Sc content is more than x~0.3 [1.15~1.16, 1.28]. As a result, for deposition of ScAlN thin films by the conventional RF magnetron sputtering using large size Sc–Al alloy targets with large Sc content, optimal conditions need to be investigated.

Besides, though with outstanding performances, SCD and/or 6H-SiC based SAW devices have lost the merit of high benefit-to-cost ratio, we need to consider other solutions, such as use of silicon. However, due to the difference in the elasticity between Si and SCD, much more SAW energy will penetrate into the base Si than SCD. Thus, consideration should be made to tackle this problem.

Furthermore, to design applicable SAW devices, it is necessary to employ the full set of material constants, but at the beginning, only Ref. [1.17] provided the full material constants of $Sc_{0.4}Al_{0.6}N$, which might be derived from those of AlN and partially adjusted based on the measurement of SAW devices. However, experimental results were sometimes deviated from the calculations, and this deviation was expected to be originated from the inaccuracy of the employed material constants for ScAlN film. To make theoretical predications work for device analysis, it is of vital importance to investigate the validity of ScAlN film material constants.

1.2 Motivation

To meet the more and more stringent requirements of future mobile communication standards, performance improvements of SAW devices are highly demanded. As for the design of high performance ScAlN film based SAW devices, the following topics should be considered carefully, such as

1. Establishment of the deposition techniques for ScAlN thin films with large Sc content applicable to mass production,

2. Determination of optimal structures for high performance SAW/BAW devices, and

3. Determination of ScAlN material constants for SAW/BAW device simulation and design.

1.3 Purpose

This thesis discusses applicability of ScAlN thin films for realization of high performance SAW/BAW devices. For the purpose, to fulfill the three demands described above, the following topics are discussed.

1. Deposition of high quality ScAlN thin films by the large size ScAl alloy targets with high Sc content applicable to mass production,

2. Determination of optimal structures for high performance SAW/BAW devices, and

3. Determination of ScAlN material constants for SAW/BAW device design and simulation.

1.4 Organization of this thesis

Chapter 2 describes the deposition of ScAlN thin films by conventional RF magnetron sputtering using large size Sc–Al alloy targets with large Sc content. Two 4-inch Sc–Al alloy targets with different Sc content were prepared by the sintering method instead of the conventional dissolution method, and deposited film qualities and uniformity were evaluated. In both cases, uniform ScAlN thin films were obtained throughout the 3-inch wafer. However, measured Sc content was significantly lower than that of the target. Influence of the N_2 content in the sputtering gas was also investigated, and the

result indicated that nitridation of the target surface is at least one of the major reasons causing the reduction of the Sc content in the deposited films.

Chapter 3 describes drastic enhancement of effective coupling factor K_e^2 by mass loading in layered SAW device structures such as the ScAlN film/Si substrate. This phenomenon occurs when the piezoelectric layer possesses high acoustic wave velocities. The mass loading decreases the SAW velocity, and causes SAW energy confinement close to the top surface where the interdigital transducer is placed. It is shown that this phenomenon is obvious even when an amorphous SiO_2 film is deposited on the top surface for temperature compensation. This K_e^2 enhancement was also found in various combinations of electrode, piezoelectric layer and/or substrate materials. Existence of this phenomenon was verified experimentally using the ScAlN film/Si substrate structure.

Chapter 4 examines the validity of material constants reported for the use in SAW device simulations. At first, based on the full set of material constants calculated by the first principle, bulk acoustic wave velocities are calculated for $Sc_xAl_{1-x}N$ and compared with published experimental results. Then, the effects of $Sc_xAl_{1-x}N$ film material constants with different Sc contents on acoustic characteristics are calculated and the influences of shear components on SAW characteristics are recognized. The effects of $Sc_xAl_{1-x}N$ film material constants with different Sc contents on acoustic characteristics are calculated. Then series of SAW devices are fabricated on the structure with various Cu and ScAlN thicknesses h_{Cu} and h_{ScAlN}, respectively, and measured variations of V and K_e^2 with these parameters are compared with the calculation. Good agreements

indicate the employed $Sc_xAl_{1-x}N$ material constants for SAW device simulations are reliable.

References

[1.1] L. Rayleigh, "On waves propagated along the plane surface of elastic solid," *Proc. London Math. Society* **17** (1885) p. 4.

[1.2] K. Sezawa, "Dispersion of elastic waves propagated on the surface of stratified bodies and on curved surfaces," *Bulletin of the Earthquake Research Institute, Tokyo Imperial University* (1927) p. 1.

[1.3] A. Love, and H. Edward, "Some problems of geodynamics," Cambridge University Press (1911).

[1.4] R. M. White, and F. W. Voltmer, "Direct piezoelectric coupling to surface elastic waves," *Appl. Phys. Lett.* **7** (1965) p. 314.

[1.5] L. A. Coldren, and R. L. Robert, "Surface-acoustic-wave resonator filters," *Proc. IEEE* **67** (1979) p. 147.

[1.6] G. Hueber, J. Tsutsumi, M. Seth, A. S. Morris III, and R. B. Staszewski, "Cost-efficient, high-volume transmission: advanced transmission design and architecture of next generation RF modems and front-ends," *IEEE Micro. Mag.* **16** (2015) p. 26.

[1.7] B. A. Auld, J. J. Gagnepain, and M. Tan, "Horizontal shear waves on corrugated surfaces," *Electron. Lett.* **2** (1976) p. 650.

[1.8] K. Hashimoto, "Surface Acoustic Wave Devices in Telecommunications," Springer-Verlag, Germany, (2000).

[1.9] K. Tsubouchi, K. Sugai, and N. Mikoshiba, "AlN material constants evaluation and SAW properties on AlN/Al$_2$O$_3$ and AlN/Si," *Proc. IEEE Ultrason. Symp.* (1981) p. 375.

[1.10] S. Fujii, T. Odawara, H. Yamada, T. Omori, K. Hashimoto, H. Torii, and S. Shikata, "Low propagation loss in a one-port SAW resonator fabricated on single-crystal diamond for super-high-frequency applications," *IEEE Trans. Ultrason. Ferroelectr. Freq. Control* **60** (2013) p. 986.

[1.11] N. Farrer, L. Bellaiche, "Properties of hexagonal ScN versus wurtzite GaN and InN," *Phys. Rev. B - Condens. Matter* **66** (2002) 2012031.

[1.12] V. Ranjan, S. Bin-Omran, D. Sichuga, R. S. Nichols, L. Bellaiche, and A. Alsaad, "Properties of GaN/ScN and InN/ScN superlattices from first principles," *Phys. Rev. B -Condens. Matter* **72** (2005) p. 1.

[1.13] A. Alsaad, and A. Ahmad, "Piezoelectricity of ordered (Sc$_x$Ga$_{1-x}$N) alloys from first principles," *Eur. Phys. J. B* **54** (2006) p. 151.

[1.14] T. Yokoyama, Y. Iwazaki, Y. Onda, T. Nishihara, Y. Sasajima, and M. Ueda, "Highly piezoelectric co-doped AlN thin films for wideband FBAR applications," *IEEE Trans. Ultrason. Ferroelectr. Freq. Control* **62** (2015) p. 1007.

[1.15] M. Akiyama, T. Kamohara, K. Kano, A. Teshigahara, Y. Takeuchi, and N. Kawahara, "Enhancement of piezoelectric response in scandium aluminum nitride alloy thin films prepared by dual reactive co-sputtering," *Adv. Mater.* **21** (2009) p. 593.

[1.16] M. Akiyama, K. Kano, and A. Teshigahara, "Influence of growth temperature and scandium concentration on piezoelectric response of scandium aluminum nitride alloy thin films," *Appl. Phys. Lett.* **95** (2009) p. 1621071.

[1.17] K. Hashimoto, S. Sato, A. Teshigahara, T. Nakamura, and K. Kano, "High Performance Surface Acoustic Resonators in 1-3 GHz Range Using ScAlN/6H-SiC Structure," *IEEE Trans. Ultrason., Ferroelec., and Freq. Contr.* **60** (2013) p. 637.

[1.18] K. Hashimoto, T. Fujii, S. Sato, T. Omori, C. Ahn, A. Teshigahara, K. Kano, H. Umezawa, and S. Shikata, "High Q surface acoustic wave resonators in 2-3 GHz range using ScAlN/Single crystalline diamond structure," *Proc. IEEE Ultrason. Symp.* (2012) p. 1926.

[1.19] T. W. Grudkowski, J. F. Black, T. M. Reeder, D. E. Cullen, and R. A. Wagner, "Fundamental−mode VHF/UHF miniature acoustic resonators and filters on silicon," *Appl. Phys. Lett.* **37** (1980) p. 993.

[1.20] K. M. Lakin, J. S. Wang. "Acoustic bulk wave composite resonators," *Appl. Phys. Lett.* **3** (1981) p. 125.

[1.21] K. Hashimoto, "RF bulk acoustic wave filters for communications," Artech House, Boston, MA., USA (2009).

[1.22] R. Aigner, "MEMS in RF filter applications: thin film bulk acoustic wave technology," in *Sensors Update* **12** (2003) p.175.

[1.23] T. Yanagitani, K. Arakawa, K. Kano, A. Teshigahara, and M. Akiyama, "Giant shear mode electromechanical coupling coefficient k_{15} in c-axis tilted ScAlN films," *Proc. IEEE Ultrason. Symp.* (2010) p. 2095.

[1.24] M. Moreira, J. Bjurström, I. Katardjev, and V. Yantchev, "Aluminum scandium nitride thin-film bulk acoustic resonators for wide band applications," *Vacuum* **86** (2011) p. 23.

[1.25] K. Arakawa, T. Yanagitani, K. Kano, A. Teshigahara, and M. Akiyama, "Deposition techniques of c-axis-tilted ScAlN films by conventional RF magnetron sputtering," *Proc. IEEE Ultrason. Symp.* (2010) p.1050.

[1.26] R. Matloub, A. Artieda, C. S. Sandu, E. Milyutin, and P. Muralt, "Electromechanical properties of $Al_{0.9}Sc_{0.1}N$ thin films evaluated at 2.5 GHz film bulk acoustic resonators," *Appl. Phys. Lett.* **99** (2011) 92903.

[1.27] M. Akiyama, T. Tabaru, K. Nishikubo, A. Teshigahara, and K. Kano, "Preparation of scandium aluminum nitride thin films by using scandium aluminum alloy sputtering target and design of experiments," *J. Cera. Soc. Jpn.* **118** (2010), p. 1166.

[1.28] A. Zukauskaite, G. Wingqvist, J. Palisaitis, J. Jensen, P. O. Persson, R. Matloub, and L. Hultman, "Microstructure and dielectric properties of piezoelectric magnetron sputtered w-$Sc_xAl_{1-x}N$ thin films," *J. Appl. Phys.* **111** (2012) 093527.

2 Deposition of high quality ScAlN thin films by traditional RF sputtering process

2.1 Introduction

Soon after Akiyama *et al*. demonstrated that wurtzite $Sc_xAl_{1-x}N$ (ScAlN) exhibits extraordinary strong piezoelectricity [2.1~2.2], a large number of research projects were launched all over the world, and its properties were investigated from various aspects [2.1~2.31].

Until now, majority of ScAlN films was deposited by co-sputtering using either two targets (Al and Sc) or a pure Al target on which multiple Sc pellets are placed or inlaid. However, co-sputtering is not suitable for mass production because of difficulty in controlling film uniformity within a wafer. Besides, since reported Sc content of the targets is relatively low, and the material electromechanical coupling factor k^2 was not so enlarged dramatically. Akiyama *et al*. and Yanagitani *et al*. independently reported deposition of ScAlN films using a three-inch alloy target with large Sc content [2.3, 2.4, 2.7] by the conventional RF magnetron sputtering. They could succeed in depositing high quality films with large k^2. Furthermore, as reported by Akiyama *et al*., the growth temperature and scandium concentration has an important effect on the deposited film qualities [2.2]. Moreover, it is worth to note that, when the growth temperature is high, e.g., 580 ℃, the piezoelectric response will deteriorate severely around x~0.3 to 0.4. This phenomenon is believed to be originated from phase instabilities [2.13]. Thus, the deposition conditions need to be considered more carefully.

15

This chapter describes deposition of ScAlN thin films by the conventional RF magnetron sputtering using large size Sc–Al alloy targets with large Sc content. Two 4-in. Sc–Al alloy targets with different Sc content were prepared by the sintering method instead of the conventional dissolution method, and deposited film qualities and uniformity were evaluated. In both cases, uniform ScAlN thin films were obtained throughout the three-inch wafer. As for the significantly lower measured Sc content than that of the target, influence of the N_2 content in the sputtering gas was also investigated, and the result indicated that nitridation of the target surface is at least one of the major reasons causing the reduction of the Sc content in the deposited films.

Besides, variation of deposited film qualities was observed with the accumulated sputtering time.

2.2 Deposition of ScAlN films and their characterization

Two 4-in. Sc–Al alloy targets with chemical composition of $Sc_{0.43}Al_{0.57}$ and $Sc_{0.32}Al_{0.68}$ prepared by Furuya Metal Co. Ltd. were installed in an RF magnetron sputtering system (Anelva SPC350-UHV), which equips an ultra-clean turbo molecular pump and a load-lock system. The sputtering condition used for the deposition is shown in Table 2.1. Nominal purity of Ar and N_2 gases is 99.9999% and 99.9999%, respectively. The deposition rate was circa 0.8 μm/h under this condition. Deposited ScAlN films were characterized by the X-ray fluorescence spectrometry (XFS) for chemical composition, the atomic force microscopy (AFM) for surface roughness, and the X-ray diffraction

(XRD) for crystallographic quality. In following experiments, 3-in. (100) Si wafers with high resistivity were used as the substrate.

2.2.1 Deposition by $Sc_{0.43}Al_{0.57}$ target

At first, we tested the case when employing the $Sc_{0.43}Al_{0.57}$ target. The sputtering condition used for the deposition is the same with that shown in Table 2.1. Under the same deposition condition, we characterized the deposited film from $T=0$ h to $T=60$ h by use of XRD, the results are shown in Fig. 2.1, where the measured XRD rocking curves for the deposited ScAlN films were plotted. It was shown that c-axis preferred orientation around $2\theta=36°$ didn't show up for deposited films except No. 4 and No. 7.
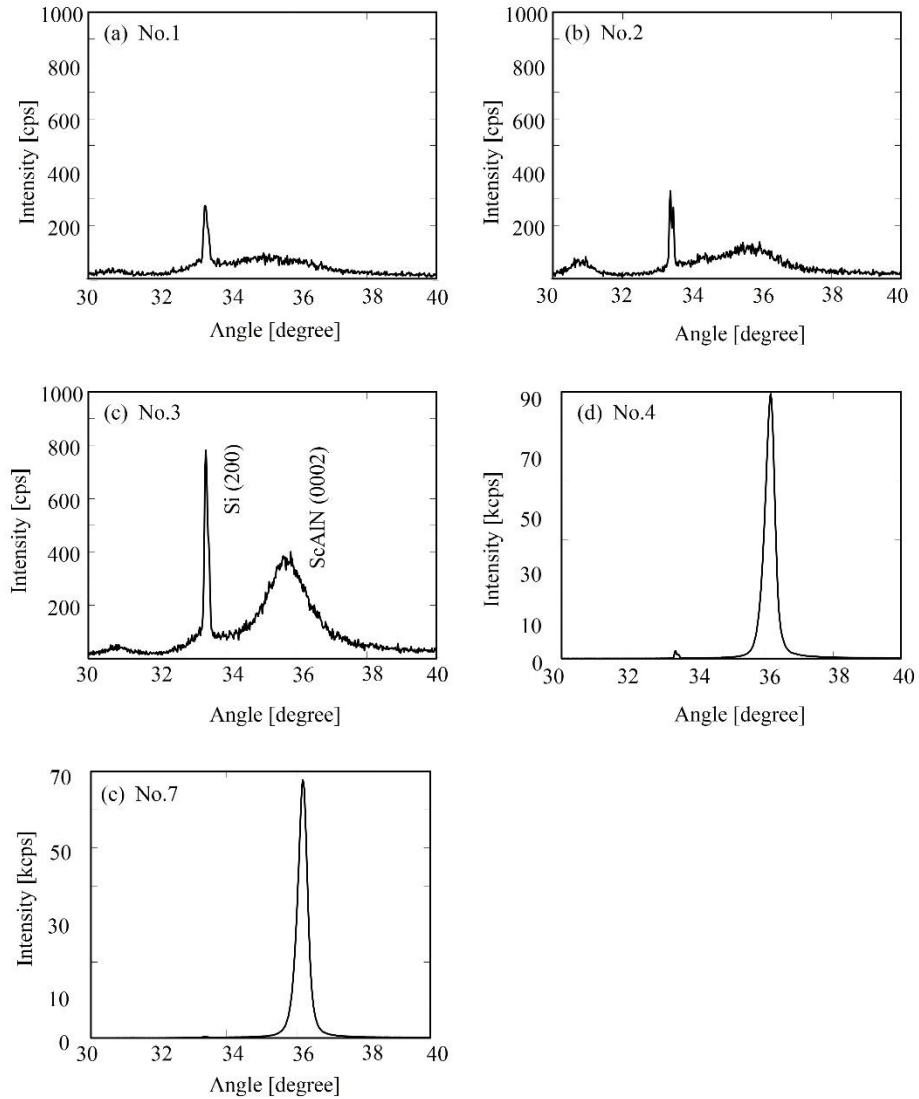
Figure 2.1 θ-2θ curve of deposited ScAlN film when the $Sc_{0.43}Al_{0.57}$ target was employed.

Figure 2.2 shows a measured XRD rocking curve of the (0002) plane for a deposited ScAlN film when the $Sc_{0.43}Al_{0.57}$ target was employed (cumulative deposition time T = 16.5 h and T=42 h). The full width at half maxima (FWHM) was 4.65 ° and 3.25 °, respectively. This indicates that the c-axis of ScAlN grains is well aligned normal to the surface. This property is necessary for developing high performance acoustic wave devices operating in the GHz range. However, as Fig. 2.1 shows, the FWHM for

the other cases are not so good as expected, and this will be further exploited in the following part.

(a) No.4   (b) No.7
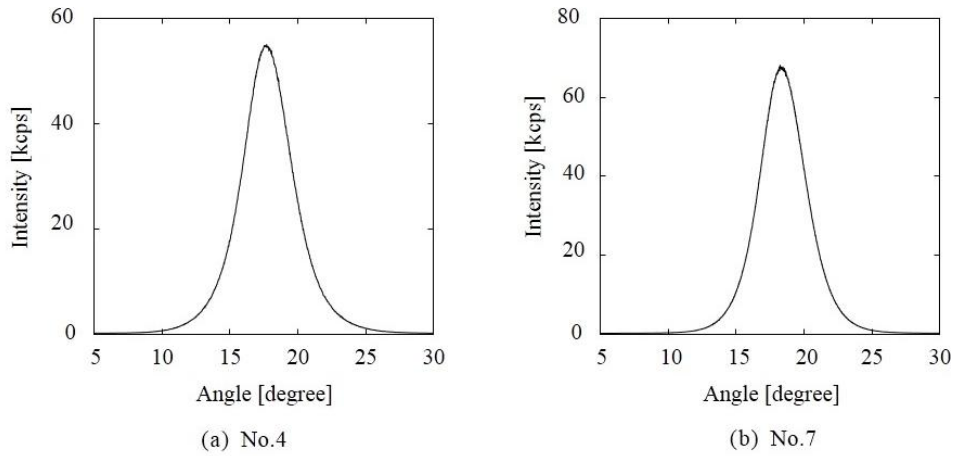
Figure 2.2 Rocking curve of deposited ScAlN film when the $Sc_{0.43}Al_{0.57}$ target was employed, (a) cumulative deposition time T=16.5 h, (b) cumulative deposition time T=42 h

Table 2.1 Deposition condition

Background pressure (Pa)	$<5 \times 10^{-5}$
Total gas pressure (Pa)	5×10^{-1}
N_2 flow (sccm)	12
Ar flow (sccm)	24
Substrate temperature (^{o}C)	200
Target size (in.)	4
Target to substrate distance (mm)	50
RF power (W)	250
Pre-sputtering time (min)	10
Sputtering time (min)	130
Film thickness (μm)	1.6

For high frequency SAW device applications, the scattering loss at the particle grains is a main factor that contributes to the propagation loss [2.32], thus we need to evaluate this surface roughness (R_a). Figure 2.3 shows the top surface of the deposited ScAlN thin film observed by AFM (cumulative deposition time T = 16.5 h), where the particle size of ScAlN film is approximately 80 nm. Besides, we employed equation

(2.1) to calculate the arithmetic average surface roughness, where it means the average value of the absolute amplitude for a given length.

$$R_a = \frac{1}{l} \int_0^l |Z(x)| dx \qquad (2.1)$$

According to equation 2.1, R_a is 1.8 nm. This is not very small, but it is possible to evaluate the SAW devices.
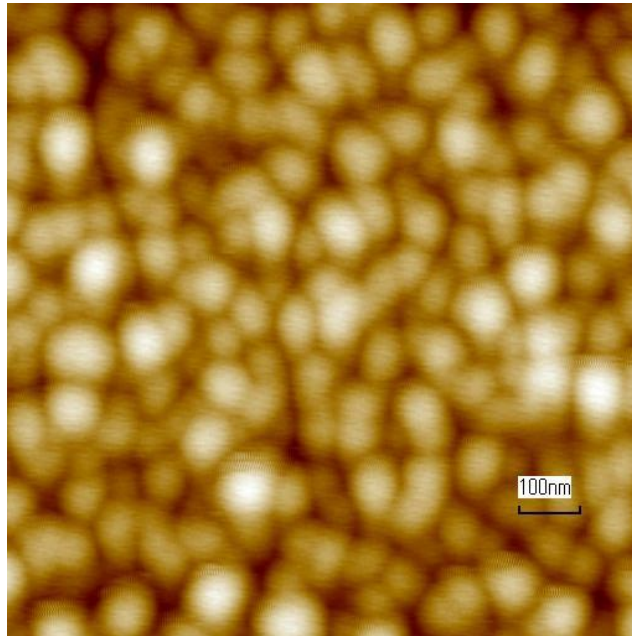
Figure 2.3 AFM image of deposited ScAlN film when the $Sc_{0.43}Al_{0.57}$ target was employed.

Figure 2.4 shows variation of the Sc content measured in a 3 inch wafer. Owing to the alloy target, variation of Sc content was very small. Nevertheless, the measured values of circa 32% (in the wafer center) are significantly lower than that of the target.
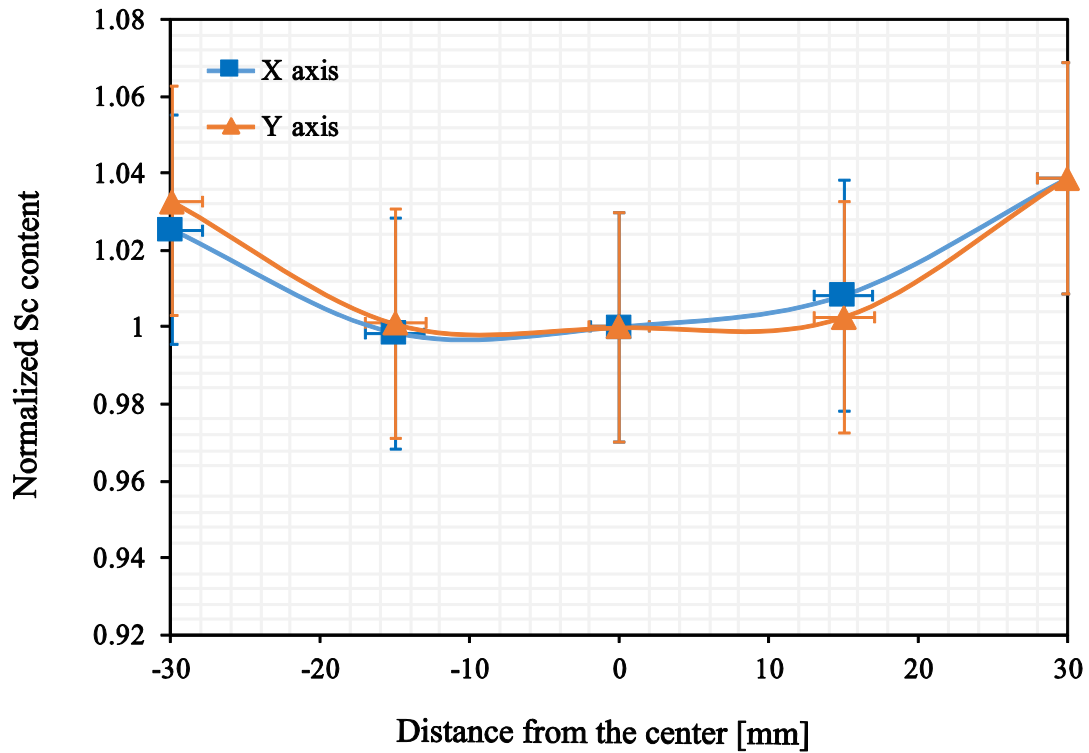
Figure 2.4 Uniformity of the Sc content in the deposited ScAlN film across a wafer when the $Sc_{0.43}Al_{0.57}$ target was employed.

Besides, the XRF measurement shows the Sc content for the deposited ScAlN film is ~45 at. % and 50 at. % at cumulative T=35 h and T=60 h, respectively. Figure 2.5 (b) shows the grain size on the target surface, which did not change so much compared with the initial state shown in Fig. 2.5(a).
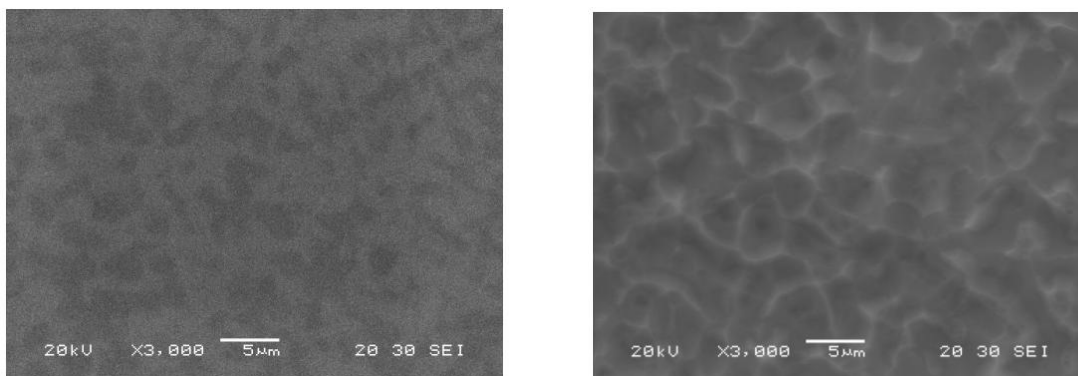
Figure 2.5 SEM result of the deposited ScAlN film, when (a) T=0 h, (b) T=60 h

As the current sputtering system is not equipped with in-situ thickness measurement system, the deposition rate has to be calculated in advance to guarantee a well-controlled thickness and good uniformity. Though in some cases, the deposition conditions vary over time, either on the scale of the deposition time and over months (mainly due to target erosion), we assume that the target status is stable during our experiments. Therefore, we calculate the deposition rate from measuring the film thickness for a given time period. We will use the optical spectral reflectance to measure the film thickness. Since the average measured film thickness is 1.6 μm, the deposition rated can be determined as 17.8 nm/min. It is also worth to note that, the optical reflectance spectrum method, relies on the knowledge of the index of reflection, which is dependent on the deposited film qualities and cannot be measured in advance. Thus, for low quality films, due to the deviation of the refractive index from the ones used in the fitting procedure, the uncertainty during the measurement can reach about 10%.

Moreover, it is also quite important to investigate on the film uniformity over the wafer, which is one of the key factors in deciding whether the deposition techniques can be applicable to mass production or not. The uniformity can be controlled by adjusting appropriately the spatial distribution of the plasma, which means tuning the deposition parameters. Figure 2.6 shows that the film thickness distribution when the $Sc_{0.43}Al_{0.57}$ target was used. The overall thickness distribution is acceptable and can be improved by introducing the substrate rotation system.
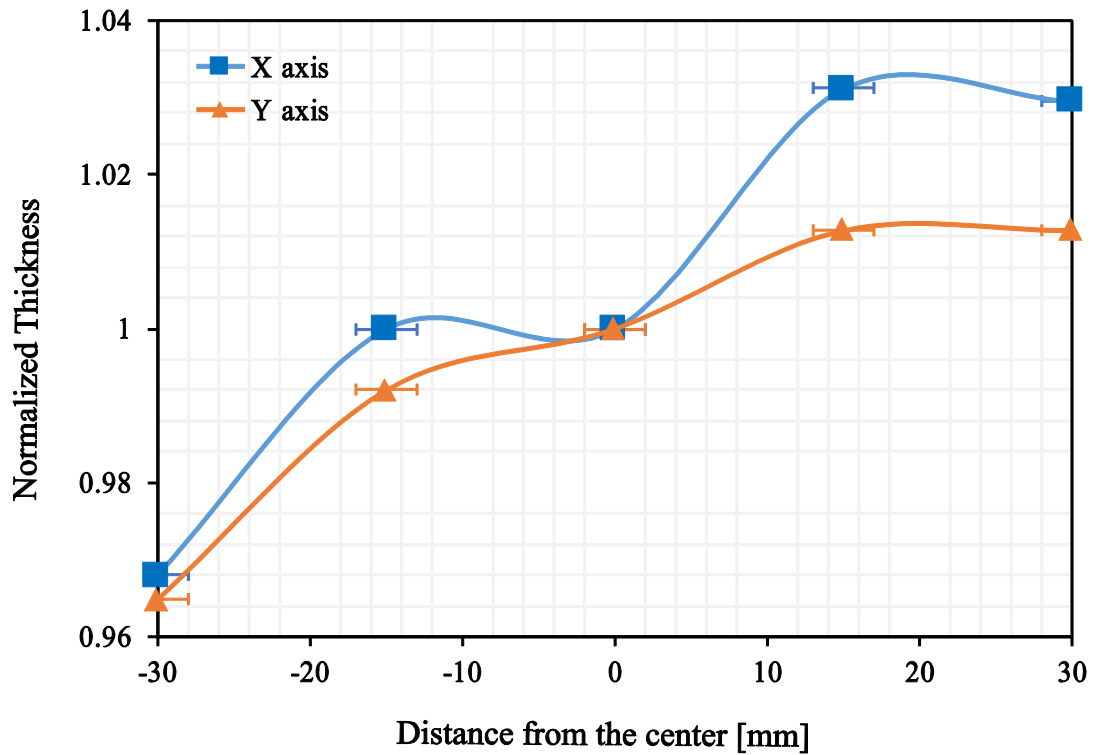
Figure 2.6 Deposited ScAlN film thickness distribution on a 4-in. Si (100) wafer. The thickness is normalized to the thickness at the center of the wafer.

Figure 2.7 shows how the Sc content and the FWHM of the rocking curve changed with the cumulative deposition time T. Although the Sc content increased gradually with T, its total change was very small. Furthermore, the film quality became worse with T, and the (0002) peak was not observed quite often. Although the target surface was polished, the film quality could not be recovered. This deterioration might be attributed to inclusion of the cubic phase ScN, which was observed when the Sc content is large [2.13].
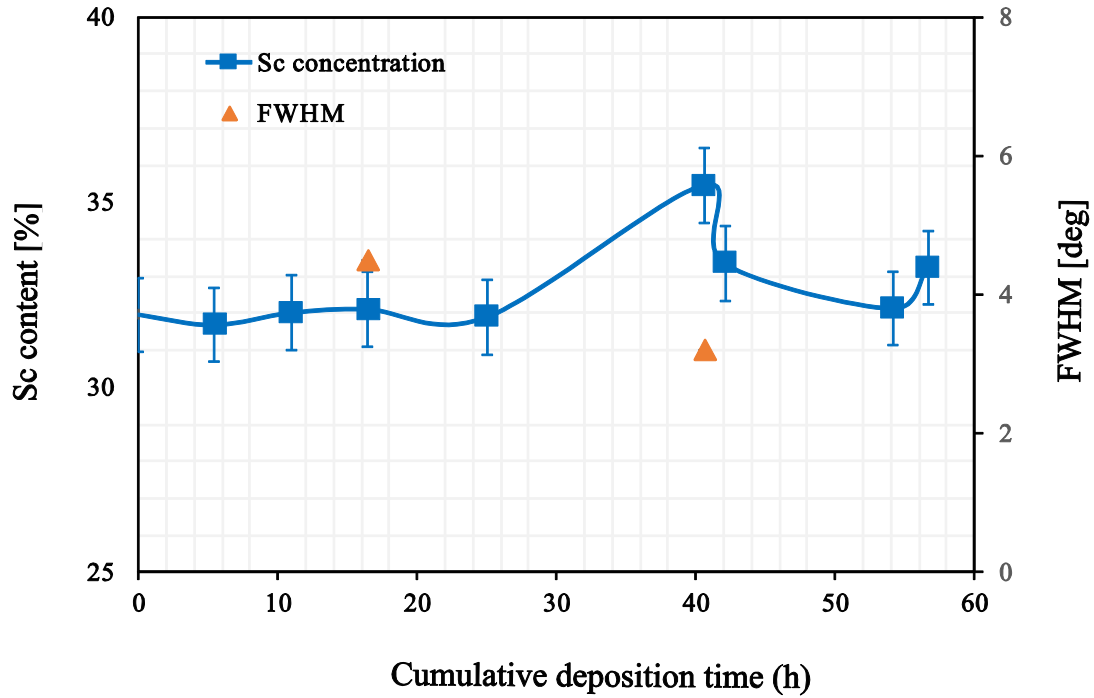
Figure 2.7 Variation of Sc content and FWHM of the rocking curve in the deposited ScAlN film with the cumulative deposition time T when the $Sc_{0.43}Al_{0.57}$ target was employed.

2.2.1 Deposition by $Sc_{0.32}Al_{0.68}$ target

As shown before, to deposit c-axis oriented ScAlN films, we need to reduce the Sc content in the alloy target. Thus, we prepared the 32% ScAl alloy target. The deposition parameters were set the same as the 43% case, where the resulted sputtering rate was ~12.6 nm/min. Meanwhile, to get the same film thickness as the 43% case, the deposition time was adjusted to 130 min., other parameters were kept the same.

Figure 2.8 shows the θ-2θ curve of the deposited ScAlN films for cumulative deposition time from T= 0 h to T = 35.2 h. It is clearly shown that the c-axis orientation is better than that of the 43% case, and the FWHM is becoming stable when the

cumulative deposition time increases. Besides, the peak around $2\theta=32^{\rm o}$ is the diffraction

peak for AlN (100). When the deposition time increases, the c-axis orientation for

ScAlN film showed up and the crystallography structure also improved, especially for

Fig. 2.8 (e)-(j), which mean the quality of the deposited films improved after cumulative

time T~10 hours. The trend for the 2θ and the FWHM of the deposited films can be

clearly shown in Fig. 2.8 (k)-(l), where the FWHM can reduce to about $3^{\rm o}$ while keeping

the 2θ~$36^{\rm o}$. This means preferred c-axis orientation can be achieved under these

conditions. Furthermore, the AFM measurements for those samples are shown in Fig.

2.9, where the grain size after cumulative time T~3.5 hours is similar to the 43% case,

which is ~80nm. Though the average $R_{\rm a}$ is ~2.4nm, a little worse than the 43% case, it

is acceptable for our SAW device application purpose.
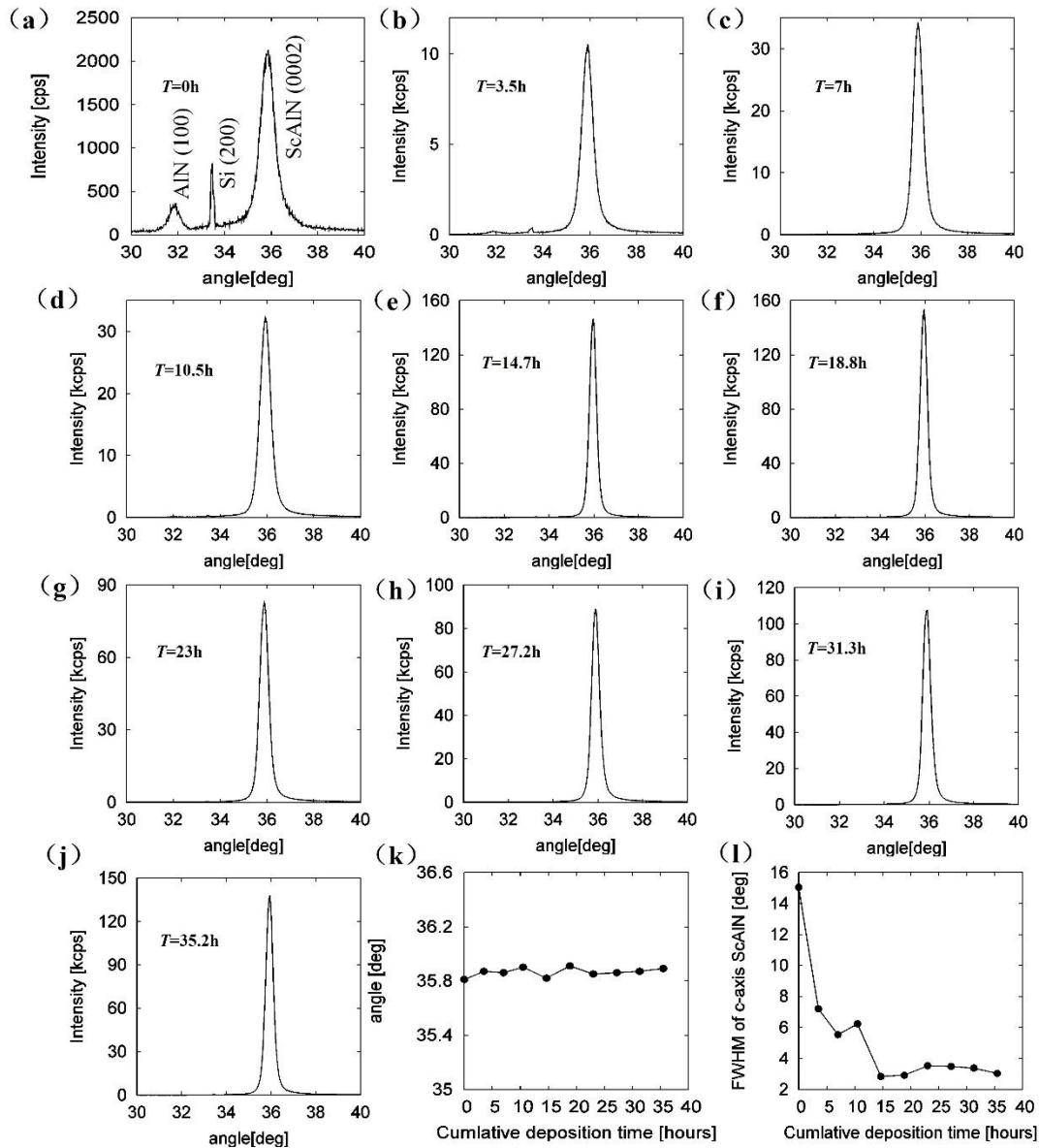
Figure 2.8 θ-2θ curve of deposited ScAlN film when $Sc_{0.43}Al_{0.57}$ target was employed, (a)-(j) stands for cumulative deposition time T=0 to T=35.2h, (k) θ-2θ curve peak changing with T, (l) FWHM changing with T
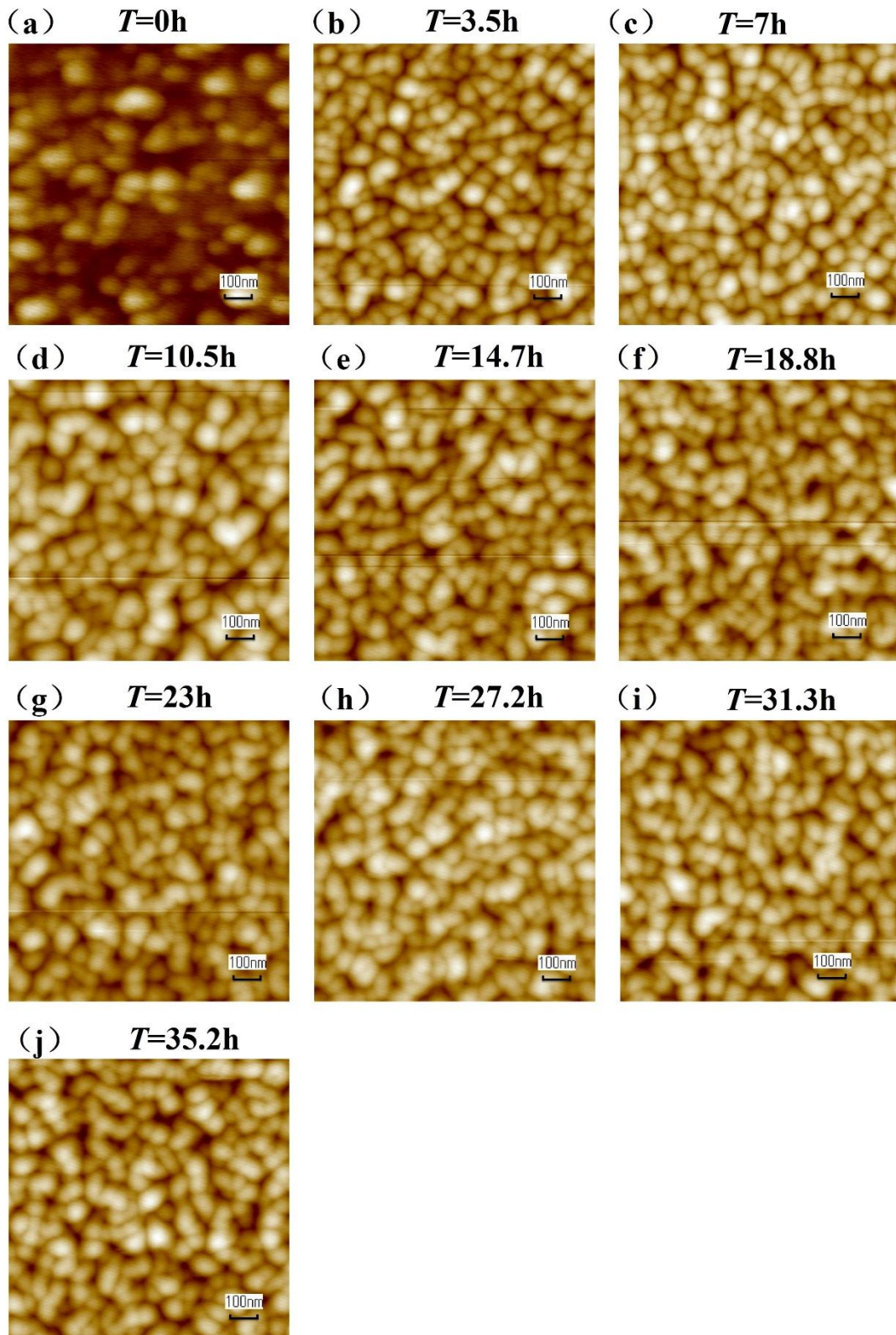
Figure 2.9 AFM result of the deposited ScAlN films when $Sc_{0.43}Al_{0.57}$ target was employed, (a)-(j) stands for cumulative deposition time T=0 to T=35.2h

As is well known, the Sc concentration along with the *c*-axis orientation determines the piezoelectric coefficient. Though the deposited films are of good orientations, we still need to know about the Sc concentration in the deposited films. Thus, by using XRF, we also derived the variation of Sc content and FWHM to cumulative time T when $Sc_{0.32}Al_{0.68}$ target was used. Similar to the case when the $Sc_{0.43}Al_{0.57}$ target was employed, the Sc content of the deposited film was approximately 22% which was significantly lower than that of the target. On the other hand, the FWHM became better with an increase in T in this case. This may be due to reduction of outgassing during sputtering with a T increase, thanks to the equipped load lock system.
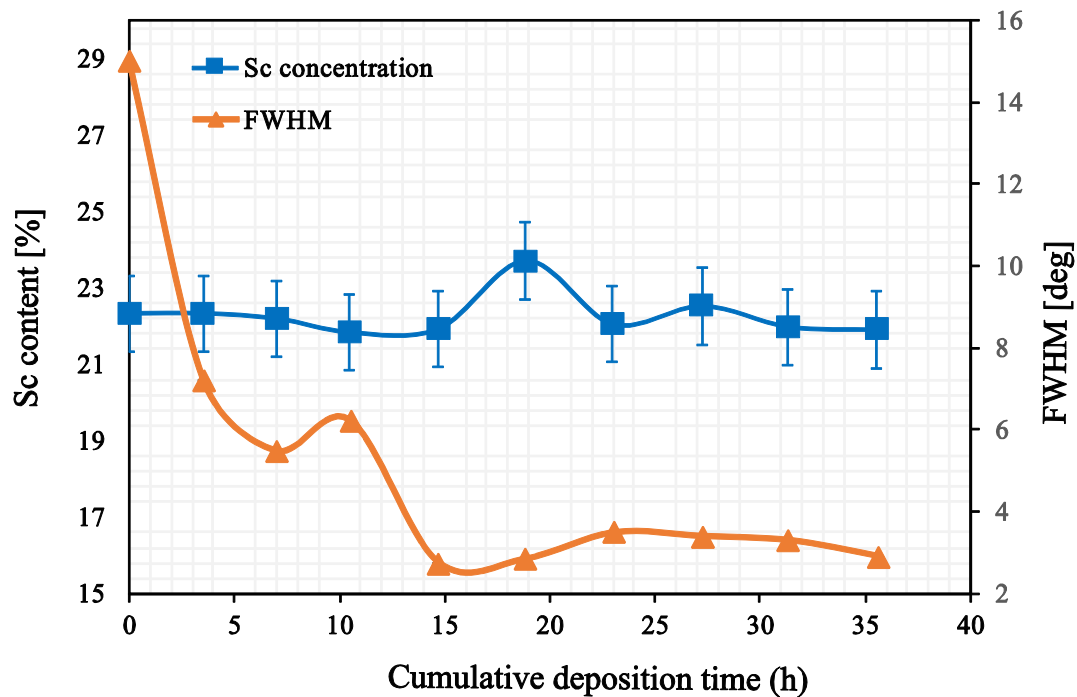
Figure 2.10 Variation of Sc content and FWHM of the rocking curve in the deposited ScAlN film with the cumulative deposition time T when the $Sc_{0.32}Al_{0.68}$ target was employed.

2.3 Design and fabrication of one-port SAW resonator

First, SAW properties on ScAlN film/Si substrate structures were analyzed using software VCALL distributed by the author's group [2.29]. The IDT was assumed to be placed on the top surface of the structure. Since the material constants for the Sc content of 22% and 32% have not been reported, we use the material constants of 43% Sc content that have been reported in Ref. [2.3]. Figures 2.11(a) and 2.11(b) show, respectively, calculated V and K_e^2 for SAWs propagating on the ScAlN film/Si substrate structure as a function of the ScAlN thickness h_{ScAlN} relative to the SAW wavelength λ. Besides, the above calculation doesn't take the influence of the IDT into account, thus, we need to consider the influence of the IDTs, and the results are shown in Fig. 2.12.

As can be seen from both Fig. 2.11 and Fig. 2.12, two propagating modes exist. When there're no electrodes included, the second (Sezawa) mode exhibits relatively large K_e^2 (2.86%) at $h_{ScAlN}/\lambda = 0.633$, where V is also large (5,414 m/s). Astonishingly, when the mass loading effects of the IDTs is taken into account, the K_e^2 for the Sezawa mode can be improved about 3 times when $h_{ScAlN}/\lambda = 0.15$. This means that wideband SAW filters operating over 2 GHz are realizable using finger width about 0.675 μm. Since this phenomenon is quite interesting and of vital importance, we will discuss this issue separately in Chapter 3.

Next, one port SAW resonators were fabricated on the ScAlN film/Si substrate structure to check piezoelectricity of deposited ScAlN films. ScAlN films deposited using the $Sc_{0.43}Al_{0.57}$ target ($T = 16.5$ h) and the $Sc_{0.32}Al_{0.68}$ target ($T = 15$ h) were employed in the following experiments. Measured FWHM, R_a and grain size of the

former film were 3.25 °, 1.8 nm, and 80 nm, respectively, while those of latter one were

2.94 °, 2.4 nm, and 80 nm, respectively.
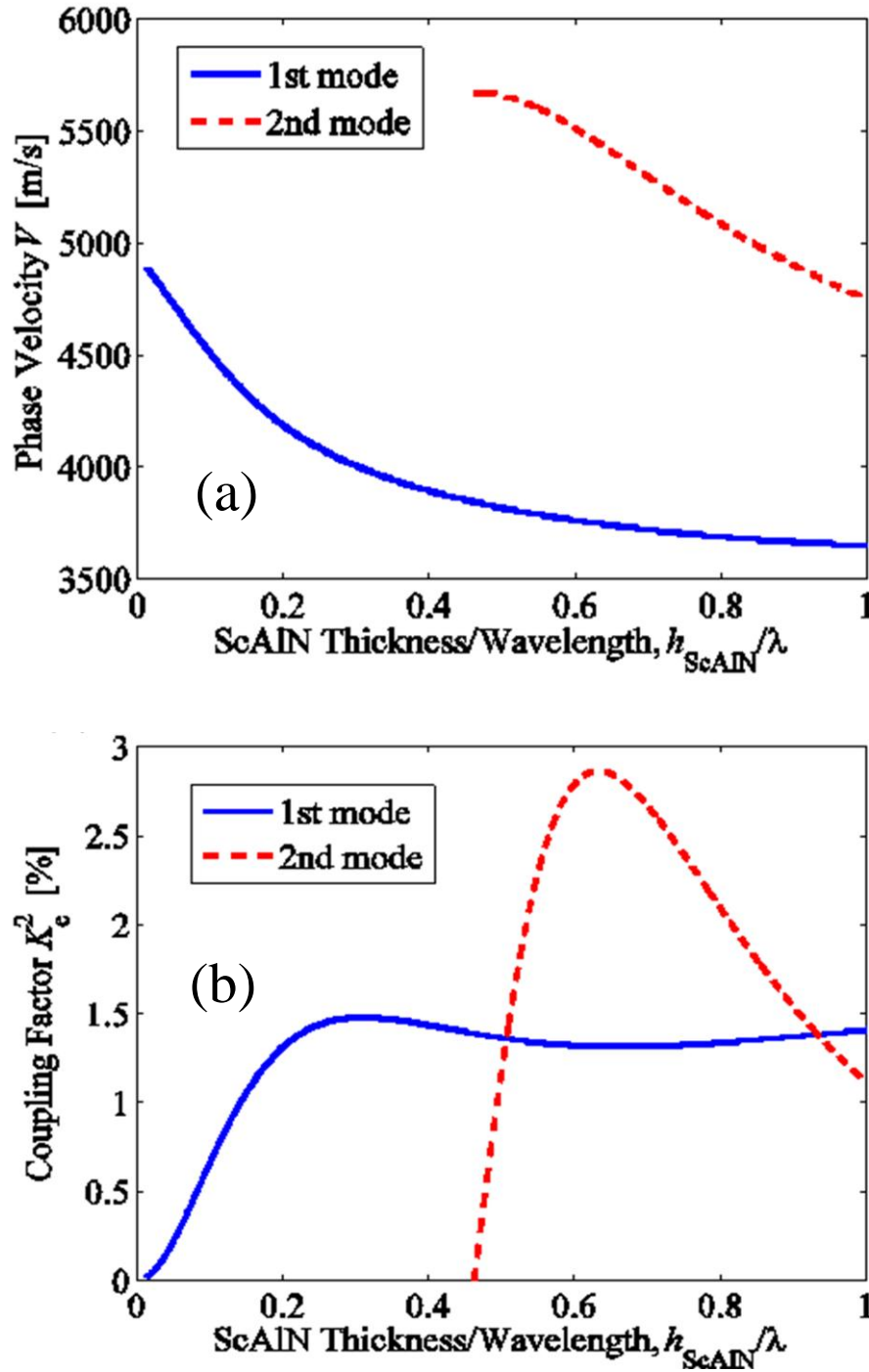
Figure 2.11 SAW propagating on the ScAlN film/Si substrate structure. (a) Phase velocity V for SAW as a function of the ScAlN film thickness h_{ScAlN}/λ, (b) Effective coupling factor K_e^2 for SAW as a function of the ScAlN film thickness h_{ScAlN}/λ.
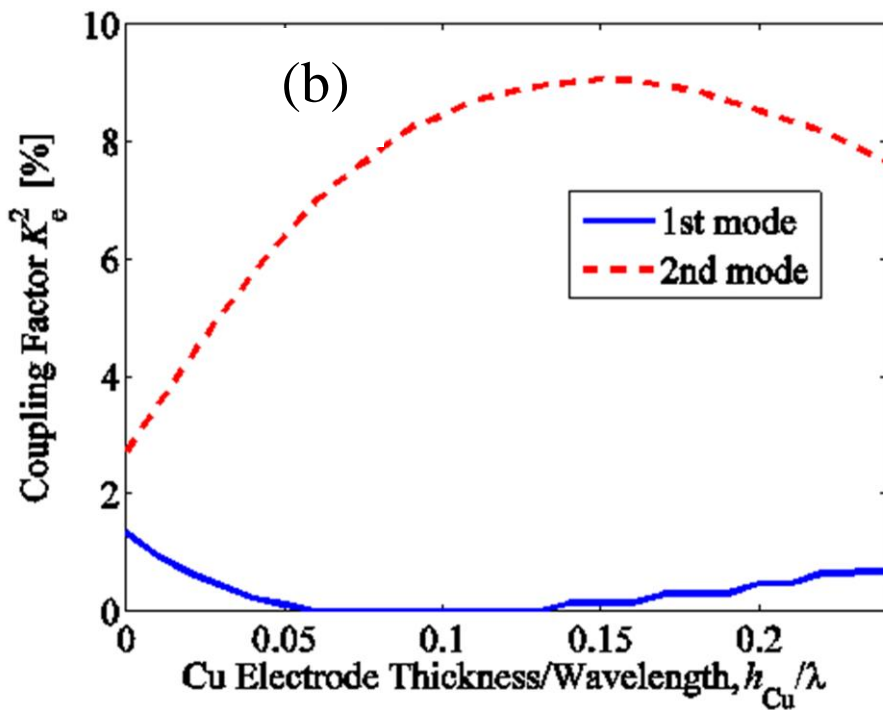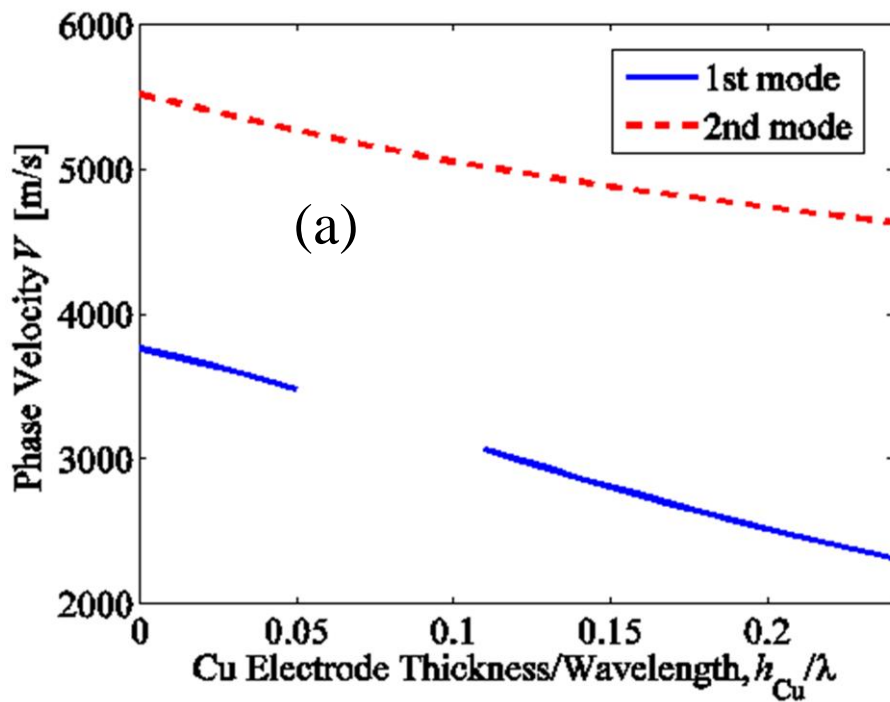
Figure 2.12 SAW propagating on the ScAlN film/Si substrate structure. (a) Phase velocity V for SAW as a function of the ScAlN film thickness h_{ScAlN}/λ, (b) Effective coupling factor K_e^2 for SAW as a function of the ScAlN film thickness h_{ScAlN}/λ.

Copper of 270 nm thickness was chosen as the electrode so as to obtain relatively large SAW reflection coefficient. Fabricated resonators had 80 IDT fingers and 40 reflector fingers, and the IDT periodicity and aperture were 2.7 μm and 54 μm, respectively. The device design is given in Table 2.2.

Table 2. 2 Device design parameters

ScAlN thickness, h_{ScAlN}	1.6 μm
Wavelength, λ	2.7 μm
Finger width, w	0.65 μm
Aperture, W	20λ
Number of IDT finger pairs	80
Number of reflector fingers	40
Cu electrode thickness, h_{Cu}	270 nm

Figure 2.13 shows the measured input impedance $|Z|$ of the fabricated one-port SAW resonators. Estimated SAW phase velocities from the resonance frequencies were 5,549 m/s and 5,700 m/s for the $Sc_{0.43}Al_{0.57}$ and $Sc_{0.32}Al_{0.68}$ cases, respectively. In spite of the difference of the Sc content, discrepancies are not obvious between the experimental and theoretical velocities. It is seen that with an increase of the Sc content, the electromechanical coupling factor K_e^2 increased while the quality factor Q decreased for the resonance. From the fitting, K_e^2 and Q were estimated as 2.7% and 305 for the $Sc_{0.43}Al_{0.57}$ case while they were 1.3% and 910 for the $Sc_{0.32}Al_{0.68}$ case. These values are significantly lower than the theoretical one described above. This is due to the reduction of Sc content from 43%, where K_e^2 takes a sharp maximum [2.1~2.2].
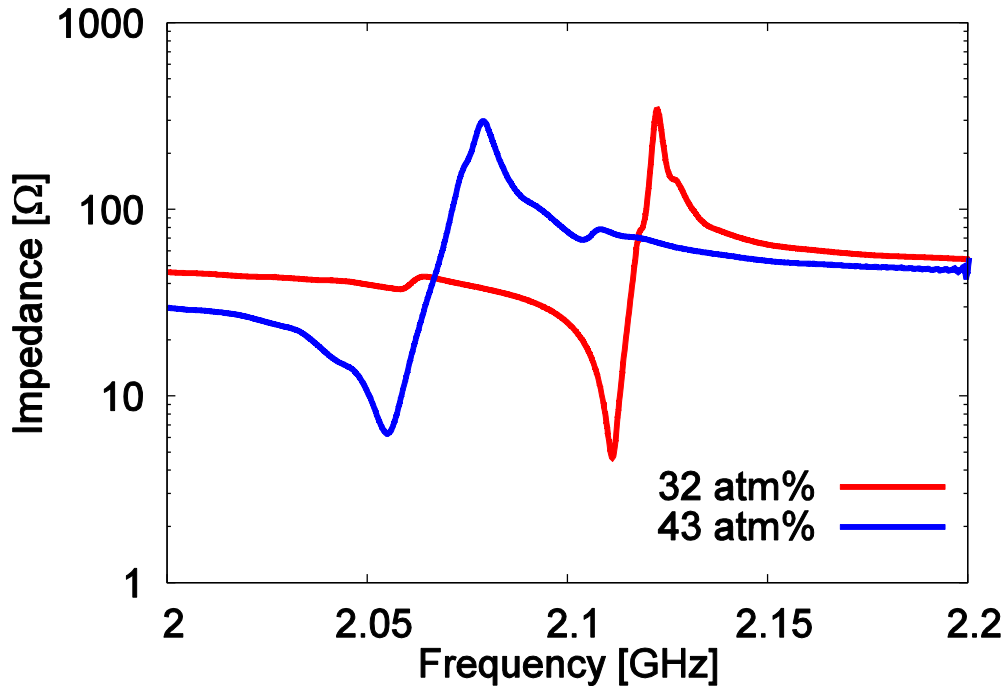
Figure 2.13 Comparison of SAW resonator impedance |Z| with on ScAlN film/Si substrate structure when Sc content is 43% and 32%.

2.4 Influence of N₂ content in sputter gas

In the experiments described above, significant deviation was observed in the Sc content between the deposited films and the target. When a Sc–Al alloy film using 100% Ar gas was deposited, the deviation was negligible. From this result, it was expected that nitridation of the target surface plays an important role in this phenomenon.

Figure 2.14 shows variation of the sputtering rate when the N_2 flow rate was changed and the other conditions were same as those given in Table 2.1. The main valve conductance was adjusted manually so as to keep the total pressure unchanged. The $Sc_{0.32}Al_{0.68}$ target was used in this experiment. It is seen that the deposition rate

decreases monotonically with an increase in the flow rate. Deposited films were metallic when the N_2 flow rate was less than 2 sccm. This result indicates that when the flow rate is large, the target surface is nitrided, and ScAlN clusters emanated from the target are deposited on a substrate. When the flow rate is small, on the other hand, ScAl clusters are emanated from the target and are nitrided.

Figure 2.14 also shows variation of Sc content in the deposited film. The Sc content also decreases with the flow rate, and becomes almost constant when the flow rate is larger than 9 sccm. Strong correlation of the Sc content with the deposition rate indicates that nitridation of the target surface is at least one of the main reasons causing the reduction of the Sc content in the deposited films.

Figure 2.15 shows variation of the FWHM of the rocking curve and the surface roughness with the N_2 flow rate. The FWHM seems to take a minimum value at the flow rate of about 6 to 9 sccm. On the other hand, clear tendency was not observed for the surface roughness.
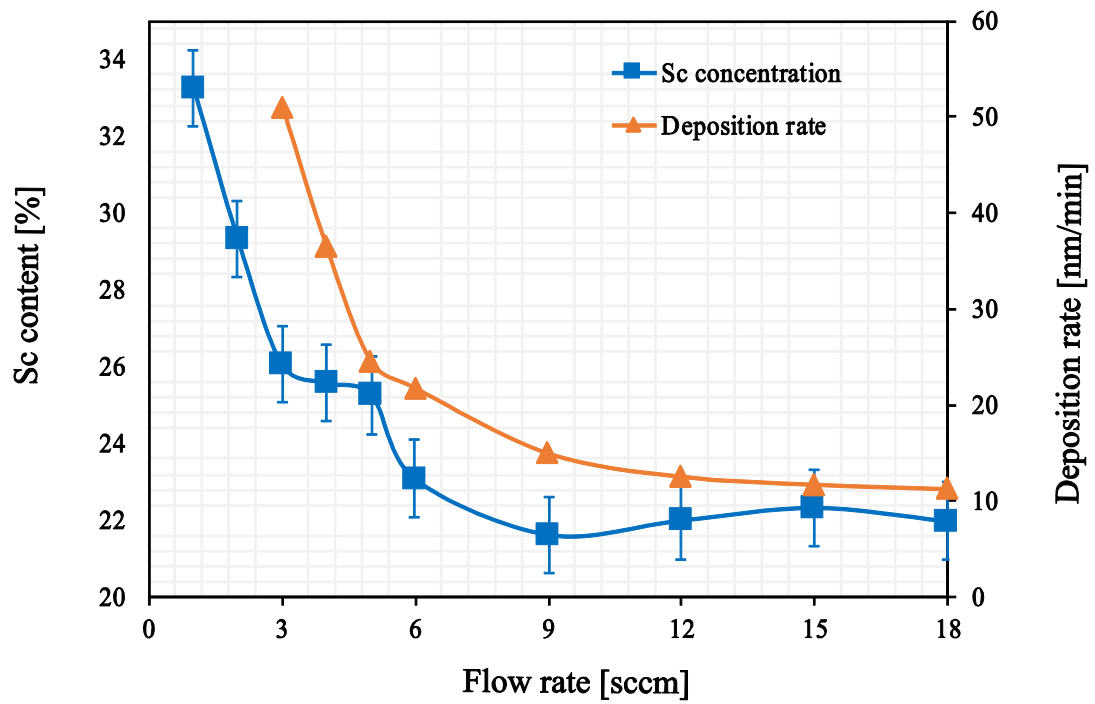
Figure 2.14 Variation of Sc content and deposition rate with N_2 flow rate for $Sc_{0.32}Al_{0.68}$ target.
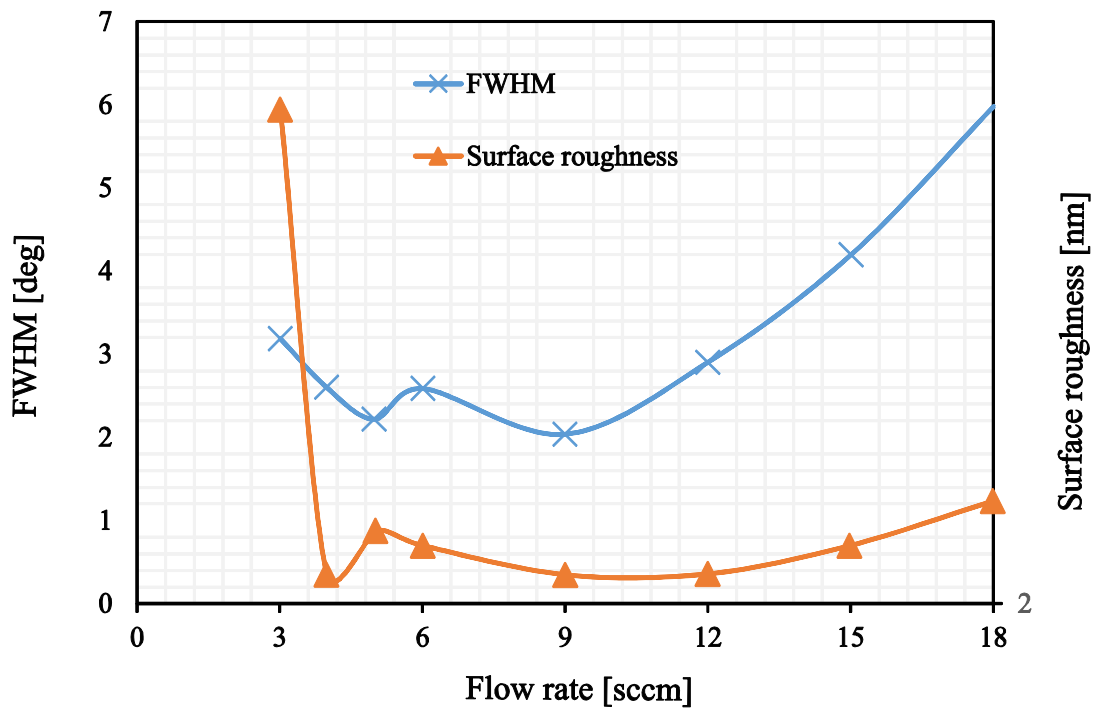
Figure 2.15 Variation of FWHM and the surface roughness with the N_2 flow rate for $Sc_{0.32}Al_{0.68}$ target.

2.5 Conclusion

This chapter discussed deposition of ScAlN thin films by the conventional RF magnetron sputtering using a large size Sc–Al alloy target with high Sc content. Two 4-in. Sc–Al alloy targets with different Sc to Al ratio were prepared, and deposited film qualities and uniformity were evaluated. When a target with Sc content of 43 at. % was used, high quality and uniform c-axis-oriented ScAlN films were obtained throughout the three inch wafer. However, measured Sc content was significantly lower than that of the target. In addition, the film quality became worse and was not stable with an increase in total sputtering time. On the other hand, when the $Sc_{0.43}Al_{0.57}$ target was employed, film quality became better and better with an increase in total sputtering time. One-port SAW resonators were fabricated on the ScAlN film/Si substrate structure and their performances were discussed. Influence of the N_2 content in the sputtering gas was also investigated, and the result indicated that nitridation of the target surface is at least one of the reasons causing the reduction of the Sc content in the deposited films from that in the target.

References

[2.1] M. Akiyama, T. Kamohara, K. Kano, A. Teshigahara, Y. Takeuchi, and N. Kawahara, "Enhancement of piezoelectric response in scandium aluminum nitride alloy thin films prepared by dual reactive co-sputtering," *Adv. Mater.* **21** (2009) p. 593.

[2.2] M. Akiyama, K. Kano, and A. Teshigahara, "Influence of growth temperature and scandium concentration on piezoelectric response of scandium aluminum nitride alloy thin films," *Appl. Phys. Lett.* **95** (2009) 162107.

[2.3] T. Yanagitani, K. Arakawa, K. Kano, A. Teshigahara, and M. Akiyama, "Giant shear mode electromechanical coupling coefficient k_{15} in c-axis tilted ScAlN films," *Proc. IEEE Ultrason. Symp.* (2010) p. 2095.

[2.4] K. Arakawa, T. Yanagitani, K. Kano, A. Teshigahara, and M. Akiyama, "Deposition techniques of c-axis-tilted ScAlN films by conventional RF magnetron sputtering," *Proc. IEEE Ultrason. Symp.* (2010) p. 1050.

[2.5] G. Wingqvist, F. Tasnádi, A. Zukauskaite, J. Birch, H. Arwin, and L. Hultman, "Increased electromechanical coupling in w-Sc$_x$Al$_{1-x}$N," *Appl. Phys. Lett.* **97** (2010) 112902.

[2.6] C. Höglund, J. Birch, B. Alling, J. Bareño, Z. Czigány, P. O. Å. Persson, G. Wingqvist, A. Zukauskaite, and L. Hultman, "Wurtzite-structure Sc$_{1-x}$Al$_x$N solid solution films grown by reactive magnetron sputter epitaxy-structural characterization and first-principles calculations," *J. Appl. Phys.* **107** (2010) 123515.

[2.7] M. Akiyama, T. Tabaru, K. Nishikubo, A. Teshigahara, and K. Kano, "Preparation of scandium aluminum nitride thin films by using scandium aluminum alloy sputtering target and design of experiments," *J. Ceram. Soc. Jpn.* **118** (2010) p. 1166.

[2.8] M. Moreira, J. Bjurström, I. Katardjev, and V. Yantchev, "Aluminum scandium nitride thin-film bulk acoustic resonators for wide band applications," *Vacuum* **86** (2011) p. 23.

[2.9] R. Matloub, A. Artieda, C. Sandu, E. Milyutin, and P. Muralt, "Electromechanical properties of $Al_{0.9}Sc_{0.1}N$ thin films evaluated at 2.5 GHz film bulk acoustic resonators," *Appl. Phys. Lett.* **99** (2011) 092903.

[2.10] K. Hashimoto, S. Sato, A. Teshigahara, T. Nakamura, and K. Kano, "High Performance Surface Acoustic Resonators in 1-3 GHz Range Using ScAlN/6H-SiC Structure," *Tech. Dig. Int. Microwave Symp.* (2012) TU1B-5.

[2.11] K. Hashimoto, S. Fujii, S. Sato, T. Omori, C. Ahn, A. Teshigahara, K. Kano, H. Umezawa, and S. Shikata, "High Q surface acoustic wave resonators in 2-3 GHz range using ScAlN/Single crystalline diamond structure," *Proc. IEEE Ultrason. Symp.* (2012) p. 1926.

[2.12] R. Matloub, M. Hadad, A. Mazzalai, N. Chidambaram, G. Moulard, C. S. Sandu, T. Metzger, and P. Muralt, "Piezoelectric $Al_{1-x}Sc_xN$ thin films: A semiconductor compatible solution for mechanical energy harvesting and sensors," *Appl. Phys. Lett.* **102** (2013) 152903.

[2.13] A. Teshigahara, K. Hashimoto, and M. Akiyama, "Scandium aluminum nitride: Highly piezoelectric thin film for RF SAW devices in multi GHz range," *Proc. IEEE Ultrason. Symp.* (2012) p. 1917.

[2.14] K. Umeda, H. Kawai, A. Honda, M. Akiyama, T. Kato, and T. Fukura, "Piezoelectric properties of ScAlN thin films for piezo-MEMS devices," *Proc. MEMS2013* (2013) p. 733.

[2.15] A. Konno, M. Sumisaka, A. Teshigahara, K. Kano, K. Hashimoto, H. Hirano, M. Esashi, M. Kadota, and S. Tanaka, "ScAlN Lamb wave resonator in GHz range released by XeF$_2$ etching," *Proc. IEEE Ultrason. Symp.* (2013) p. 1376.

[2.16] K. Hashimoto, S. Sato, A. Teshighara, T. Nakamura, and K. Kano, "High Performance Surface Acoustic Resonators in 1-3 GHz Range Using ScAlN/6H-SiC Structure," *IEEE Trans. Ultrason. Ferroelectr. Freq. Control* **60** (2013) p. 637.

[2.17] S. Barth, H. Bartzsch, D. Gloess, P. Frach, T. Herzog, S. Walter, and H. Heuer, "Sputter deposition of stress controlled piezoelectric AlN and AlScN films for ultrasonic and energy harvesting applications," *Proc. IEEE Ultrason. Symp.* (2013) p. 1351.

[2.18] S. Mishin, M. Gutkin, A. Bizyukov, and V. Sleptsov, "Method of controlling coupling coefficient of Aluminum Scandium Nitride deposition in high volume production," *In 2013 Joint Conf. IEEE Int. Freq. Control Symp. & Euro. Freq. Time Forum* (2013) p. 126.

[2.19] S. Zhang, W. Y. Fu, D. Holec, C. J. Humphreys, and M. A. Moram, "Elastic constants and critical thicknesses of ScGaN and ScAlN," *J. Appl. Phys.* **114** (2013) 243516.

[2.20] Y. Zhang, W. Zhu, D. Zhou, Y. Yang, and C. Yang, "The preparation of ScAlN(002) alloy thin films deposited on Si(100) substrates by DC reactive magnetron sputtering," *J. Mat. Sci.: Mat. Electro.* **26** (2015) p. 2151.

[2.21] T. Yanagitani and M. Suzuki, "Electromechanical coupling and gigahertz elastic properties of ScAlN films near phase boundary," *Appl. Phys. Lett.* **105** (2014) 122907.

[2.22] M. Suzuki, T. Yanagitani, and H. Odagawa, "Polarity-inverted ScAlN film growth by ion beam irradiation and application to overtone acoustic wave (000-1)/(0001) film resonators," *Appl. Phys. Lett.* **104** (2014) 172905.

[2.23] A. Konno, M. Kadota, J. Kushibiki, Y. Ohashi, M. Esashi, Y. Yamamoto, and S. Tanaka, "Determination of full material constants of ScAlN thin film from bulk and leaky Lamb waves in MEMS-based samples," *Proc. IEEE Ultrason. Symp.* (2014) p. 273.

[2.24] W. Wang, P. M. Mayrhofer, X. He, M. Gillinger, Z. Ye, X. Wang, A. Bittner, U. Schmid, and J. K. Luo, "High performance AlScN thin film based surface acoustic wave devices with large electromechanical coupling coefficient," *Appl. Phys. Lett.* **105** (2014) 133502.

[2.25] S. Barth, H. Bartzsch, D. Glöß, P. Frach, O. Zywitzki, T. Herzog, S. Walter, and H. Heuer, "Sputter deposition of stress controlled piezoelectric AlN and AlScN films

for ultrasonic and energy harvesting applications," *IEEE Trans. Ultrason. Ferroelectr. Freq. Control* **61** (2014) p. 1329.

[2.26] H. Ichihashi, T. Yanagitani, M. Suzuki, S. Takayanagi, and M. Matsukawa, "Effect of Sc concentration on shear wave velocities in ScAlN films measured by micro-Brillouin scattering technique," *Proc. IEEE Ultrason. Symp.* (2014) p. 2521.

[2.27] M. Zhu, L. Hua, and F. Xiong, "First principles study on the structural, electronic, and optical properties of Sc-doped AlN," *Russ. J. Phys. Chem.* **88** (2014) p. 722.

[2.28] Y. Zhang, W. Zhu, D. Zhou, Y. Yang, and C. Yang, "Effects of sputtering atmosphere on the properties of *c*-plane ScAlN thin films prepared on sapphire substrate," *J. Mater. Sci.* **26** (2015) p. 472.

[2.29] http://www.te.chiba-u.jp/~ken/freesoft.html

[2.30] T. Yokoyama, Y. Iwazaki, Y. Onda, T. Nishihara, Y. Sasajima, and M. Ueda, "Highly piezoelectric co-doped AlN thin films for wideband FBAR applications," *IEEE Trans. Ultrason. Ferroelectr. Freq. Control* **62** (2015) p. 1007.

[2.31] V. Felmetsger, M. Mikhov, M. DeMiguel-Ramos, M. Clement, J. Olivares, T. Mirea, E. Iborra, "Sputtered Al$_{(1-x)}$Sc$_x$N thin films with high areal uniformity for mass production," *In 2015 Joint Conf. IEEE Int. Freq. Control Symp. & Euro. Freq. Time Forum* (2015) p. 117.

[2.32] J. B. Lee, S. H. Kwak, and H. J. Kim, "Effects of surface roughness of substrates on the *c*-axis preferred orientation of ZnO films deposited by RF magnetron sputtering," *Thin Solid Films*, **423** (2003) p. 262.

3 Determination of optimal structures for high performance SAW/BAW devices

3.1 Introduction

As discussed in the first two chapters, the effective electromechanical coupling factor K_e^2 is a key parameter to determine the realizable filter bandwidth and the minimum insertion loss. Recently, much effort has been done on the research of scandium doped AlN (ScAlN) films due to the strong piezoelectricity [3.1~3.25]. But in some cases, the measured K_e^2s are much bigger than the calculated ones. Though it may be partially due to the inaccurate material constants, according to our calculation in Chapter 2, electrode mass loading effect is also necessary to be taken into account.

As is well known, in many cases, K_e^2 of SAW is much lower than that of bulk acoustic waves (BAWs) even when the same piezoelectric material is chosen. This is because the SAW field distribution does not match well to the electric field generated by the interdigital transducer (IDT), and thus K_e^2 can be sometimes enhanced when heavy electrodes are used and/or the IDT is inlaid in the layered substrate. This effect is well known also for the BAW devices [3.26], and is widely used in practical device design.

In general, mass loading by IDTs has not been taken into account for K_e^2 estimation in SAW device structures. This is because K_e^2 does not vary so much with the mass loading for Rayleigh SAWs, which are intrinsically guided to the surface by the surface mechanical boundary conditions. On the other hand, K_e^2 is enhanced by the

mass loading for shear-horizontal (SH) type SAWs, because the mass loading enhances the SAW energy concentration near the surface [3.27].

This chapter describes drastic enhancement of K_e^2 by mass loading in layered SAW device structures such as the ScAlN film/Si substrate. This phenomenon occurs when the piezoelectric layer possesses relatively high acoustic wave velocities, and the SAW energy confinement is enhanced by the mass loading.

At first, the ScAlN film/Si (001) substrate structure is taken as an example, and it is shown that K_e^2 is considerably enhanced by the mass loading of the electrodes. Then it is shown that such K_e^2 enhancement is quite often seen in SAW device structures composed of a thin piezoelectric film and a high velocity base substrate. It should be noted that this phenomenon is obvious even when an amorphous SiO_2 film is deposited uniformly on the top surface for temperature compensation.

Finally K_e^2 enhancement by mass loading was verified experimentally using the ScAlN film/Si substrate structure.

3.2 Simulation

3.2.1 Simulation setup

Figure 3.1 shows the device model of the Cu electrode/$Sc_{0.43}Al_{0.57}N$ film/Si structure used in the simulation. As illustrated in the figure, six configurations for counter-electrode and IDT are employed. In configurations (a) and (b), the crossed electric field is dominant due to the existence of the counter-electrode when the ScAlN thickness is

small. On the other hand, the in-line field is dominant in configurations (c) and (d) in the case. Material constants for $Sc_{0.43}Al_{0.57}N$ were taken from Ref. [3.15], while those of Si, Cu, Al and SiO_2 were taken from Ref. [3.29].
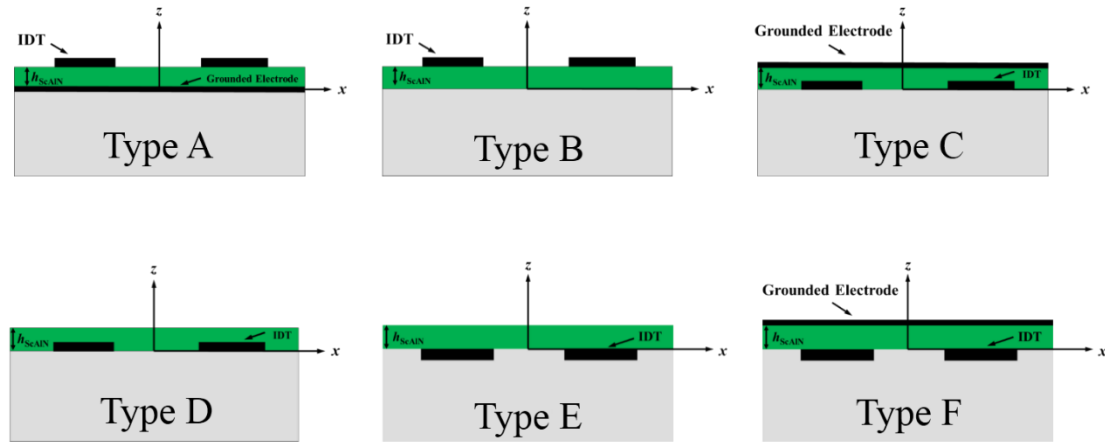
Figure 3.1 Model structure used for simulation

3.2.2 Influence of ScAlN film thickness

At first, the SAW phase velocity V and the K_e^2 are estimated for the ScAlN/Si structure without taking the influence of the IDT mass loading into account. The calculation was performed by the software VCALL [3.27~3.28]. Figure 3.2 shows estimated V and K_e^2 as a function of the h_{ScAlN}/λ, where h_{ScAlN} is the ScAlN thickness. Multiple propagation modes exist, and are labeled in the order of their phase velocities.

As can be seen from Fig. 3.2 (a), V for all the four configurations are almost the same, both for the Rayleigh and Sezawa modes. Differences in velocities show the piezoelectric stiffness effect of the electric field. Judging from the difference, it seems the devices are more stiffened by the crossed electric field. As for Fig. 3.2 (b), though

the electric field distribution in the piezoelectric film is different, type C and type D configurations offer larger K_e^2 for Rayleigh mode than type A and type B. This result implies that K_e^2 for these two modes is preliminary determined by how well the electric field of the SAW matches with that generated by the IDT. Namely, much energy of the Rayleigh mode is distributed close to the boundary between the piezoelectric film and the Si substrate while that of the Sezawa mode is not for all these structures.

It is seen that, for type A and type B configurations, the second (Sezawa) mode exhibits relatively large K_e^2, which take the maximum value of 3.3% and 3.2% at $h_{ScAlN}/\lambda=0.55$ and $h_{ScAlN}/\lambda=0.6$, where V is 5,570 m/s and 5,420 m/s, respectively. On the other hand, in type C and D configurations, Rayleigh mode shows much larger K_e^2 of 6.3% and 9.1%, where $h_{ScAlN}/\lambda=0.6$ and $h_{ScAlN}/\lambda=0.5$, V is 3,770 m/s and 3,810 m/s.

For the former two cases, the maximum K_e^2 for the Sezawa mode is much smaller than the value of 6.1% obtainable in the ScAlN/SCD structure. This is due to difference in the elasticity between Si and SCD, which determines the SAW energy penetration into the base substrate. In contrast, K_e^2 for the Rayleigh mode is comparable with that in the ScAlN/SCD structure. On the other hand, for the latter two cases, the maximum K_e^2 for the Rayleigh mode is much larger than the former two cases. The difference may be explained by the difference in the electric field carried by these modes. It fits well with the electric field generated by the IDT for the Rayleigh mode while not for the Sezawa mode.

(a)

(b)
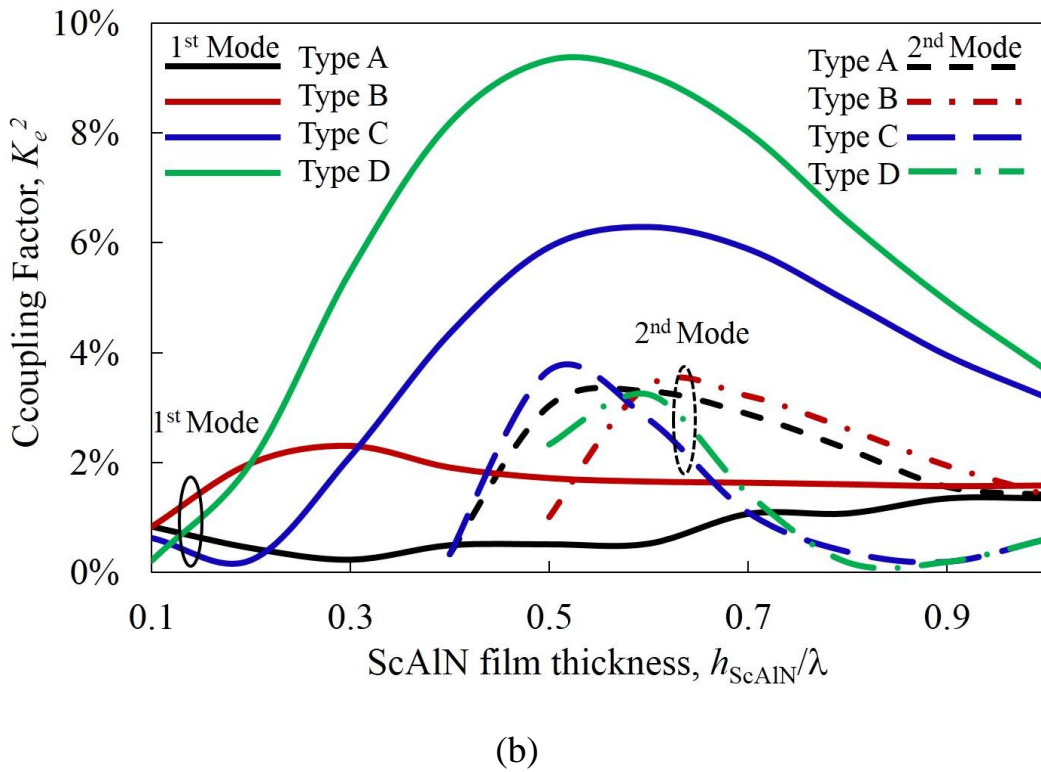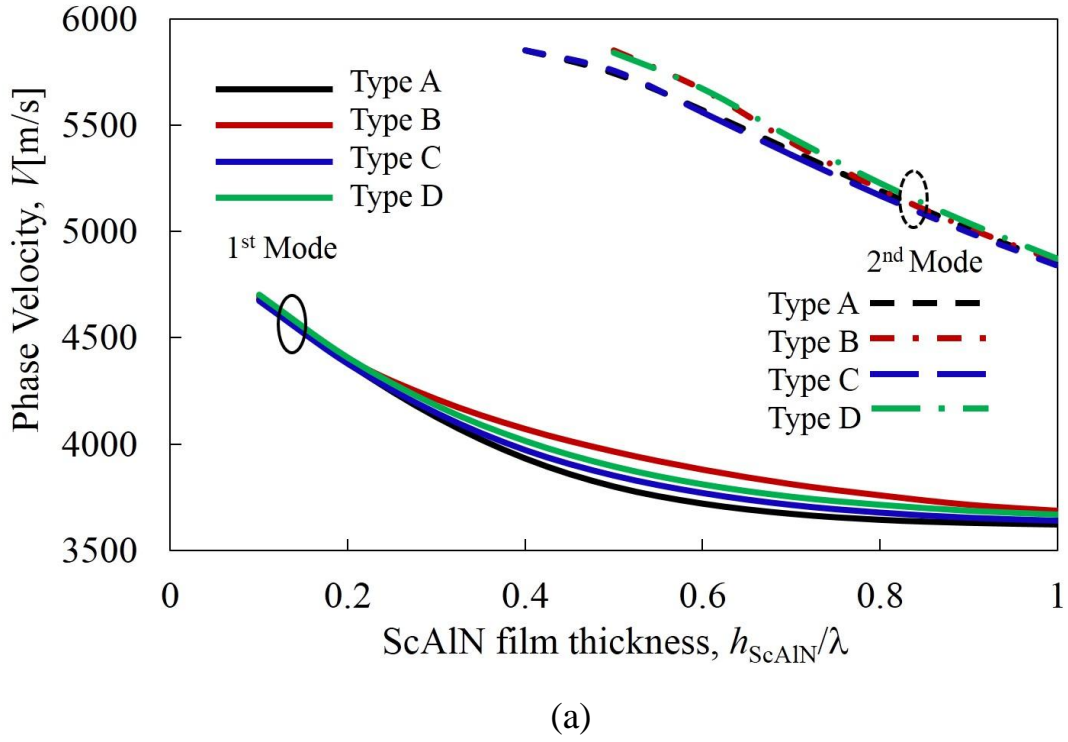
Figure 3.2 SAW properties on ScAlN/Si structure when mass loading is not taken into account. (a) Variation of V with h_{ScAlN}/λ, (b) Variation of K_e^2 with h_{ScAlN}/λ.

3.2.3 Influence of IDT mass loading

Next, h_{ScAlN} is fixed at the value giving the maximum K_e^2 for these four structures, and influence of the Cu electrode thickness h_{Cu} is investigated. The simulation was performed by the software SYNCL [3.27~3.28], which calculates the input admittance of the infinitely long IDT of the device structure as a function of the driving frequency f. Material constants employed in the simulation are the same as before.

The resonance and anti-resonance frequencies, f_r and f_a, respectively, are determined from the calculated input admittance for the fundamental (Rayleigh) and second (Sezawa) modes, and their effective SAW velocity V and K_e^2 are estimated using the following equations:

$$V=f_r\lambda \tag{3.1}$$

and

$$K_e^2=(\pi f_r/2f_a)\cot(\pi f_r/2f_a). \tag{3.2}$$

Figure 3.3 show variation of V and K_e^2 in Cu/ScAlN/Si structure as a function of h_{Cu}/λ. It is seen that when the IDT is placed on the top surface, K_e^2 for the Sezawa mode dramatically increases with h_{Cu}/λ, and takes a maximum value of 7.3% and 8.7% for type A and type B configurations at h_{Cu}/λ~0.12 and h_{Cu}/λ~0.15 respectively, which are more than two times larger than the values at h_{Cu}/λ~0. In contrast, K_e^2 for the Rayleigh mode decreases with h_{Cu}/λ for both cases. This confirms variation of K_e^2 is due to that of the SAW field distribution to fit with the electric field. Owing to the mass loading, V is reduced, but the value is still large (4,969 m/s) at the thickness.

On the other hand, when the IDT is embedded, K_e^2 for the Rayleigh mode decreases monotonically with the increment of h_{Cu}/λ as shown in Figs. 3.3 and 3.4 for type C to type F configurations, no matter whether the IDT is inlaid in the substrate or placed on the boundary. It is interesting to note that as for the Sezawa mode, K_e^2 depends on whether the IDT is embedded or not. Namely, K_e^2 decreases gradually when the IDT is placed on the boundary (type C and type D in Fig. 3.3) while it increases when IDT is embedded (type E and type F in Fig. 3.4).

Since the type B configuration is most desirable from a view point of device fabrication and offers high velocity, relatively large K_e^2 for the Sezawa mode and small K_e^2 for the Rayleigh mode, attention will be focused on the structure for further discussions.
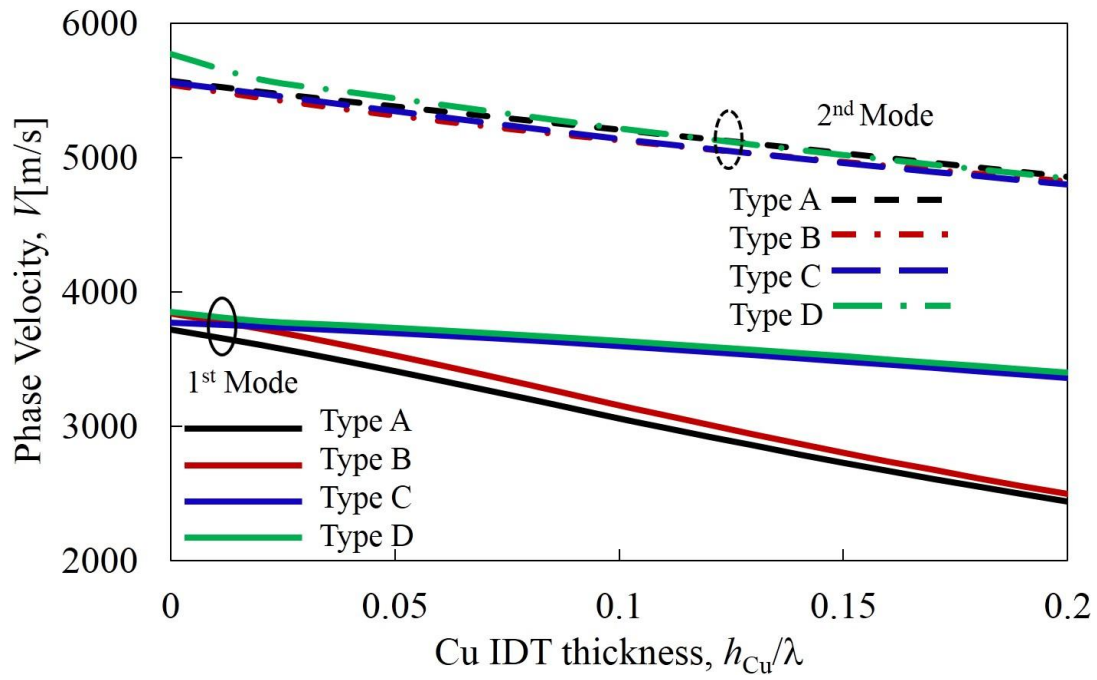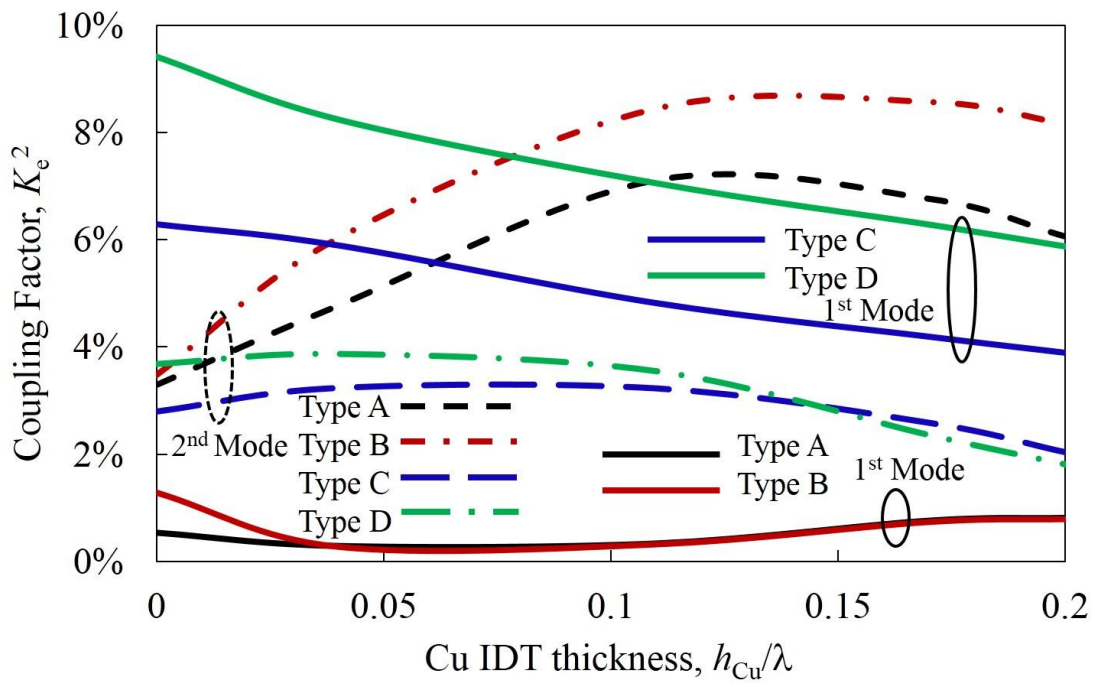
Figure 3.3 SAW properties on ScAlN/Si structure when mass loading is not taken into account. (a) Variation of V with h_{ScAlN}/λ, (b) Variation of K_e^2 with h_{ScAlN}/λ.

(a)

(b)
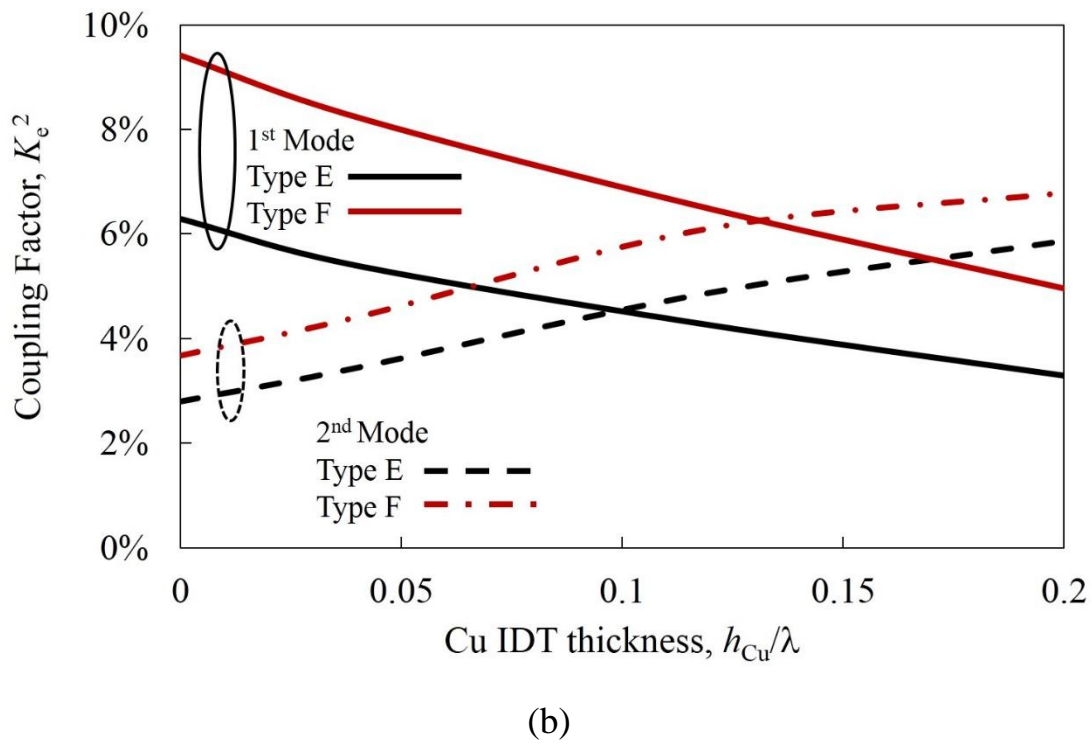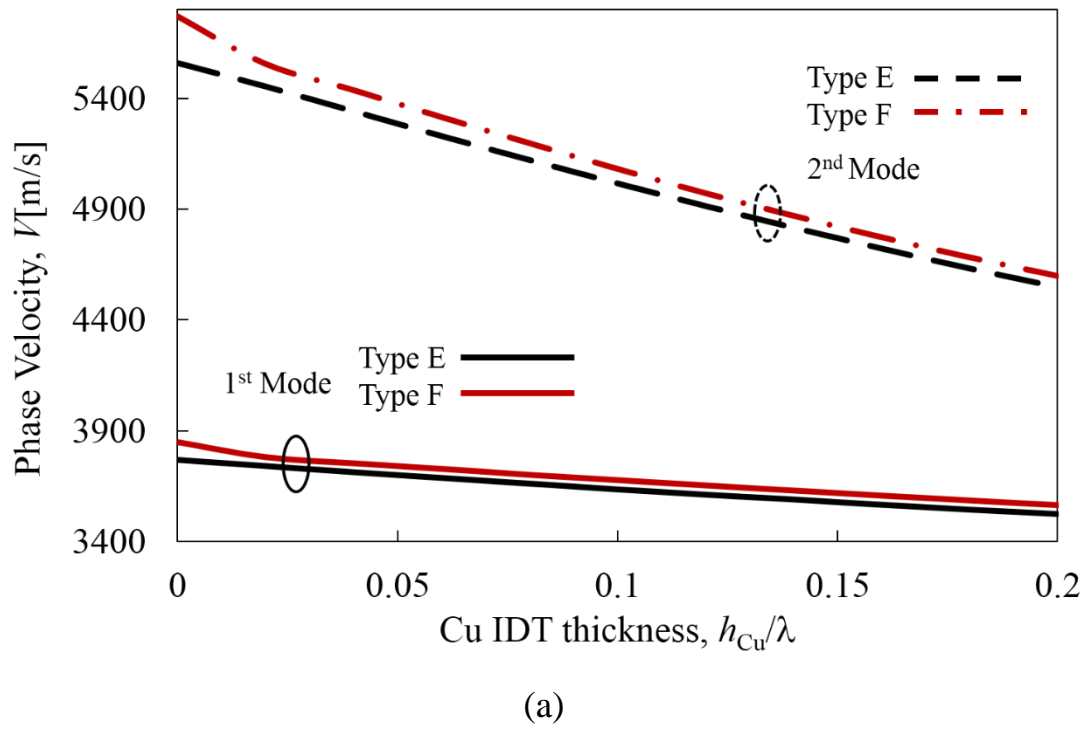
Figure 3.4 SAW properties on ScAlN/Si structure when mass loading is taken into account. (a) Variation of V with h_{ScAlN}/λ, (b) Variation of K_e^2 with h_{ScAlN}/λ.

Figure 3.5 shows the displacement field distributions in four different thicknesses for type B configuration, namely, h_{Cu}/λ=0.01, 0.05, 0.15 and 0.20. When the K_e^2 is large, namely h_{Cu} is close to optimal, the SAW energy tends to be concentrated close to the surface of the piezoelectric layer. This means the field for the Sezawa mode fits well with the electric field under the situation.

(a)   (b)

(c)   (d)
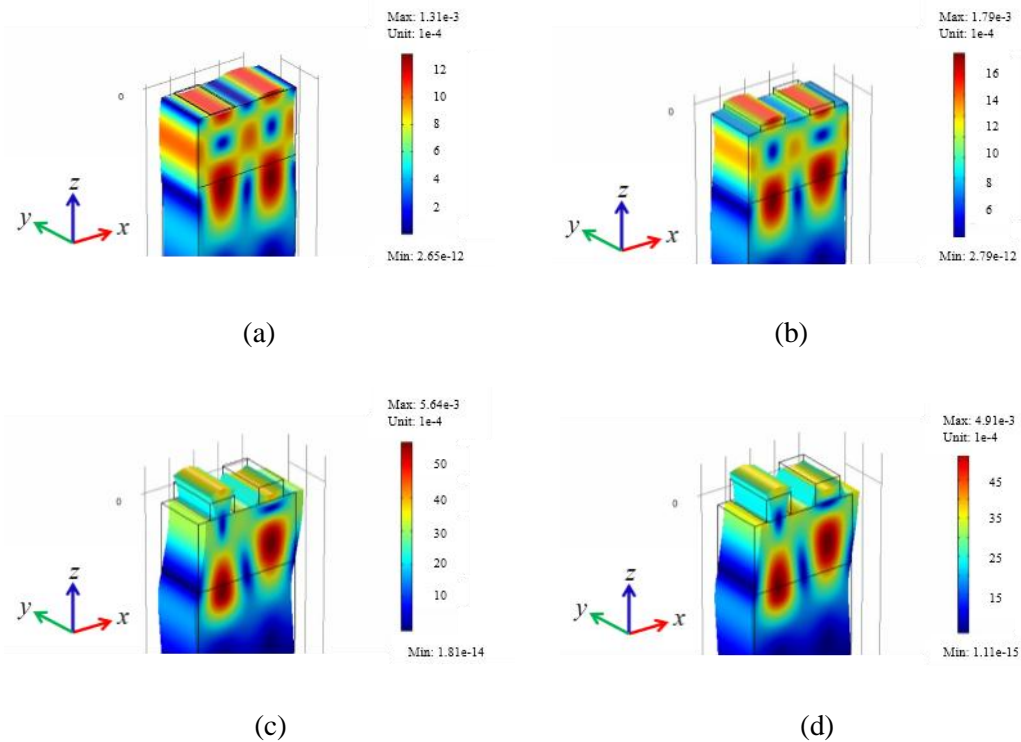
Figure 3.5 Displacement field distributions (Unit: μm) on Cu/ScAlN/Si structure with h_{ScAlN}/λ=0.62 when (a) h_{Cu}/λ =0.01, (b) h_{Cu}/λ =0.10, (c) h_{Cu}/λ =0.15 and (d) h_{Cu}/λ =0.20.

This result confirms variation of K_e^2 is due to variation of the SAW field distribution to fit with the electric field. Owing to the mass loading, V is reduced, but the value is still large (4,883 m/s) at the thickness.

It is known that large K_e^2 is obtainable for the Rayleigh mode in the structure when the IDT is placed at the boundary between the piezoelectric layer and the substrate

instead of the top surface [3.31]. This means that for obtaining large K_e^2 for the Rayleigh mode, the field should be concentrated close to the boundary instead of the top surface. Thus the mass loading offers negative impact to the K_e^2.

Figure 3.6 shows change of K_e^2 with h_{ScAlN} and h_{Cu}. The maximum K_e^2 of 9.5% is achievable when $h_{Cu}/\lambda \sim 0.15$ and $h_{ScAlN}/\lambda \sim 0.55$, where V is 5,080 m/s. It is seen that h_{ScAlN}/λ giving large K_e^2 is less sensitive to h_{Cu}/λ. This implies that the optimal structure can be determined through the following procedures: (1) find the optimal piezoelectric layer thickness with ignoring the IDT thickness, and (2) fix the piezoelectric layer thickness to this optimal value, and find the optimal electrode thickness.
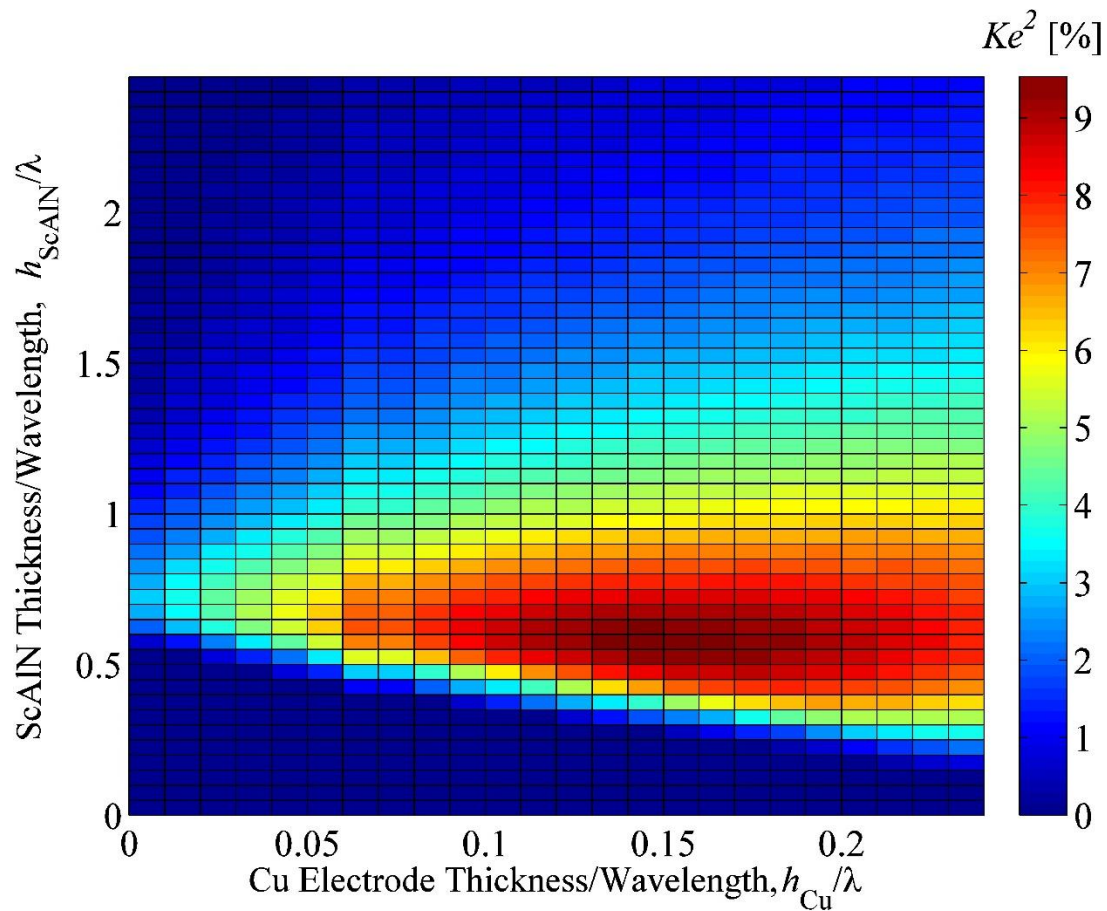
Figure 3.6 Variation of K_e^2 with h_{ScAlN}/λ and h_{Cu}/λ on Cu/ScAlN/Si structure.

This K_e^2 enhancement is also found when other electrode, piezoelectric and/or substrate materials are employed. Table 3.1 shows the maximum K_e^2 for some representative structures. The Cu/ScAlN/SCD structure also offers the K_e^2 enhancement (from 5.5% to 9.8%). This enhancement is smaller than that of the Cu/ScAlN/Si structure (from 2.9% to 9.5%). This is because fast acoustic wave velocities in the SCD offer SAW energy confinement in the piezoelectric layer even when the mass loading is not given. It is interesting to note that choice of sapphire as the base substrate exhibits smaller K_e^2 enhancement than the other choices. It is seen that Cu offers larger K_e^2 enhancement than Al due to difference in the mass density.

Table 3.1. Maximum K_e^2 of mode achieved on different structures.

Structure	K_e^2[%]	V[m/s]	h_{IDT}/λ	$h_{(Sc)AlN}/\lambda$	K_e^2 w/o IDT[%]
Cu/ScAlN/SCD	9.8	5,782	0.11	0.71	5.5
Al/ScAlN/SCD	9.0	5,869	0.19		
Cu/ScAlN/ Sapphire	7.1	5,331	0.16	0.57	2.8
Al/ScAlN/ Sapphire	6.5	5,382	0.23		
Cu/ScAlN/Si	9.1	4,883	0.15	0.62	2.9
Al/ScAlN/Si	7.7	4,876	0.24		
Cu/AlN/SCD	1.98	8,478	0.074	0.6	1.25
Cu/AlN/Si	0.8	5,897	0.28	0.5	0.45

SCD: (001)<100>, Si: (001)<100>, Sapphire: (0001) <1000>

When pure AlN is used, the K_e^2 enhancement also exists. But for the AlN/Si substrate case, much larger mass loading is necessary than the ScAlN/Si case. This is because acoustic wave velocities in AlN are much larger than those in ScAlN.

3.2.4 Influence of SiO$_2$ mass loading

Because the K_e^2 enhancement described in this chapter is owed to the mass loading, addition of a uniform layer on the IDT is another choice. Here this dissertation investigates use of SiO$_2$ uniform layer to the K_e^2 enhancement. The SiO$_2$ and electrode thicknesses can be adjusted to achieve large K_e^2 and temperature compensation simultaneously.

First, h_{ScAlN} is fixed at the value giving the maximum K_e^2 for the four structures, and h_{Cu} is fixed at zero, the configurations from type A to type D are shown in Fig. 3.7. Figure. 3.8 show variation of V and K_e^2 in SiO$_2$/Cu/ScAlN/Si structure as a function of the SiO$_2$ thickness h_{SiO2}/λ. It is seen that K_e^2 for the Sezawa mode for type A and type B increases with h_{SiO2}/λ, and takes maximum values of 6.2% and 7.4%, respectively at h_{SiO2}/λ~0.25.
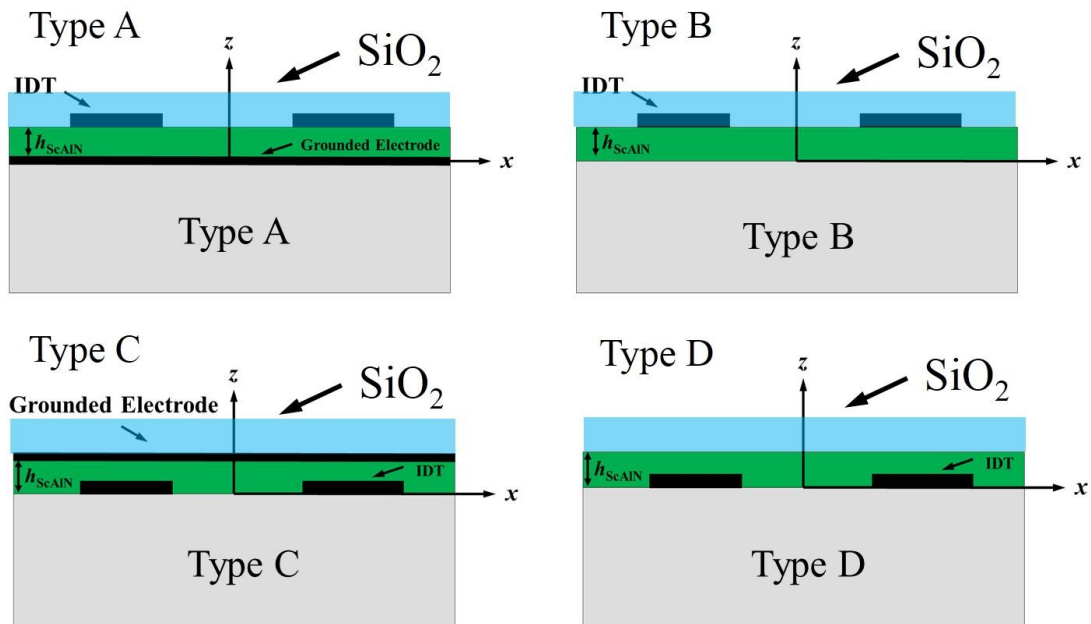
Figure 3.7 Four configurations for counter-electrode and IDT on ScAlN film/Si substrate structure.

On the other hand, K_e^2 for the Sezawa mode decreases with h_{SiO2}/λ, for type C and type D configurations, and goes to about zero at $h_{SiO2}/\lambda \sim 0.25$. In contrast, K_e^2 for the Rayleigh mode decreases with h_{SiO2}/λ for all cases. This confirms variation of K_e^2 is caused by the mass loading, which changes the SAW field distribution. Owing to the mass loading, V is reduced, but the value is still large (about 5,000 m/s) at $h_{SiO2}/\lambda \sim 0.25$.

Then, the influence of finite electrode thickness when the SiO_2 overlay is given will be discussed. Here, the SiO_2 film is assumed to cover not only the electrodes but also the gap between electrodes uniformly (see the inset in Fig. 3.9).

Figure 3.9 shows variation of V and K_e^2 for the Sezawa mode with h_{SiO2} on $SiO_2/Cu/ScAlN/Si$ structure at three different electrode thicknesses while h_{ScAlN} is fixed at 0.55λ. It is seen that when h_{Cu} is small, K_e^2 increases with h_{SiO2}, and the maximum K_e^2 of 8.1% is achievable when both h_{SiO2} and h_{Cu} are set properly. The maximum K_e^2 is scarcely dependent on h_{Cu}, and h_{SiO2} giving the maximum value becomes small with an increase in h_{Cu}.

The uniform SiO_2 deposition results in small reduction in the maximum K_e^2 because SiO_2 in the gap region increases the static capacitance of the IDT.
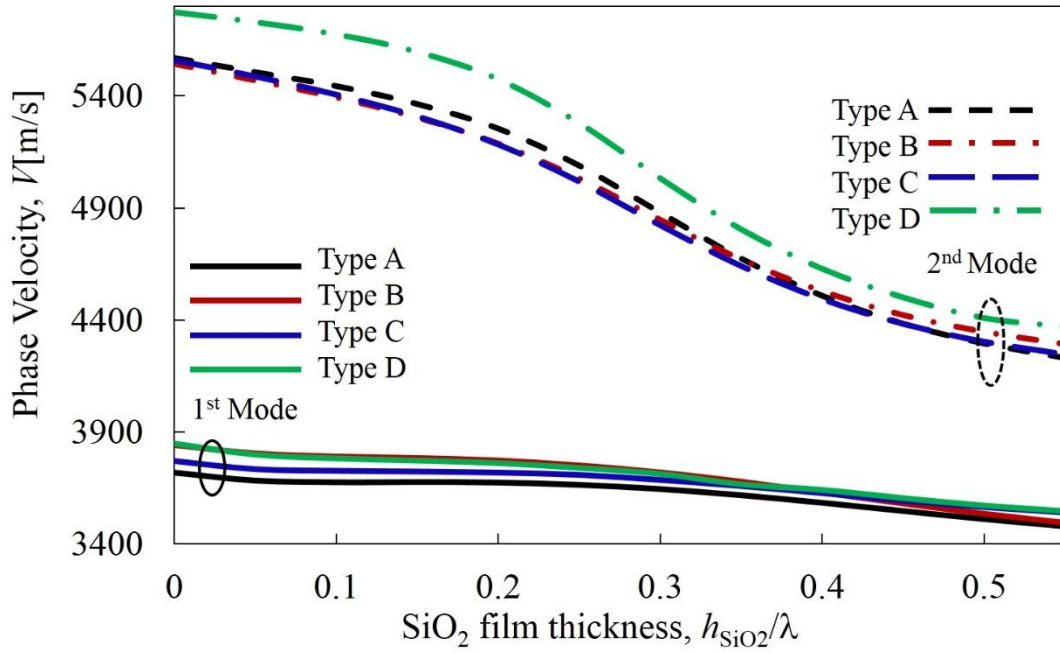
(a)
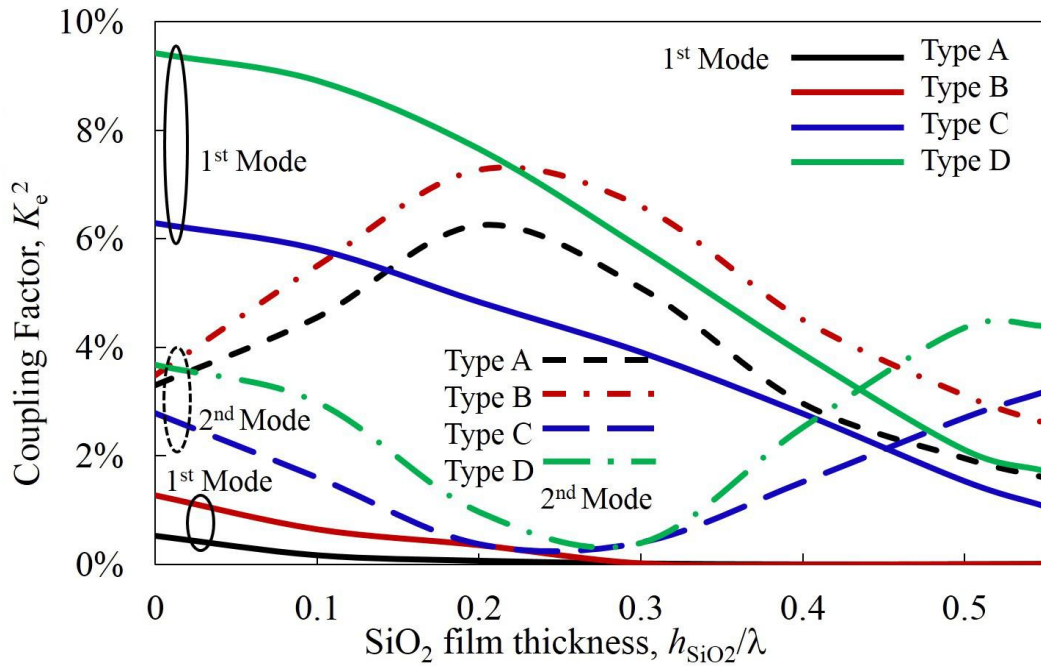
(b)

Figure 3.8 Theoretical SAW properties on $SiO_2/Cu/ScAlN/Si$ structure when $h_{ScAlN}/\lambda = 0.55$. (a) Variation of V with h_{SiO_2}/λ, (b) Variation of K_e^2 with h_{SiO_2}/λ.
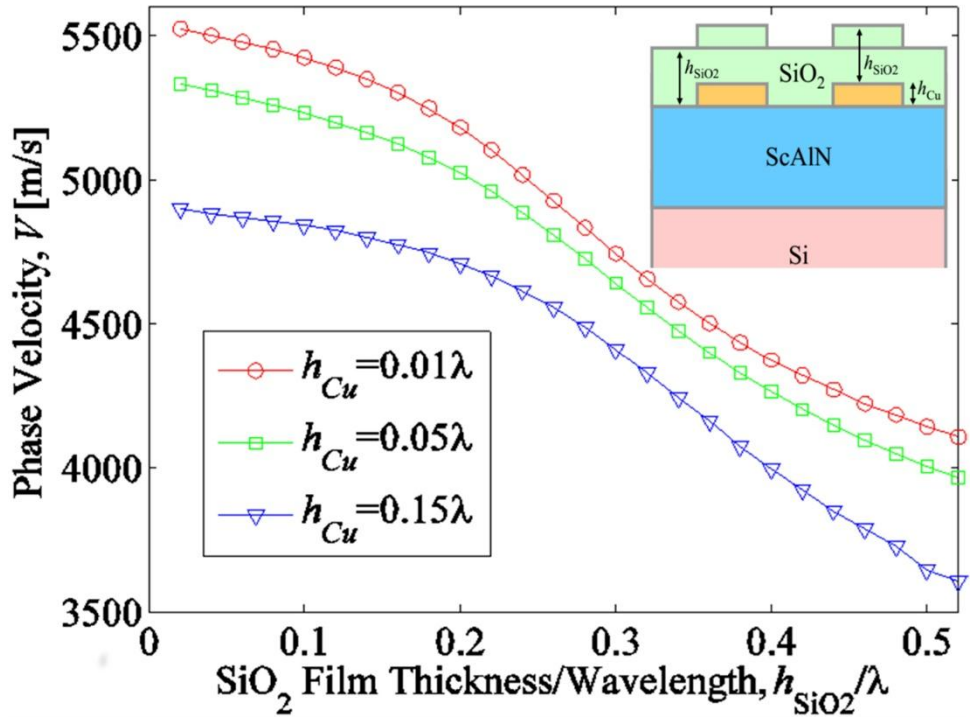
(a)
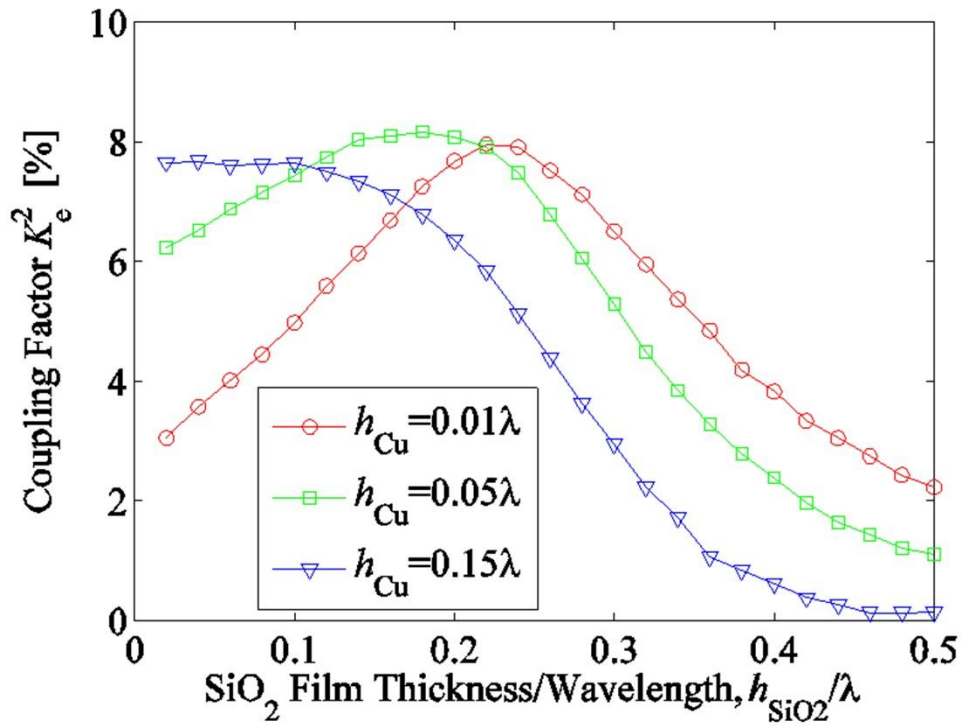
(b)

Figure 3.9 Theoretical SAW properties for Sezawa mode on Type B structure when h_{ScAlN}/λ =0.55. (a) Variation of V with h_{SiO2}/λ, (b) Variation of K_e^2 with h_{SiO2}/λ.

3.3 Experiments

For experimental verification of this phenomenon, a series of one port SAW devices were fabricated on the ScAlN film/Si (100) substrate structure, where ScAlN thin films are deposited by conventional RF magnetron sputtering techniques, by use of 4-inch Sc-Al alloy targets described in Chapter 2. The device design parameters are given in Table 3.2. The Sc content r estimated by the X-ray fluorescence spectrometry was circa 30%.

Table 3. 2 Device design parameters

ScAlN thickness, h_{ScAlN}	1.6 μm
Wavelength, λ	2.0, 2.2, 2.4 μm
Finger width, w	0.5 μm
Aperture, W	20λ
Number of IDT finger pairs	80
Number of reflector fingers	40
Cu electrode thickness, h_{Cu}	20, 100, 200 nm

Figure 3. 10 shows measured K_e^2 of the Sezawa mode as a function of h_{Cu}. It is seen that K_e^2 increases monotonically with h_{Cu}, and K_e^2 of about 2% is obtained when $h_{Cu}/\lambda \sim 0.1$. The value is about three times larger than that when $h_{Cu}/\lambda \sim 0.01$. Achieved K_e^2 is much smaller than that shown in Fig. 3.3(b), and although Fig. 3.3(b) also indicated that K_e^2 mostly saturates at $h_{Cu}/\lambda \sim 0.01$, the experimental curve does not show such tendency. These discrepancies may be caused by inaccurate material constants of ScAlN, or difference in Sc content r, i.e., smaller Sc content r gives larger V and smaller K_e^2. Larger V tends to increase the Cu thickness giving maximum K_e^2 as indicated in Section 3.2.3.
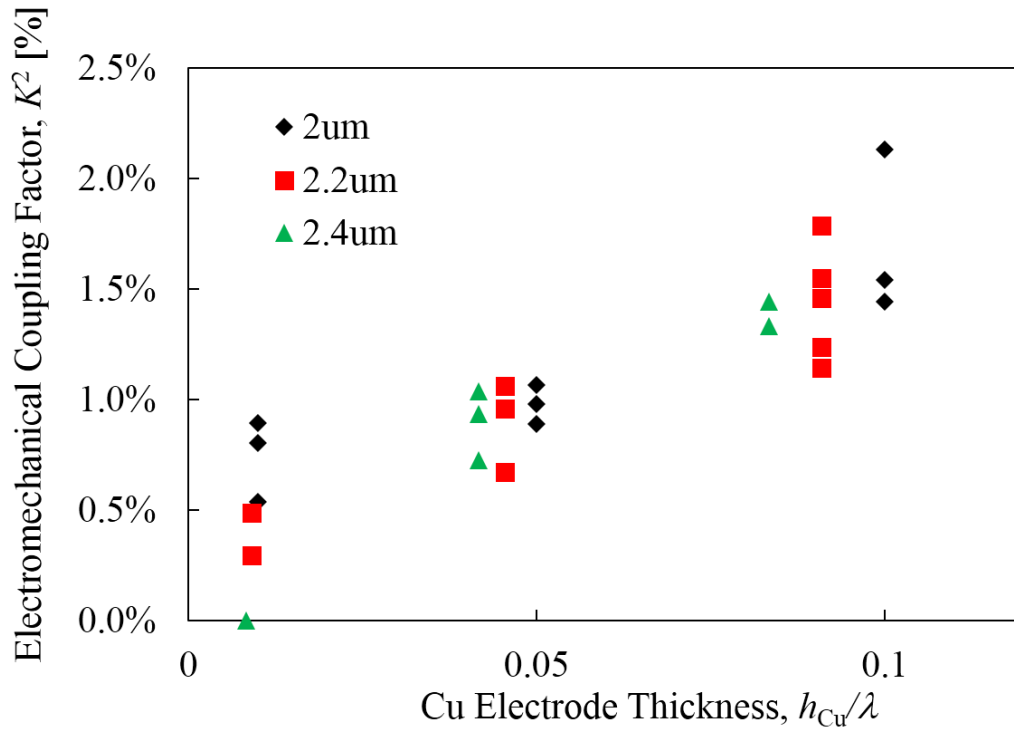
Figure 3.10 K_e^2 on ScAlN/Si structure changing with h_{Cu}/λ.

3.4 Conclusion

This chapter described drastic enhancement of K_e^2 by mass loading in layered SAW device structures such as the ScAlN film/Si substrate. This phenomenon occurs when the piezoelectric layer possesses high acoustic wave velocities, and the SAW energy confinement is enhanced by the mass loading.

At first, the ScAlN/Si structure was chosen, and it was shown that K_e^2 is considerably enhanced by the mass loading of the IDTs. It was also shown that such K_e^2 enhancement also occurs in various layered SAW device structures.

Furthermore, it was shown that this phenomenon is obvious even when an amorphous SiO_2 film is deposited on the top surface for temperature compensation although the SiO_2 film is non-piezoelectric.

Finally K_e^2 enhancement by mass loading was verified experimentally using the ScAlN film/Si substrate structure.

It was thought that a high velocity material such as SCD and SiC had to be used as the base substrate for realizing high performance SAW devices using the ScAlN layer [3.14~3.15]. However, the present results indicate that comparable performances can be achievable even when inexpensive Si is used for the purpose. This fact is very feasible for commercialization of ScAlN-based SAW devices because SCD and SiC are expensive and their availability is limited.

Besides, the disagreement between the experimental and calculated values may be caused by the inaccurate material constants of ScAlN, i.e., smaller Sc concentration r gives larger V and smaller K_e^2, different SAW characteristics will be achieved when different set of material constants are employed, thus it's of vital importance to verify the material constants employed for device simulations. This issue will be discussed in the following chapter.

References

[3.1] M. Akiyama, T. Kamohara, K. Kano, A. Teshigahara, Y. Takeuchi, and N. Kawahara, "Enhancement of piezoelectric response in scandium aluminum nitride alloy thin films prepared by dual reactive co-sputtering," *Adv. Mater.* **21** (2009) p. 593.

[3.2] M. Akiyama, K. Kano, and A. Teshigahara, "Influence of growth temperature and scandium concentration on piezoelectric response of scandium aluminum nitride alloy thin films," *Appl. Phys. Lett.* **95** (2009) 162107.

[3.3] T. Yanagitani, K. Arakawa, K. Kano, A. Teshigahara, and M. Akiyama, "Giant shear mode electromechanical coupling coefficient k_{15} in c-axis tilted ScAlN films," *Proc. IEEE Ultrason. Symp.* (2010) p. 2095.

[3.4] K. Arakawa, T. Yanagitani, K. Kano, A. Teshigahara, and M. Akiyama, "Deposition techniques of c-axis-tilted ScAlN films by conventional RF magnetron sputtering," *Proc. IEEE Ultrason. Symp.* (2010) p. 1050.

[3.5] G. Wingqvist, F. Tasnádi, A. Zukauskaite, J. Birch, H. Arwin, and L. Hultman, "Increased electromechanical coupling in w-Sc$_x$Al$_{1-x}$N," *Appl. Phys. Lett.* **97** (2010) 112902.

[3.6] M. Moreira, J. Bjurström, I. Katardjev, and V. Yantchev, "Aluminum scandium nitride thin-film bulk acoustic resonators for wide band applications," *Vacuum* **86** (2011) p. 23.

[3.7] R. Matloub, A. Artieda, C. Sandu, E. Milyutin, and P. Muralt, "Electromechanical properties of $Al_{0.9}Sc_{0.1}N$ thin films evaluated at 2.5 GHz film bulk acoustic resonators," *Appl. Phys. Lett.* **99** (2011) 092903.

[3.8] M. A. Caro, S. Zhang, T. Riekkinen, M. Yliammi, M. A. Moram, O. Lopez-Acevedo, J. Molarius, and T. Laurila, "Piezoelectric coefficients and spontaneous polarization of ScAlN," *J. Phys.: Condens. Matter* **24** (2015) 245901.

[3.9] S. Zhang, W. Y. Fu, D. Holec, C. J. Humphreys, and M. A. Moram, "Elastic constants and critical thicknesses of ScGaN and ScAlN," *J. Appl. Phys.* **114** (2013) 243516.

[3.10] S. Takayanagi, T. Yanagitani, and M. Matsukawa, "*c*-Axis tilted or *c*-Axis parallel ScAlN films/substrate SAW devices with high electromechanical coupling," *Proc. Symp. Ultrasonic Electron.* (2013) p. 143.

[3.11] M. Suzuki, T. Yanagitani, and H. Odagawa, "Polarity-inverted ScAlN film growth by ion beam irradiation and application to overtone acoustic wave (000-1)/(0001) film resonators," *Appl. Phys. Lett.* **104** (2014) 172905.

[3.12] R. Matloub, M. Hadad, A. Mazzalai, N. Chidambaram, G. Moulard, C. S. Sandu, T. Metzger, and P. Muralt, "Piezoelectric $Al_{1-x}Sc_{x}N$ thin films: A semiconductor compatible solution for mechanical energy harvesting and sensors," *Appl. Phys. Lett.* **102** (2013) 152903.

[3.13] A. Teshigahara, K. Hashimoto, and M. Akiyama, "Scandium aluminum nitride: Highly piezoelectric thin film for RF SAW devices in multi GHz range," *Proc. IEEE Ultrason. Symp.* (2012) p. 1917.

[3.14] K. Hashimoto, T. Fujii, S. Sato, T. Omori, C. Ahn, A. Teshigahara, K. Kano, H. Umezawa, and S. Shikata, "High Q surface acoustic wave resonators in 2-3 GHz range using ScAlN/Single crystalline diamond structure," *Proc. IEEE Ultrason. Symp.* (2012) p. 1926.

[3.15] K. Hashimoto, S. Sato, A. Teshighara, T. Nakamura, and K. Kano, "High Performance Surface Acoustic Resonators in 1-3 GHz Range Using ScAlN/6H-SiC Structure," *IEEE Trans. Ultrason. Ferroelectr. Freq. Control* **60** (2013) p. 637.

[3.16] A. Konno, M. Sumisaka, A. Teshigahara, K. Kano, K. Hashimo, H. Hirano, M. Esashi, M. Kadota, and S. Tanaka, "ScAlN Lamb wave resonator in GHz range released by XeF$_2$ etching," *Proc. IEEE Ultrason. Symp.* (2013) p. 1376.

[3.17] S. Mishin, M. Gutkin, A. Bizyukov, and V. Sleptsov, "Method of controlling coupling coefficient of Aluminum Scandium Nitride deposition in high volume production," *In 2013 Joint Conf. IEEE Int. Freq. Control Symp. & Euro. Freq. Time Forum* (2013) p. 126.

[3.18] K. Umeda, H. Kawai, A. Honda, M. Akiyama, T. Kato, and T. Fukura, "Piezoelectric properties of ScAlN thin films for piezo-MEMS devices," *Proc. MEMS2013* (2013) p. 733.

[3.19] A. Konno, M. Kadota, J. Kushibiki, Y. Ohashi, M. Esashi, Y. Yamamoto, and S. Tanaka, "Determination of full material constants of ScAlN thin film from bulk and leaky Lamb waves in MEMS-based samples," *Proc. IEEE Ultrason. Symp.* (2014) p. 273.

[3.20] T. Yanagitani, and M. Suzuki, "Electromechanical coupling and gigahertz elastic properties of ScAlN films near phase boundary," *Appl. Phys. Lett.* **105** (2014) 122907.

[3.21] H. Ichihashi, T. Yanagitani, M. Suzuki, S. Takayanagi, and M. Matsukawa, "Effect of Sc concentration on shear wave velocities in ScAlN films measured by micro-Brillouin scattering technique," *Proc. IEEE Ultrason. Symp.* (2014) p. 2521.

[3.22] C. Höglund, J. Bareno, J. Birch, B. Alling, Z. Czigany, and L. Hultman. "Cubic $Sc_{1-x}Al_xN$ solid solution thin films deposited by reactive magnetron sputter epitaxy onto ScN (111)," *J. Appl. Phys.* **105** (2009) 132862.

[3.23] C. Höglund, B. Alling, J. Birch, M. Beckers, P. O. Persson, C. Baehtz, and L. Hultman, "Effects of volume mismatch and electronic structure on the decomposition of ScAlN and TiAlN solid solutions," *Phys. Rev. B* **81** (2010) 224101.

[3.24] V. Felmetsger, M. Mikhov, M. DeMiguel-Ramos, M. Clement, J. Olivares, T. Mirea, and E. Iborra, "Sputtered $Al_{(1-x)}Sc_xN$ thin films with high areal uniformity for mass production," *In 2015 Joint Conf. IEEE Int. Freq. Control Symp. & Euro. Freq. Time Forum* (2015) p. 117.

[3.25] A. Zukauskaite, G. Wingqvist, J. Palisaitis, J. Jensen, P. O. Persson, R. Matloub, and L. Hultman, "Microstructure and dielectric properties of piezoelectric magnetron sputtered w-Sc_xAl_{1-x}N thin films," *J. Appl. Phys.* **111** (2012) 093527.

[3.26] K. M. Lakin, J. Belsick, J. F. McDonald, and K. T. McCarron, "High performance stacked crystal filters for GPS and wide bandwidth applications," *Proc. IEEE Ultrasonics Symp.* (2001) p.827.

[3.27] K. Hashimoto, T. Omori, and M. Yamaguchi, "Extended FEM/SDA Software for Characterising Surface Acoustic Wave Propagation in Multi-Layered Structures," *IEEE Trans. Ultrason. Ferroelectr. Freq. Control* **56** (2009) p. 2559.

[3.28] http://www.te.chiba-u.jp/~ken/freesoft.html

[3.29] B. A. Auld, "Acoustic field and waves in solids," Krieger, Malabar, FL, 1989, 2nd ed., Vol 1, p. 365.

[3.30] Q. Zhang, T. Han, J. Chen, W. Wang, and K. Hashimoto, "Enhanced coupling factor of surface acoustic wave devices employing ScAlN/Diamond layered structure with embedded electrodes," *Diamond Relat. Mater.* **58** (2015) p. 31.

[3.31] M. Sumisaka, K. Yamazaki, S. Fujii, G. Tang, T. Han, Y. Suzuki, S. Otomo, T. Omori, and K. Hashimoto, "Sputter deposition of ScAlN using large size alloy target with high Sc content and reduction of Sc content in deposited films," *Jpn. J. Appl. Phys*. **54** (2015) 07HD06.

4 Determination of ScAlN material constants for SAW/BAW device design and simulation

4.1 Introduction

Chapter 3 mentioned experimental results are sometimes deviated from the calculations, which are believed to be originated from the inaccuracy of the employed material constants for ScAlN film. Thus, it is of vital importance to investigate the validity of ScAlN film material constants employed for simulations.

As is well known, experimental data are not necessary as an initial guess in the first principle calculation. In fact, possibility of Sc-doped AlN in wurtzite phase was predicted by the calculation [4.1]. Such facts proved the feasibility of the first principle calculation, and it became a popular research topic in recent years [4.1~4.4].

Since the successful deposition of ScAlN film, the material constants have been highly demanded [4.5~4.35]. At first, elastic constants of ScAlN films have been calculated by Tasnádi [4.9] and Zhang [4.23]. Though this may be enough for X-ray diffraction (XRD) analysis of material lattice characteristics [4.7], the piezoelectric response of ScAlN films were not given.

There are 3 available sets of material constants for SAW/BAW device simulations. The first set for ScAlN is distributed by Teshigahara, et al. from Denso corp., where the Sc concentration is 40%, and the data may be derived based on that of pure AlN and adjusted according to experimental devices [4.19]. The second set is derived from measuring the characteristics of bulk and leaky lamb waves in MEMS devices by

Konno, where the Sc concentration is also 40% [4.26]. The third one is published by Caro et al., where the full set of $Sc_xAl_{1-x}N$ material constants calculated by first principle calculation [4.30].

Based on the 3 sets of material constants, the admittances for SAW devices of Cu IDT/ScAlN film/Si (001) substrate structure were calculated, where $h_{ScAlN}/\lambda = 0.633$, $h_{Cu}/\lambda = 0.15$, and Sc concentration is 40%. Besides, the normalization factor for frequency is V_{norm}/p, where $V_{norm} = 5840$m/s and $p = 1\mu$m. The comparison is shown in Fig. 4.1
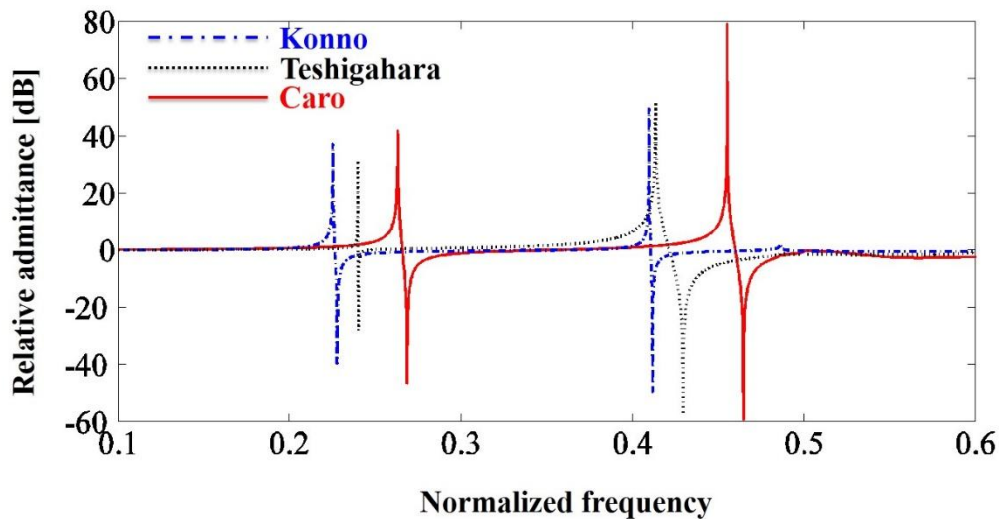
Figure 4.1 Comparison of calculated SAW admittances with 3 different sets of material constants.

Table 4.1 shows the comparison of values for V, K_e^2 of different modes when employing different material constants. It can be seen quite clearly that, the differences in V and K_e^2 are quite big, both for the Rayleigh mode and the Sezawa mode. Though it seems, V of the Sezawa mode is quite similar for Konno's and Teshigahara's constants, the K_e^2 is quite different.

Table 4.1 Comparison of V and K_e^2 using different material constants

	Konno		Teshigahara		Caro	
Mode	Rayleigh	Sezawa	Rayleigh	Sezawa	Rayleigh	Sezawa
V [m/s]	2630	4781	2802	4826	3073	5313
K_e^2 [%]	2.78	1.19	0.31	8.81	4.86	4.95

It seems the difference of device characteristics introduced by material constants is quite big, thus the validity of the material constants need to be evaluated. The validity of the above mentioned material constants had already been partially verified by BAW devices [4.30]. However, validity of the material constants for shear vibration which is dominant in SAWs has not been reported yet. This chapter describes verification of the material constants using SAW devices.

At first, based on the full set of material constants reported by Caro, *et al.* [4.30], BAW velocities for ScAlN are calculated and compared with the published experimental data measured on some BAW devices.

Then, influence of the Sc content on acoustic wave characteristics are numerically analyzed. It was shown that the accuracy of the shear components give significant impact to the properties of SAW modes.

Finally, a series of SAW resonators are fabricated on the $Sc_{0.4}Al_{0.6}N$ film/Si substrate structures. It is seen that the agreement between the calculation and experimental results is well not only for the h_{Cu} dependence but also for the h_{ScAlN} dependence. The same comparison was also carried out for the cases with $x=22\%$ and $x=32\%$, and good coincidence of the same level was obtained.

4.2 Simulation

4.2.1 Simulation procedure

The simulation was performed by the software SYNC2L, which calculates the input admittance of the infinitely long IDT of the device structure as a function of the driving frequency f [4.35~4.36]. Material constants for ScAlN were taken from Ref. [4.30], while those of Si, and Cu were taken from Ref. [4.37]. The reasons for selecting Cu as electrodes are as followed. To enhance the effective electromechanical coupling factor K_e^2, the electrodes need to achieve certain thickness, which usually means relative thick electrodes, such as Al. However, theoretical analysis suggests that Cu electrodes can serve the same purpose to enhance the K_e^2, while keeping the electrodes not so thick as Al. Besides, since the electrical conductivity for Cu is relatively large, the use of Cu electrodes will be helpful to keep the production yield ability without badly increasing ohmic loss.

4.2.2 Influence of Sc content on acoustic wave characteristics

Figure 4.2 shows the comparisons of calculated BAW velocities in $Sc_xAl_{1-x}N$ film with published data from Refs. [4.27~4.29], where the film thickness is fixed at $h_{ScAlN}/\lambda=1$. The calculation fits quite well with the experiments for the range from $x=0$ to $x\sim0.3$, where x stands for the Sc content in the film. Though there seems to be a growing discrepancy between the calculation and experimental results when Sc content is larger than $x\sim0.3$, this can be interpreted as unfavorable deposition conditions for $Sc_xAl_{1-x}N$ films [4.5, 4.16].

Figure 4.3 shows the BAW velocities in $Sc_xAl_{1-x}N$ film, where x ranges from 0 to 0.5. It is seen that longitudinal and shear horizontal (SH) BAW velocities decrease monotonically with an increase in x. On the other hand, the shear vertical (SV) BAW velocity decreases very slowly, and takes a minimum at $x\sim0.4$. Thus, it is quite interesting to note that when x is lower than ~0.12, the SH branch will be the fast shear BAW and SV branch will be the slow shear BAW. On the other hand, when x is larger than ~0.12, the SH branch will be the slow shear BAW and SV branch will be the fast shear BAW. Besides, in the figure, the velocity of SV-type surface skimming bulk wave (SSBW) for the Si (001) substrate is also given. It can be used to identify whether the Sezawa mode is leaky or non-leaky. Namely, when the SAW velocity is larger than the SSBW velocity, SV BAW in the Si substrate will couple with the SAW, and part of the SAW energy will be leaked into the substrate.

In the ScAlN/Si structure, the Sezawa mode can possess larger V and larger K_e^2 than the Rayleigh mode. As will be shown later, the velocity of the Sezawa mode is mostly determined by that of the SV BAW in the ScAlN layer. Since the accuracy of the shear components give significant impact to the properties of SAW modes, thus estimation of the shear components is of vital importance.
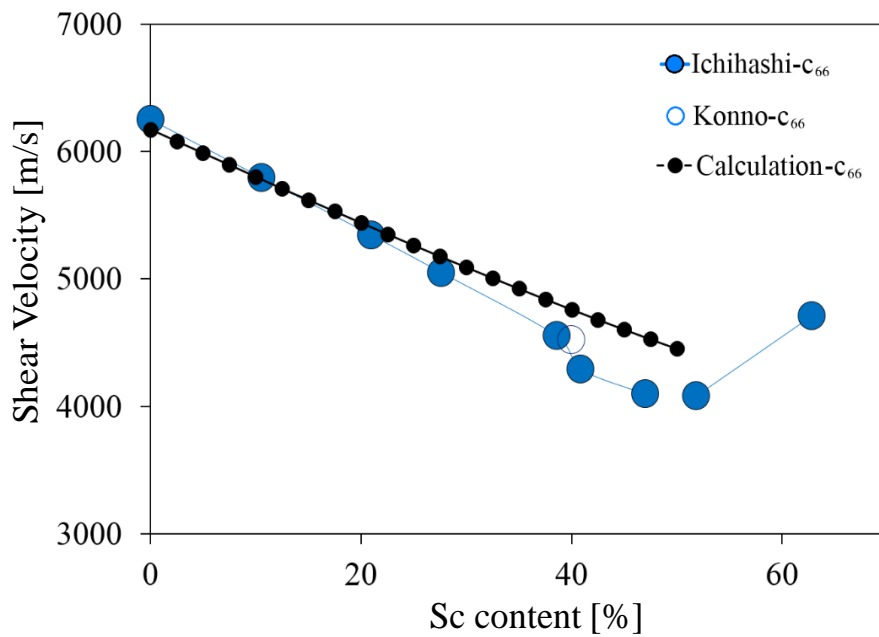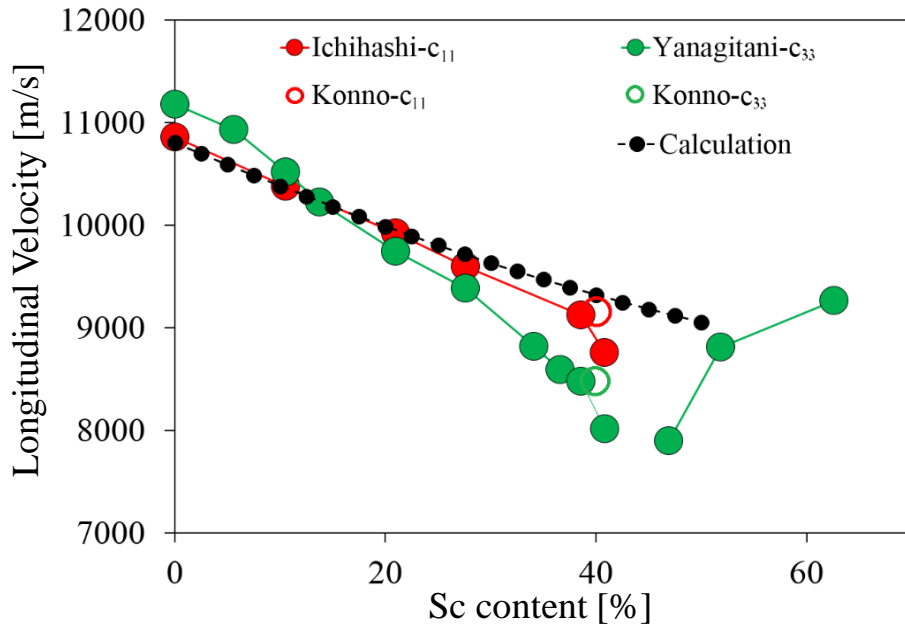
Figure 4.2 Comparison of calculated BAW velocities with experimental ones as a function of Sc content

x, (a) Longitudinal BAW velocity ($v_l = (c_{11}/\rho)^{1/2}$), b) Shear horizontal BAW velocity ($v_s = (c_{66}/\rho)^{1/2}$).
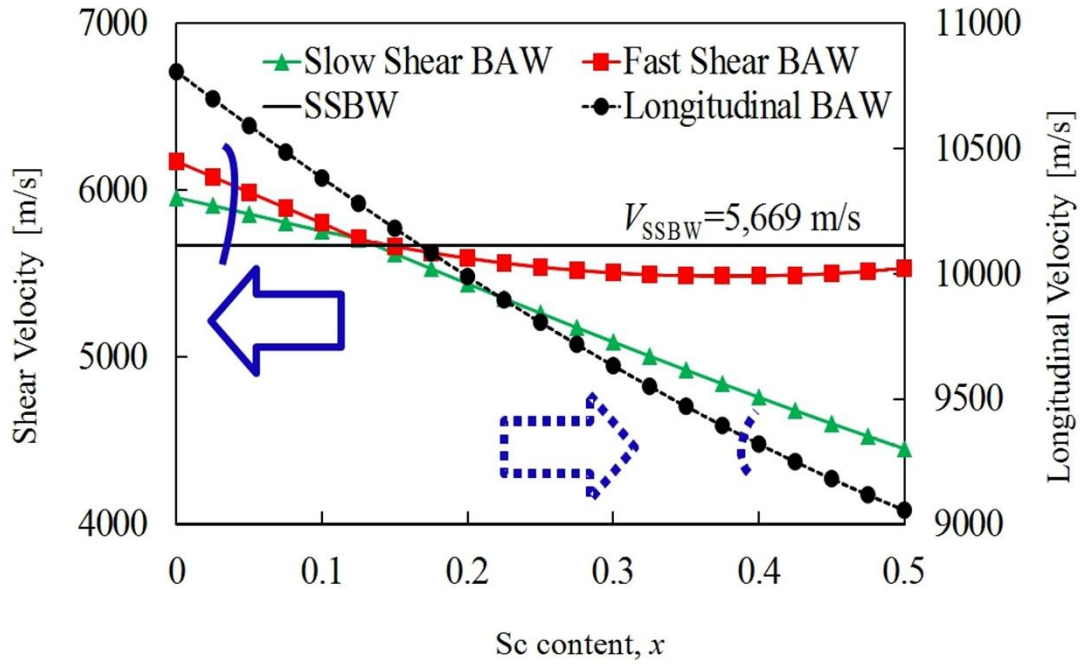
Figure 4.3 Change of slow shear BAW velocity, fast shear BAW velocity and longitudinal BAW velocity in ScAlN film as a function of Sc content. The black solid line stands for velocity of SV-type surface skimming bulk wave (SSBW) in Si (001) substrate.

4.2.3 SAW dispersion characteristic

Though the influences of different material constants have already been recognized in the beginning of this chapter, detailed calculations of V and K_e^2 are still not given. Thus, based on the design principles established in Chapter 3, a full description of the calculation process will be given here.

By use of the constants and VCALL, V and K_e^2 for $Sc_xAl_{1-x}N$ film/Si (001) substrate structure were calculated as a function of h_{ScAlN}/λ, where Sc content x was fixed at 0, 0.2 and 0.4. The calculation was performed without the influence of the IDT

mass loading effects. Figure 4.4 shows the existence of two modes, which are labeled in the order of their phase velocities.

It is seen that the second (Sezawa) mode exhibits relatively large V and K_e^2. As predicated before, for a given $Sc_xAl_{1-x}N$ film thickness h_{ScAlN}/λ, the SAW phase velocity V for both of the modes will decrease with the increment of the Sc content, the necessary minimum thickness where the Sezawa mode shows up is decreasing. Meanwhile, it is crystal clear that the velocity for the Rayleigh mode is more sensitive to the Sc content, while that for the Sezawa mode doesn't change so much. Besides, as for the K_e^2, the two modes are changing differently, where the K_e^2 for Rayleigh mode doesn't change so much with x, while that for the Sezawa mode is enhanced greatly, which means the K_e^2 for Sezawa mode is more sensitive to the Sc content.

Next, h_{ScAlN} is fixed at 0.6λ, and influence of the Cu electrode thickness h_{Cu} is investigated. Figure 4.5 shows variation of V and K_e^2 in the $Cu/Sc_xAl_{1-x}N/Si$ structure as a function of h_{Cu}/λ, where Sc content x is fixed at 0, 0.2 and 0.4. It is seen that K_e^2 for the Sezawa mode increases with h_{Cu}/λ, and takes a maximum value of 1.6% and 5.2% at $h_{Cu}/\lambda \sim 0.12$ for x is 0.2 and 0.4, which is greatly enhanced compared those when $h_{Cu}/\lambda \sim 0$. Meanwhile, K_e^2 for the Rayleigh mode changes similarly, which takes a maximum value above 1.2% and 5.3% at a thickness bigger than $h_{Cu}/\lambda \sim 0.2$. Both K_e^2 enhancements can be explained by the mass loading effect in Chapter 3 [4.33~4.34]. Meanwhile, V for the Sezawa mode is still above 5,000 m/s, it's quite favorable for practical use along with the enhanced K_e^2. However, as for the Rayleigh mode, though the K_e^2 is increased rapidly, the too-slow velocity may limit its applications.

This K_e^2 enhancement are also found when other $Sc_xAl_{1-x}N$ films of different Sc contents are employed. Figure 4.6 shows the change of K_e^2 with Sc content x and Cu IDT thickness h_{Cu} when $Sc_xAl_{1-x}N$ film thickness is fixed at $h_{ScAlN} \sim 0.6\lambda$. It is seen that h_{ScAlN}/λ giving large K_e^2 is less sensitive to h_{Cu}/λ.
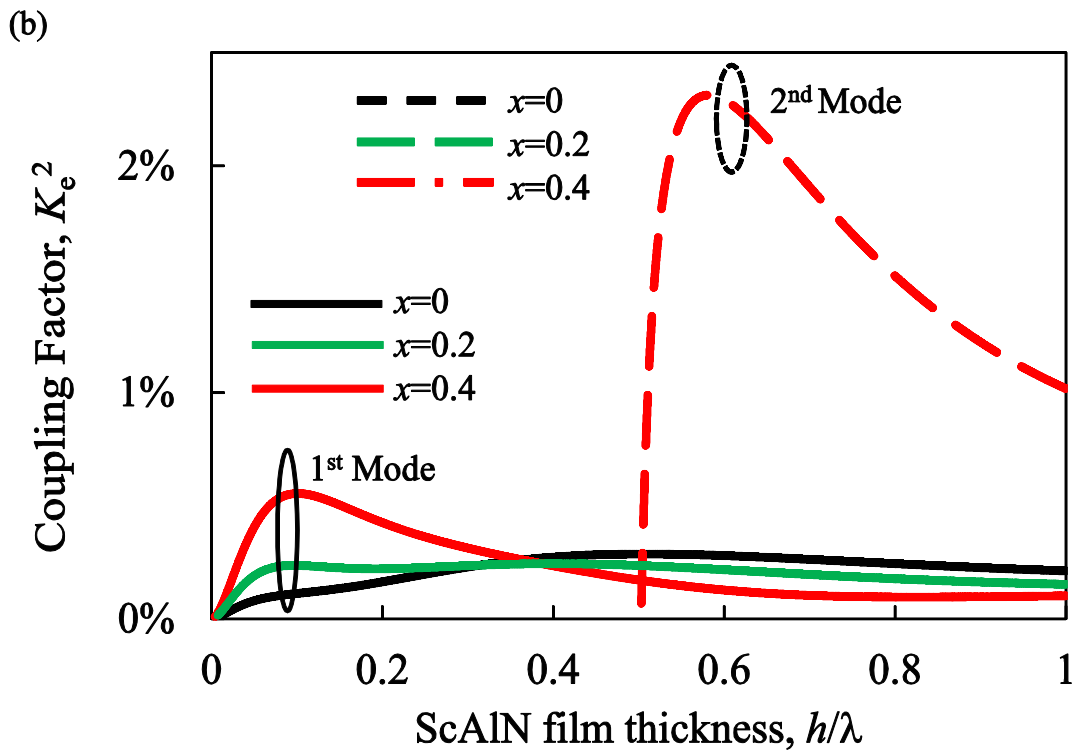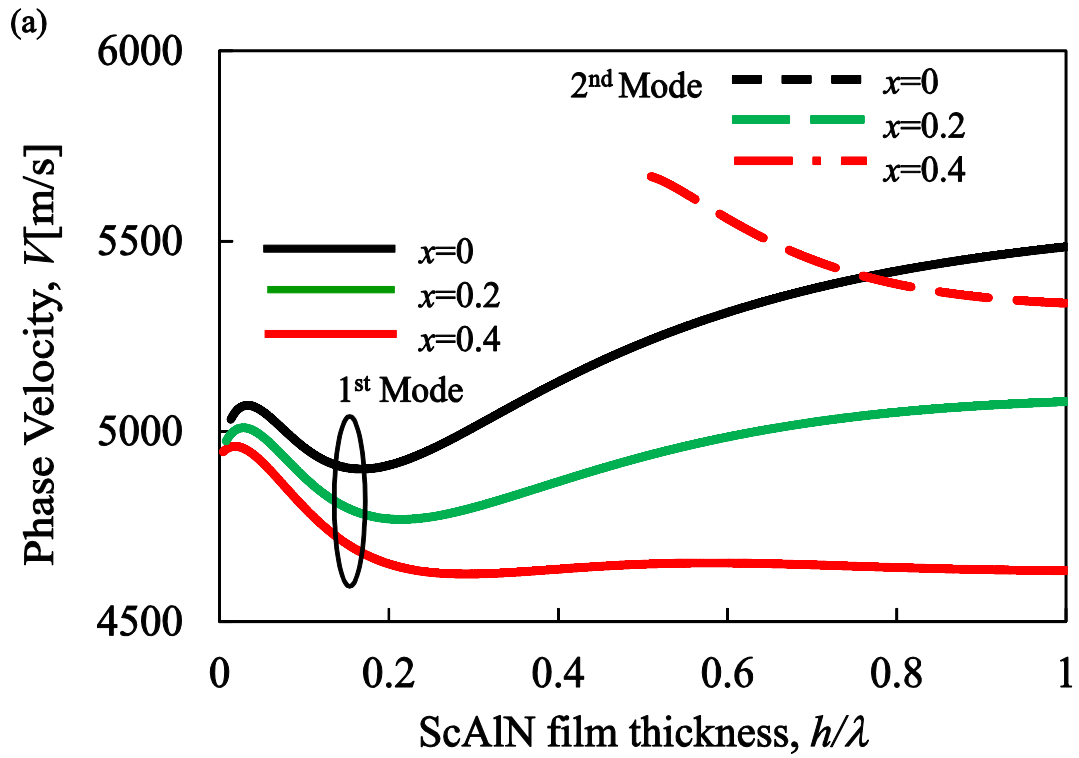
Figure 4.4 Theoretical SAW characteristics changing with h_{ScAlN}/λ on Cu/ScAlN/Si structure (a) Phase velocity changing with h_{ScAlN}/λ, (b) Effective coupling factor K_e^2 changing with h_{ScAlN}/λ.

(a)

(b)
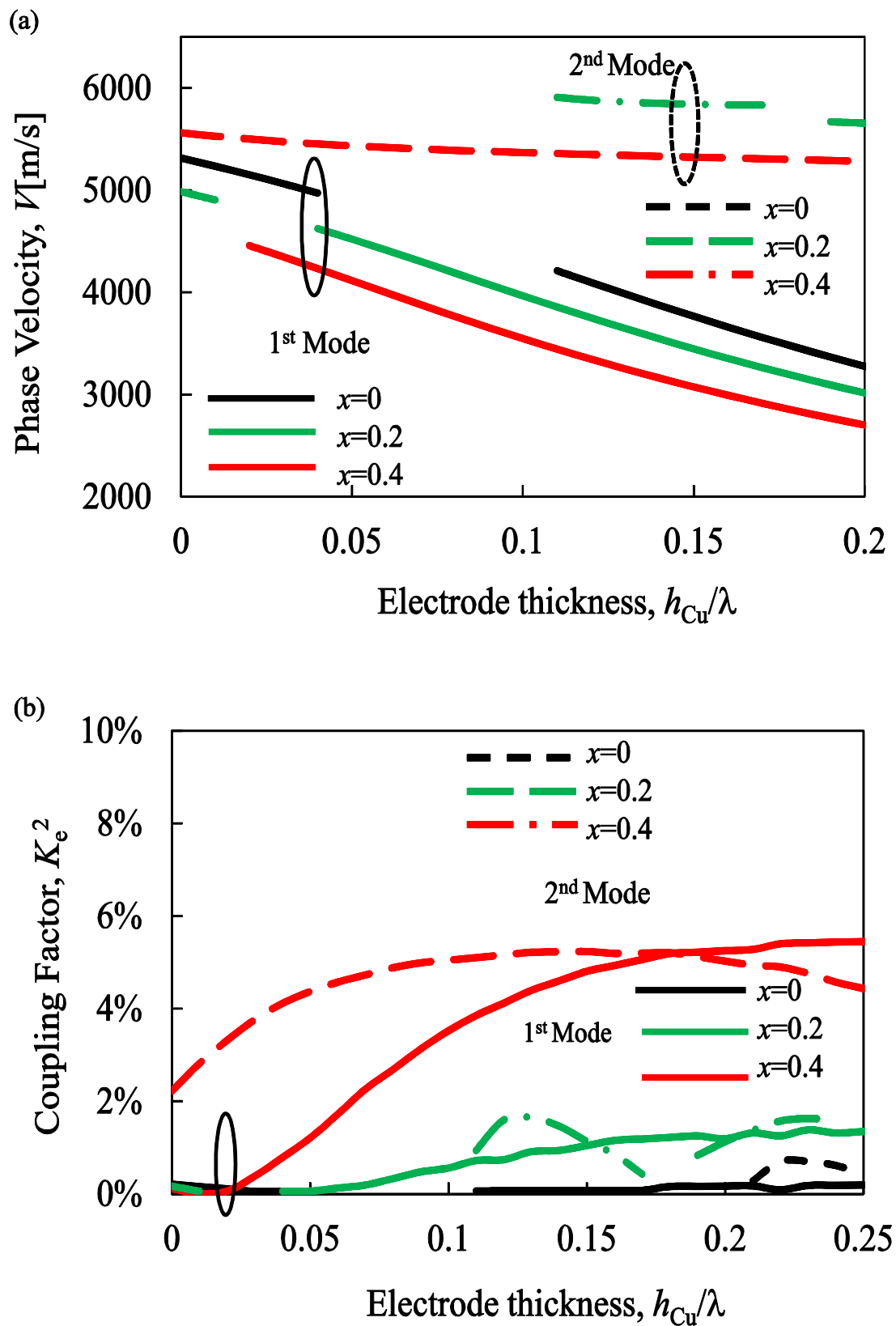
Figure 4.5 Theoretical SAW characteristics changing with h_{Cu}/λ on Cu/ScAlN/Si structure. (a) Phase velocity changing with h_{Cu}/λ, (b) Effective coupling factor K_e^2 changing with h_{Cu}/λ.
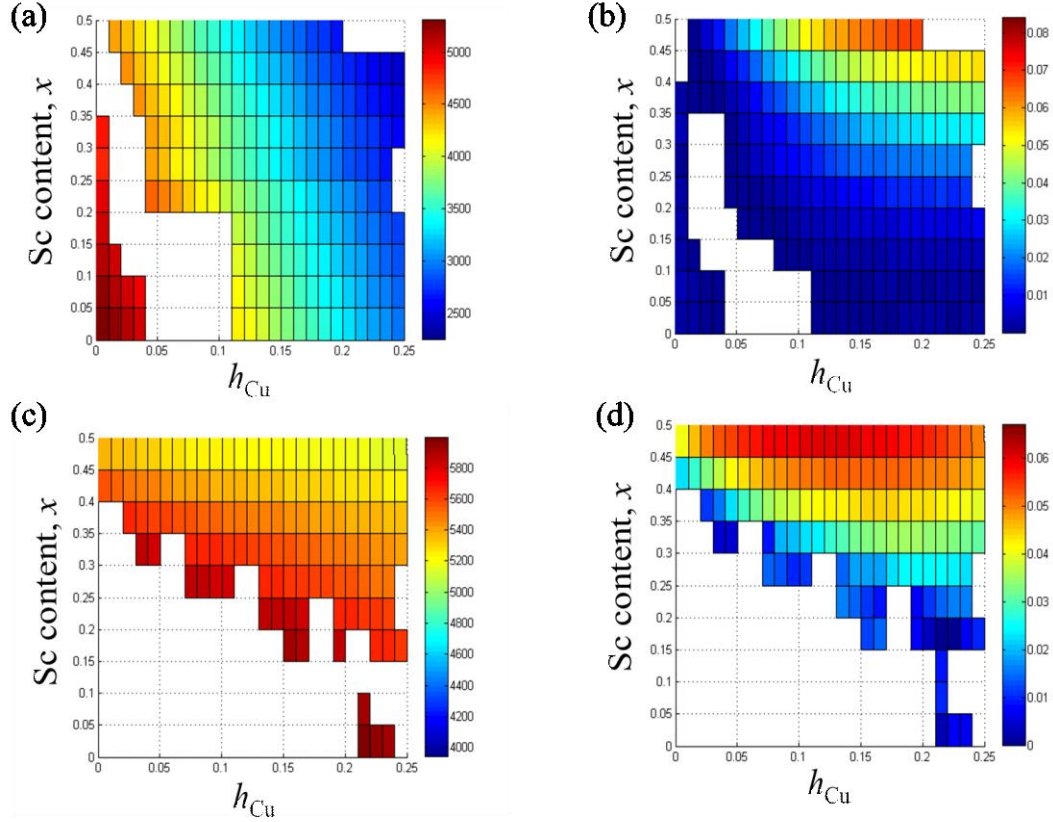
Figure 4.6 Theoretical SAW properties on Cu/ScAlN/Si structure when $h_{\text{ScAlN}}/\lambda = 0.55$. (a) Rayleigh mode V changing with Sc content x and h_{Cu}/λ, (b) Rayleigh mode K_e^2 changing with Sc content x and h_{Cu}/λ, (c) Sezawa mode V changing with Sc content x and h_{Cu}/λ, (d) Sezawa mode K_e^2 changing with Sc content x and h_{Cu}/λ.

4.3 Experiments

High quality ScAlN films were deposited by the conventional RF magnetron sputtering. $Sc_{0.43}Al_{0.57}$ and $Sc_{0.32}Al_{0.68}$ alloy targets were used [4.32], and a 3-in FZ Si (100) wafer was used as substrate. On the other hand, the $Sc_{0.40}Al_{0.60}$ film was deposited by the dual target sputtering described in Ref. [4.17].

SAW properties were measured using a series of one port SAW resonators fabricated on the structure, and their phase velocity V and effective coupling factor K_e^2

were evaluated using Eqs. (3.1)-(3.2). The design parameters are given in Table 4.2 and

the design configuration is shown in Fig. 4.7.

Table 4.2 Resonator design parameters

Sc content	22%	32%	40%
ScAlN thickness, h_{ScAlN} (μm)	1.52	1.73	1.60
Wavelength, λ (μm)	2, 2.2, 2.4		
Metallization ratio	0.5		
Aperture, W	20λ		
Gap	0.25λ		
Distance	0.25λ		
Numb. of IDT finger pairs	80		
Numb. of Reflector fingers	40		
Cu electrode thickness, h_{Cu} (nm)	20, 70, 150, 300	20, 200, 300	100, 200, 300

Figure 4.8 shows typical admittance characteristics of SAW resonators on the Cu

IDT/$Sc_{0.4}Al_{0.6}N$ film/Si substrate structure at different Cu electrode thicknesses when

h_{ScAlN}/λ=0.8 and λ=2μm. The Sezawa mode SAW phase velocities estimated from the

resonance frequencies were 5,460 m/s, 5,360 m/s and 5,300 m/s for the

h_{Cu}/λ=0.075, h_{Cu}/λ=0.1 and h_{Cu}/λ=0.15, respectively. Comparing the three admittance

curves indicates that V of the Rayleigh mode decreases faster with h_{Cu}/λ, while that of

the Sezawa mode does not change so much. This can be explained by the fact that the

Sezawa mode is mainly determined by the SV type BAW velocity, which decreases

gradually with the Sc content. By use of the equivalent circuit model [4.38], extracted Q

for the Sezawa mode is ~200 when h_{Cu}/λ=0.075, and it will become worsened when the

electrodes become thicker, which can be attributed to the increased BAW scattering

from mass loading effects. However, this deterioration phenomenon does not happen

for the Rayleigh mode, where the Q for the mode will increase with the mass loading effects. The difference in Q can be explained by the varied energy distribution in the ScAlN film, where Rayleigh mode energy is almost confined to the surface, while the Sezawa mode energy is located at a certain depth. Besides, when $h_{Cu}/\lambda=0.10$, there is a satellite resonance close to the main one. Its origin is unclear at this moment.

Figures 4.9-4.11 show how measured V and K_e^2 of the Rayleigh and Sezawa modes change with h_{Cu}/λ, when h_{ScAlN}/λ is fixed at several thicknesses. It is seen that experimental V and K_e^2 agree quite well with the theoretical ones, especially for Figs. 4.5 and 4.6, where the Sc content is relatively large, namely, 40% and 32%, respectively. The un-even distribution of the deposited ScAlN film thickness along with the on-top electrode thickness might contribute to variation of the experimental results.

When the Sc content is relatively low (~22%) shown in Fig. 4. 7, the agreement is a little poor for K_e^2. This may be due to the fact that the Sezawa mode is leaky when h_{Cu}/λ is small, e. g., when $h_{Cu}/\lambda<0.15$ for $h_{ScAlN}/\lambda=0.63$ and $h_{Cu}/\lambda<0.11$ for $h_{ScAlN}/\lambda=0.75$. Besides, it is well known that the non-piezoelectric cubic phase often coexists with the piezoelectric wurtzite one. Since the calculation in Ref. [4.29] was applied to pure wurtzite phase, inclusion of the cubic phase may cause the deviations of velocity and K_e^2 from real values.
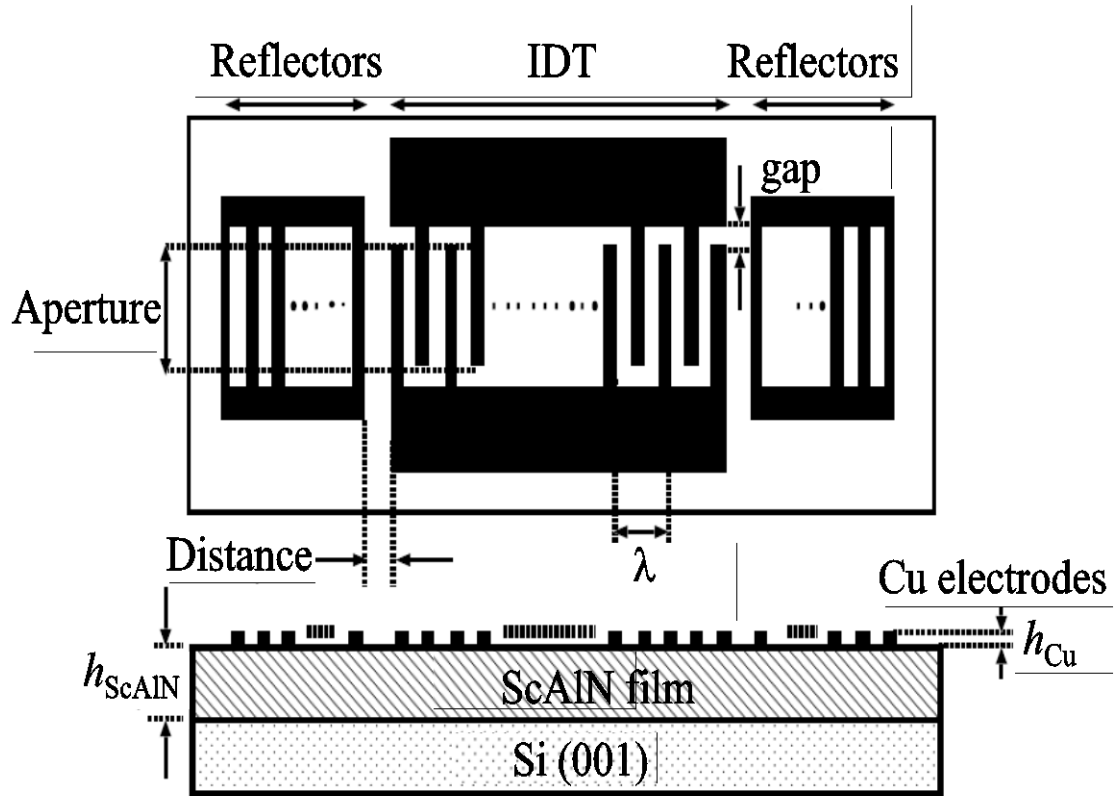
Figure 4.7 Configuration of Cu IDT/Sc$_x$Al$_{1-x}$N film/Si substrate structure based one-port synchronous SAW resonators with short-circuited design.
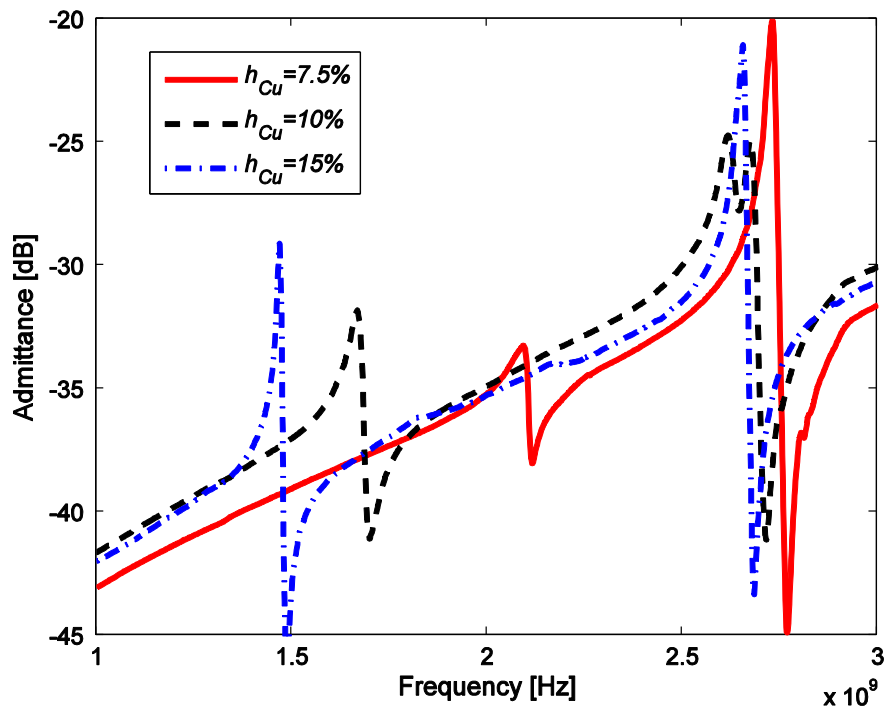
Figure 4.8 Typical admittance characteristics of fabricated SAW resonators when Sc content is 40%, ScAlN film thickness h_{ScAlN} =0.8λ, and h_{Cu}=0.075λ, 0.1λ, 0.15λ.
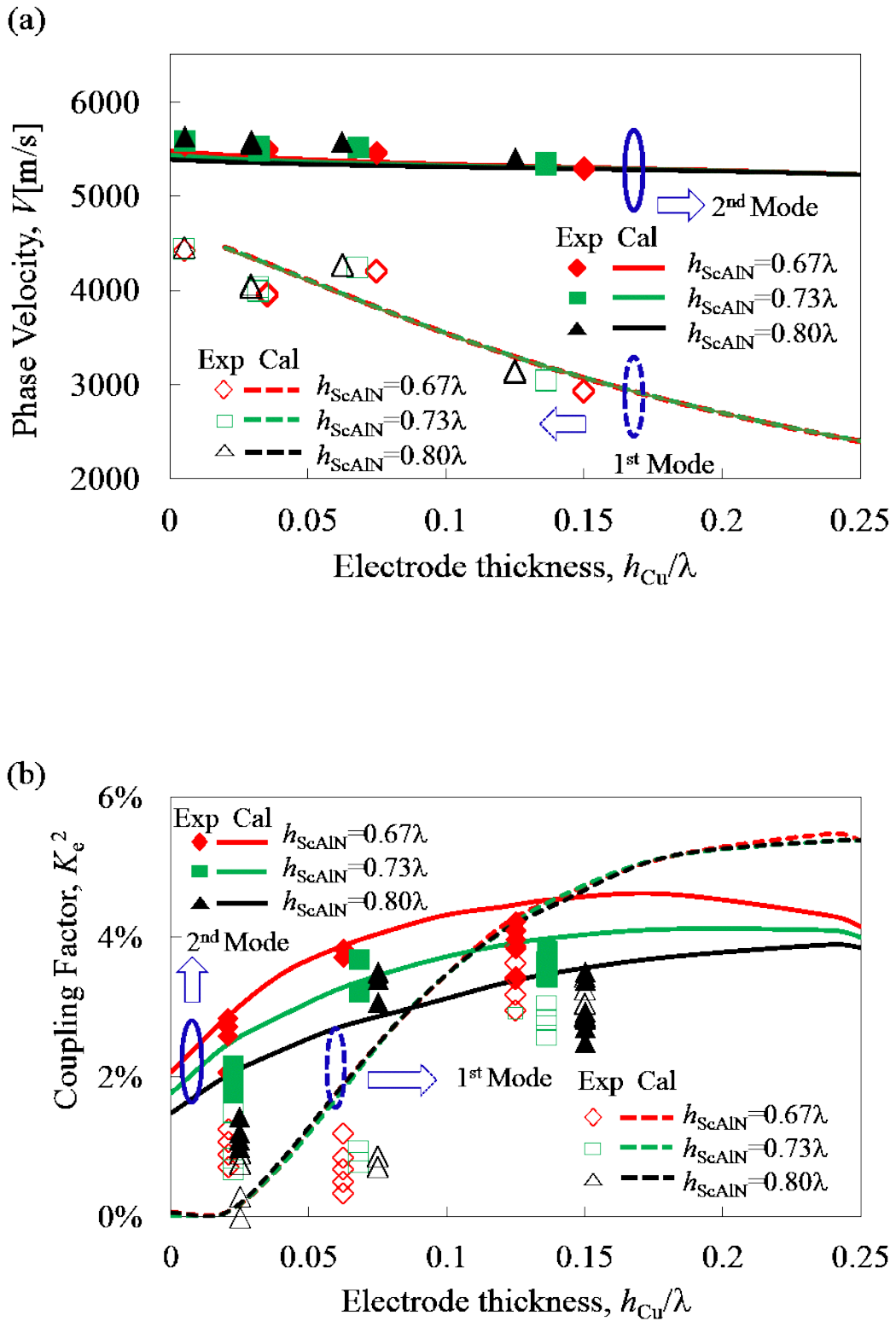
Figure 4.9 Comparison between theoretical (lines) and experimental (symbols) results when Sc content

is 40%, ScAlN film thickness h_{ScAlN} =0.67λ, h_{ScAlN} =0.73λ and h_{ScAlN} =0.8λ. The calculations are done by

use of SYNC2L for h_{Cu}=0 through 0.25λ where the ScAlN film thickness.
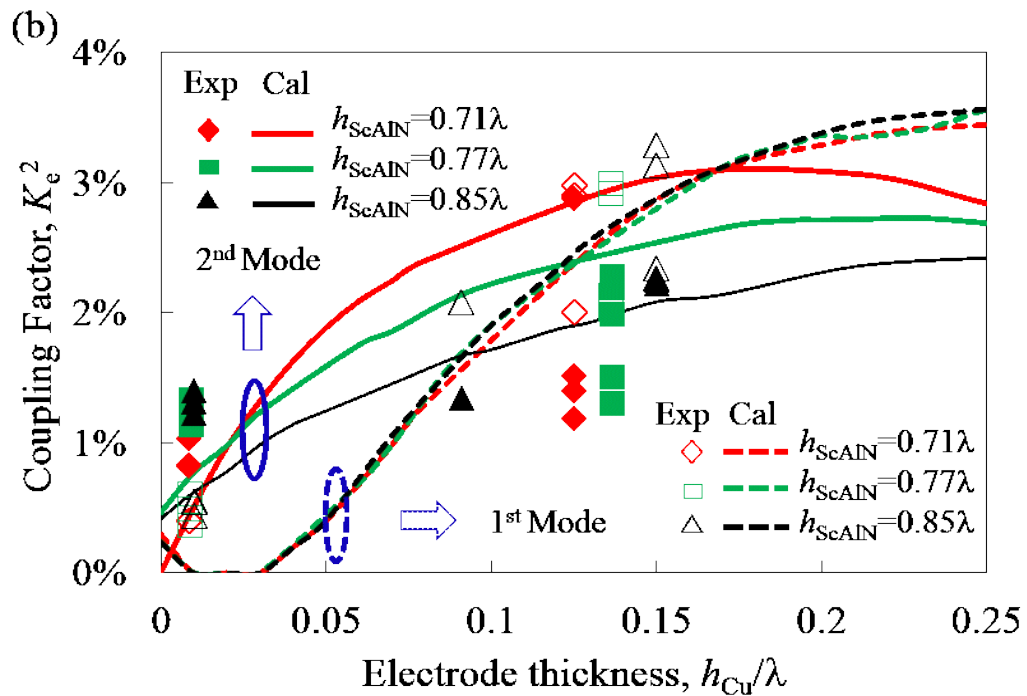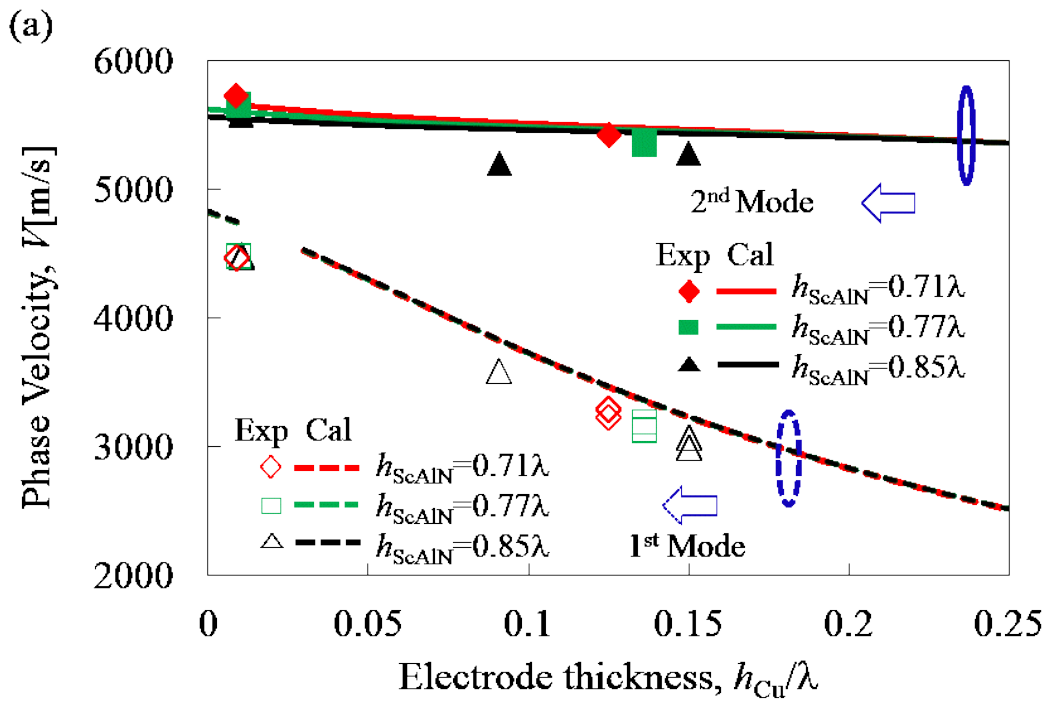
Figure 4.10 Comparison between theoretical (lines) and experimental (symbols) results when Sc content is 32%, ScAlN film thickness h_{ScAlN} =0.71λ, h_{ScAlN} =0.77λ and h_{ScAlN} =0.85λ. The calculations are done by use of SYNC2L for h_{Cu}=0 through 0.25λ where the ScAlN film thickness.
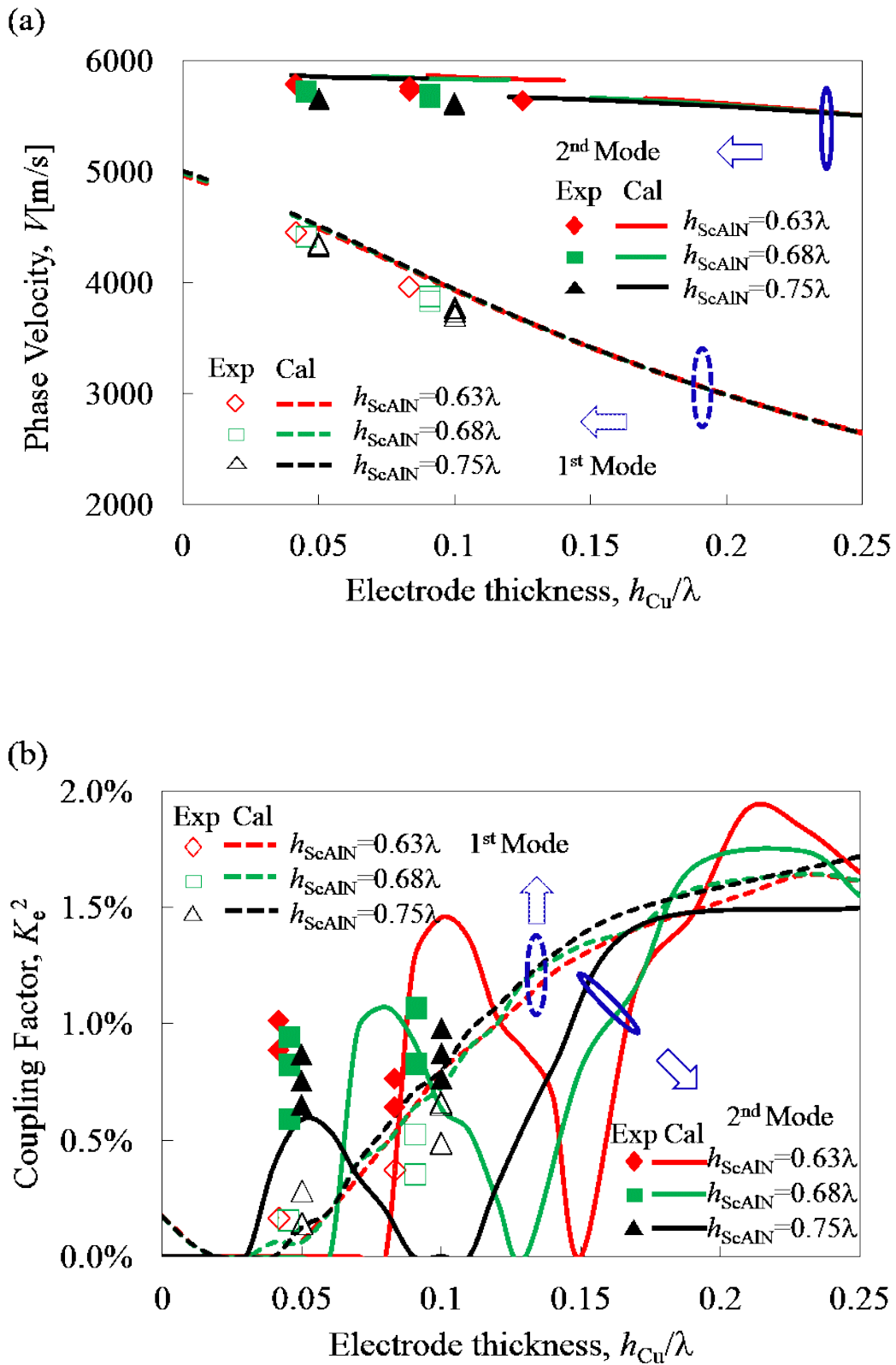
Figure 4.11 Comparison between theoretical (lines) and experimental (symbols) results when Sc content is 22%, ScAlN film thickness h_{ScAlN} =0.63λ, h_{ScAlN} =0.68λ and h_{ScAlN} =0.75λ. The calculations are done by use of SYNC2L for h_{Cu}=0 through 0.25λ where the ScAlN film thickness.

By the way, as shown in Ref. [4.5], the rapid velocity decrease at Sc concentration 30%~40% was observed experimentally by several authors. However, it did not appear in our experiment, and thus the result agreed well with the calculation based on the material constants reported in Ref. [4.30]. The difference may be due to the instability of ScAlN phase, and dependent on deposition conditions, such as substrate temperature and Sc concentration.

4.4 Conclusion

This chapter described the validity evaluation of $Sc_xAl_{1-x}N$ film material constants based on SAW characteristics. At first, the full set of material constants reported by Caro's group was employed, and the acoustic wave velocities on ScAlN film/Si substrate structures were calculated. The calculation results were compared with the published experimental data and good agreements were achieved. Then, BAW velocities in $Sc_xAl_{1-x}N$ film were calculated as a function of the Sc content, where the fast shear BAW will change differently with slow shear BAW and longitudinal BAW due to the anisotropic softening effects caused by dopant. Besides, the necessity to evaluate the effectivity of the material constants was shown since the shear velocities are so close to the SSBW velocity of the Si substrate. Series of SAW devices with various Cu and ScAlN film thicknesses were fabricated. The experimental results agreed quite well with the calculation, the agreement indicates the reliability of the employed ScAlN material constants.

References

[4.1] N. Takeuchi, "First-principles calculations of the ground-state properties and stability of ScN," *Phys. Rev. B* **65** (2002) 045204.

[4.2] N. Farrer, and L. Bellaiche, "Properties of hexagonal ScN versus wurtzite GaN and InN," *Phys. Rev. B* **66** (2002) 201203.

[4.3] V. Ranjan, S. Bin-Omran, D. Sichuga, R. S. Nichols, L. Bellaiche, and A. Alsaad, "Properties of GaN/ScN and InN/ScN superlattices from first principles," *Phys. Rev. B -Condens. Matter* **72** (2005) p. 1.

[4.4] A. Alsaad, and A. Ahmad, "Piezoelectricity of ordered ($Sc_xGa_{1-x}N$) alloys from first principles," *Euro. Phys. J. B- Condens. Matter and Complex Sys.* **54** (2006) p. 151.

[4.5] M. Akiyama, T. Kamohara, K. Kano, A. Teshigahara, Y. Takeuchi, and N. Kawahara, "Enhancement of piezoelectric response in scandium aluminum nitride alloy thin films prepared by dual reactive co-sputtering," *Adv. Mater.* **21** (2009) p. 593.

[4.6] M. Akiyama, K. Kano, and A. Teshigahara, "Influence of growth temperature and scandium concentration on piezoelectric response of scandium aluminum nitride alloy thin films," *Appl. Phys. Lett.* **95** (2009) 162107.

[4.7] M. A. Moram, and M. E. Vickers, "X-ray diffraction of III-nitrides ," *Rep. Prog. Phys.* **72** (2009) 036502.

[4.8] C. Höglund, J. Bareno, J. Birch, B. Alling, Z. Czigany, and L. Hultman, "Cubic $Sc_{1-x}Al_xN$ solid solution thin films deposited by reactive magnetron sputter epitaxy onto ScN (111)," *J. Appl. Phys.* **105** (2009) 132862.

[4.9] F. Tasnádi, B. Alling, C. Höglund, G. Wingqvist, J. Birch, L. Hultman and I. A. Abrikosov, "Origin of the anomalous piezoelectric response in wurtzite $Sc_xAl_{1-x}N$ alloys," *Phys. Rev. Lett.*, **104**, (2010) 1376011.

[4.10] C. Höglund, B. Alling, J. Birch, M. Beckers, P. O. Persson, C. Baehtz, and L. Hultman, "Effects of volume mismatch and electronic structure on the decomposition of ScAlN and TiAlN solid solutions," *Phys. Rev. B* **81** (2010) 224101.

[4.11] T. Yanagitani, K. Arakawa, K. Kano, A. Teshigahara, and M. Akiyama, "Giant shear mode electromechanical coupling coefficient k_{15} in *c*-axis tilted ScAlN films," *Proc. IEEE Ultrason. Symp.* (2010) p. 2095.

[4.12] K. Arakawa, T. Yanagitani, K. Kano, A. Teshigahara, and M. Akiyama, "Deposition techniques of *c*-axis-tilted ScAlN films by conventional RF magnetron sputtering," *Proc. IEEE Ultrason. Symp.* (2010) p. 1050.

[4.13] G. Wingqvist, F. Tasnádi, A. Zukauskaite, J. Birch, H. Arwin, and L. Hultman, "Increased electromechanical coupling in w-$Sc_xAl_{1-x}N$," *Appl. Phys. Lett.* **97** (2010) 112902.

[4.14] M. Moreira, J. Bjurström, I. Katardjev, and V. Yantchev, "Aluminum scandium nitride thin-film bulk acoustic resonators for wide band applications," *Vacuum* **86** (2011) p. 23.

[4.15] R. Matloub, A. Artieda, C. Sandu, E. Milyutin, and P. Muralt, "Electromechanical properties of $Al_{0.9}Sc_{0.1}N$ thin films evaluated at 2.5 GHz film bulk acoustic resonators," *Appl. Phys. Lett.* **99** (2011) 092903.

[4.16] A. Zukauskaite, G. Wingqvist, J. Palisaitis, J. Jensen, P. O. Persson, R. Matloub and L. Hultman, "Microstructure and dielectric properties of piezoelectric magnetron sputtered w-$Sc_xAl_{1-x}N$ thin films," *J. Appl. Phys.* **111** (2012) 093527.

[4.17] A. Teshigahara, K. Hashimoto, and M. Akiyama, "Scandium aluminum nitride: Highly piezoelectric thin film for RF SAW devices in multi GHz range," *Proc. IEEE Ultrason. Symp.* (2012) p. 1917.

[4.18] K. Hashimoto, T. Fujii, S. Sato, T. Omori, C. Ahn, A. Teshigahara, K. Kano, H. Umezawa, and S. Shikata, "High Q surface acoustic wave resonators in 2-3 GHz range using ScAlN/Single crystalline diamond structure," *Proc. IEEE Ultrason. Symp.* (2012) p. 1926.

[4.19] K. Hashimoto, S. Sato, A. Teshighara, T. Nakamura, and K. Kano, "High Performance Surface Acoustic Resonators in 1-3 GHz Range Using ScAlN/6H-SiC Structure," *IEEE Trans. Ultrason. Ferroelectr. Freq. Control* **60** (2013) p. 637.

[4.20] A. Konno, M. Sumisaka, A. Teshigahara, K. Kano, K. Hashimoto, H. Hirano, M. Esashi, M. Kadota, and S. Tanaka, "ScAlN Lamb wave resonator in GHz range released by XeF_2 etching," *Proc. IEEE Ultrason. Symp.* (2013) p. 1376.

[4.21] K. Umeda, H. Kawai, A. Honda, M. Akiyama, T. Kato, and T. Fukura, "Piezoelectric properties of ScAlN thin films for piezo-MEMS devices," *Proc. MEMS2013* (2013) p. 733.

[4.22] S. Takayanagi, T. Yanagitani, M. Matsukawa, "*c*-axis tilted or *c*-axis parallel ScAlN films/substrate SAW devices with high electromechanical coupling," *Proc. IEEE Ultrason. Electro.* (2013) p. 143.

[4.23] S. Zhang, W. Y. Fu, D. Holec, C. J. Humphreys, and M. A. Moram, "Elastic constants and critical thicknesses of ScGaN and ScAlN," *J. Appl. Phys.* **114** (2013) 243516.

[4.24] R. Matloub, M. Hadad, A. Mazzalai, N. Chidambaram, G. Moulard, C. S. Sandu, T. Metzger, and P. Muralt, "Piezoelectric $Al_{1-x}Sc_xN$ thin films: A semiconductor compatible solution for mechanical energy harvesting and sensors," *Appl. Phys. Lett.* **102** (2013) 152903.

[4.25] S. Mishin, M. Gutkin, A. Bizyukov, and V. Sleptsov, "Method of controlling coupling coefficient of Aluminum Scandium Nitride deposition in high volume production," *In 2013 Joint Conf. IEEE Int. Freq. Control Symp. & Euro. Freq. Time Forum* (2013) p. 126.

[4.26] A. Konno, M. Kadota, J. Kushibiki, Y. Ohashi, M. Esashi, Y. Yamamoto, and S. Tanaka, "Determination of full material constants of ScAlN thin film from bulk and leaky Lamb waves in MEMS-based samples," *Proc. IEEE Ultrason. Symp.* (2014) p. 273.

[4.27] T. Yanagitani and M. Suzuki, "Electromechanical coupling and gigahertz elastic properties of ScAlN films near phase boundary," *Appl. Phys. Lett.* **105** (2014) 122907.

[4.28] H. Ichihashi, T. Yanagitani, M. Suzuki, S. Takayanagi, and M. Matsukawa, "Effect of Sc concentration on shear wave velocities in ScAlN films measured by micro-Brillouin scattering technique," *Proc. IEEE Ultrason. Symp.* (2014) p. 2521.

[4.29] M. Suzuki, T. Yanagitani, and H. Odagawa, "Polarity-inverted ScAlN film growth by ion beam irradiation and application to overtone acoustic wave (000-1)/(0001) film resonators," *Appl. Phys. Lett.* **104** (2014) 172905.

[4.30] M. A. Caro, S. Zhang, T. Riekkinen, M. Ylilammi, M. A. Moram, O. Lopez-Acevedo, J. Molarius, and T. Laurila, "Piezoelectric coefficients and spontaneous polarization of ScAlN," *J. Phys.: Condens. Matter* **24** (2015) 245901.

[4.31] V. Felmetsger, M. Mikhov, M. DeMiguel-Ramos, M. Clement, J. Olivares, T. Mirea, and E. Iborra, "Sputtered Al$_{(1-x)}$Sc$_x$N thin films with high areal uniformity for mass production," *In 2015 Joint Conf. IEEE Int. Freq. Control Symp. & Euro. Freq. Time Forum* (2015) p. 117.

[4.32] M. Sumisaka, K. Yamazaki, S. Fujii, G. Tang, T. Han, Y. Suzuki, S. Otomo, T. Omori and K. Hashimoto, "Sputter deposition of ScAlN using large size alloy target with high Sc content and reduction of Sc content in deposited films," *Jpn. J. Appl. Phys.* **54** (2015) 07HD06.

[4.33] G. Tang, T. Han, A. Teshigahara, T. Iwaki and K. Hashimoto, "Enhancement of effective electromechanical coupling factor by mass loading in layered SAW device structures," *Proc. IEEE Freq. Contr. Symp.* (2015) p. 416.

[4.34] K. M. Lakin, J. Belsick, J. F. McDonald, and K. T. McCarron. "Improved bulk wave resonator coupling coefficient for wide bandwidth filters," *Proc. IEEE Ultrason. Symp.* (2001) p. 827.

[4.35] K. Hashimoto, T. Omori, and M. Yamaguchi, "Extended FEM/SDA Software for Characterizing Surface Acoustic Wave Propagation in Multi-Layered Structures," *IEEE Trans. Ultrason., Ferroelec., and Freq. Control* **56** (2009) p. 2559.

[4.36] http://www.te.chiba-u.jp/~ken/freesoft.html

[4.37] B. A. Auld, Acoustic Field and Waves in Solids, Volume I, 2nd ed., Krieger, FL (1989) p. 365.

[4.38] K. Hashimoto, "Surface Acoustic Wave Devices in Telecommunications," Springer-Verlag, Germany, (2000).

5 Conclusions and outlooks

5.1 Conclusions

To improve the performance of SAW devices, the following topics, such as deposition conditions for ScAlN films, considerations for high performance layered SAW devices were investigated. The results can be concluded as the following,

(1) Chapter 2 discussed deposition of ScAlN thin films by the conventional RF magnetron sputtering using a large size Sc-Al alloy target with high Sc content. Two 4-in. Sc–Al alloy targets with different Sc to Al ratio were prepared, and deposited film qualities and uniformity were evaluated. When a target with Sc content of 43 at. % was used, high quality and uniform c-axis-oriented ScAlN films were obtained throughout the three inch wafer. However, measured Sc content was significantly lower than that of the target. In addition, the film quality became worse and was not stable with an increase in total sputtering time. On the other hand, when the $Sc_{0.43}Al_{0.57}$ target was employed, film quality became better and better with an increase in total sputtering time. One-port SAW resonators were fabricated on the ScAlN film/Si substrate structure and their performances were discussed. Influence of the N_2 content in the sputtering gas was also investigated, and the result indicated that nitridation of the target surface is at least one of the reasons causing the reduction of the Sc content in the deposited films from that in the target.

(2) Chapter 3 described the mass loading effect on enhancement of K_e^2 in layered SAW device structures such as the ScAlN film/Si substrate. This phenomenon occurs when

the piezoelectric layer possesses high acoustic wave velocities, and the SAW energy confinement is enhanced by the mass loading. At first, the ScAlN/Si structure was chosen, and it was shown that K_e^2 is considerably enhanced by the mass loading of the IDTs. It was also shown that such K_e^2 enhancement also occurs in various layered SAW device structures. This phenomenon was obvious even when an amorphous SiO_2 film is deposited on the top surface for temperature compensation. Finally, K_e^2 enhancement by mass loading was verified experimentally using the ScAlN film/Si substrate structure.

It was thought that a high velocity material such as SCD and SiC had to be used as the base substrate for realizing high performance SAW devices using the ScAlN layer. The results indicate that comparable performances can be achievable even when inexpensive Si is used for the purpose. This fact is very feasible for commercialization of ScAlN-based SAW devices because SCD and SiC are expensive and their availability is limited.

(3) Chapter 4 described the validity evaluation of $Sc_xAl_{1-x}N$ film material constants based on SAW characteristics. At first, the full set of material constants reported by Caro's group was employed, and the BAW velocities on ScAlN film/Si substrate structures were calculated. Comparing with the published experimental data, good agreements were achieved. Then, BAW velocities in $Sc_xAl_{1-x}N$ film were calculated as a function of Sc content, and it was found that the fast shear BAW velocity changes differently with slow shear BAW velocity and longitudinal BAW velocity due to the anisotropic softening effects caused by dopant. Besides, the necessity to evaluate the

94

effectivity of the material constants was shown since the shear velocities were so close to the SSBW velocity of the Si substrate. Furthermore, series of SAW devices with various Cu IDT and ScAlN film thicknesses were fabricated. The experimental results agreed quite well with the calculation, the agreement indicates the reliability of the employed ScAlN material constants.

5.2 Outlooks

It was demonstrated that relative good uniformity, *c*-axis orientation can be achieved by the current RF sputtering deposition. Although problems exist, such as the low Sc content in the deposited film, and the not so good surface roughness, the RF sputtering shows great potential for mass production of ScAlN films.

For next step, a systematic research on the optimal deposition conditions, such as the sputtering power, distance between the target and the substrate, et al., should be done. To improve *c*-axis orientation and stress-free characteristic of the deposited films, influence of the substrate should also be considered. As for mass production applications, Sc content and thickness uniformity should also be further improved.

Besides, though high performance layered SAW devices can be designed delicately under the design rules given in Chapter 3, loss mechanisms in the structure were not fully analyzed. Thus, to design high performance SAW devices, especially devices with high quality factors and spurious free characteristics, it is necessary to analyze the SAW propagation and BAW scattering in the ScAlN film-based SAW devices not only to the depth direction but also to the in-plane direction.

List of Publications

Refereed journals papers

(1) **G. Tang**, T. Han, Q. Zhang, K. Yamazaki, T. Omori, and K. Hashimoto, "Validity evaluation of $Sc_xAl_{1-x}N$ material constants based on SAW characteristics," Journal of Micromechanics and Microengineering, **26**, 11 (2016) 115002-1~6.

(2) **G. Tang**, T. Han, A. Teshigahara, T. Iwaki, and K. Hashimoto, "Enhancement of effective electromechanical coupling factor by mass loading in layered surface acoustic wave device structures," Japanese Journal of Applied Physics, **55**, 7S1 (2016) 07KD07-1~5.

(3) **G. Tang**, T. Han, J. Chen, B. Zhang, T. Omori, and K. Hashimoto, "Model parameter extraction for obliquely propagating surface acoustic waves in infinitely long grating structures," Japanese Journal of Applied Physics, **55**, 7S1 (2016) 07KD08-1~4.

(4) **G. Tang**, T. Han, J. Chen, B. Zhang, T. Omori, and K. Hashimoto, "Thin plate model for transverse mode analysis of surface acoustic wave devices," Japanese Journal of Applied Physics, **55**, 7S1 (2016) 07KD09-1~5.

(5) Q. Zhang, T. Han, **G. Tang**, J. Chen, and K. Hashimoto, "SAW Characteristics of $AlN/SiO_2/3C$-SiC Layered Structure with Embedded Electrodes," IEEE Transactions on Ultrasonics, Ferroelectrics, and Frequency Control, **63**, 10 (2016) pp. 1608-1612.

(6) X. Ji, J. Chen, T. Han, L. Zhou, Q. Zhang, and **G. Tang**, "Enlarged phase velocities of ultra-wideband surface acoustic wave devices with relaxor based ferroelectric single crystal/diamond layered structure," Diamond and Related Materials, **66** (2016) pp.213-216.

(7) M. Sumisaka, K. Yamazaki, S. Fujii, **G. Tang**, T. Han, Y. Suzuki, S. Otomo, T. Omori and K. Hashimoto, "Sputter deposition of ScAlN using large size alloy target with high Sc content and reduction of Sc content in deposited films," Japanese Journal of Applied Physics, **55**, 7S1 (2015) 07HD06-1~4.

(8) J. Chen, Q. Zhang, T. Han, L. Zhou, **G. Tang**, B. Liu, and X. Ji, "Theoretical Analysis of Surface Acoustic Wave Propagating Property of Y cut Nano Lithium Niobate Film on Silicon Dioxide," AIP Advances, **58** (2015) 087173-1~5.

Review Paper

(1) 橋本研也,大森達也,**唐供賓**,韓韜,陳景, "無限周期構造における弾性波動斜め伝搬のモデル化," 超音波テクノ, **28**, 7/8 (2016) pp. 88-89.

Proceedings Papers for International Conferences

(1) **G. Tang**, T. Han, Q. Zhang, K. Yamazaki, T. Omori, and K. Hashimoto, "Validity evaluation of $Sc_xAl_{1-x}N$ material constants based on SAW characteristics," Proc. IEEE Ultrason. Symp. (2016) 10.1109/ULTSYM.2016.7728493 (4 pages).

(2) B. Zhang, T. Han, **G. Tang**, Q. Zhang, T. Omori, K. Hashimoto, "Modeling of Lateral SAW Propagation Including Coupling Between Different SAW Modes," Proc. IEEE Ultrason. Symp. (2016) 0.1109/ULTSYM.2016.7728496 (4 pages).

(3) Y. Huang, J. Bao, **G. Tang**, T. Aonuma, Q. Zhang, T. Omori, and K. Hashimoto, "SAW/BAW band reject filters embedded in impedance converter," Proc. IEEE Ultrason. Symp. (2016) 10.1109/ULTSYM.2016.7728411 (4 pages).

(4) Q. Zhang, T. Han, B. Zhang, **G. Tang**, Y. Huang, T. Omori, and K. Hashimoto, "Frequency Domain FEM Analysis of Reflector Scattering Characteristics for SAW Tags," Proc. IEEE Ultrason. Symp. (2016) 10.1109/ULTSYM.2016.7728495 (4 pages).

(5) T. Han, C. Zhang, Y. Hu, Y. Yang, and **G. Tang**, "Recent research results on wireless passive acoustic sensors for smart grids application," Proc. IEEE Ultrason. Symp. (2016) 10.1109/ULTSYM.2016.7728508 (4 pages).

(6) K. Hashimoto, M. Sumisaka, K. Yamazaki, S. Fujii, **G. Tang**, T. Han, Y. Suzuki, S. Otomo, and T. Omori, "Sputter Deposition of ScAlN Films by Reactive Sputtering Using Large Size ScAl Alloy Target with High Sc Content-Impact of Nitridation of Sputtering Target," Proc. Sixth International Symposium on Acoustic Wave Devices for Future Mobile Communication Systems (2015) pp.40-45.

(7) **G. Tang**, Q. Zhang, T. Han, and K. Hashimoto, "Enhancement of Effective Electromechanical Coupling Factor by Mass Loading in Layered SAW Device

Structures," Proc. Sixth International Symposium on Acoustic Wave Devices for Future Mobile Communication Systems (2015) pp.116-120.

(8) **G. Tang**, T. Han, J. Chen, T. Omori, and K. Hashimoto, "Thin Plate Model for Transverse Mode Analysis of Surface Acoustic Wave Devices," Proc. IEEE Ultrasonics Symp. (2015) 457-1~4.

(9) Q. Zhang, T. Han, **G. Tang**, J. Chen and K. Hashimoto, "SAW characteristics of $AlN/SiO_2/3C$-SiC layered structure with embedded electrodes," Proc. IEEE Ultrason. Symp. (2015) 116-1~4.

(10) **G. Tang**, T. Han, A. Teshigahara, T. Iwaki, and K. Hashimoto, "Enhancement of Effective Electromechanical Coupling Factor by Mass Loading in Layered SAW Device Structures," Proc. IEEE Freq. Contr. Symp. (2015) pp.416-419.

(11) S. Fujii, M. Sumisaka, **G. Tang**, Y. Suzuki, S. Otomo, T. Omori, and K. Hashimoto, "Highly c-axis-oriented ScAlN thin films deposited using Sc-Al alloy target," Tech. Digest, IEEE MTT-S International Microwave Symp. (2015) TH3D-2-1~4.

Proceedings Papers for Domestic Conferences

(1) Y. Huang, J. Bao, **G. Tang,** Y. Wang, T. Omori, and K. Hashimoto, "Multi-mode filter composed of single-mode SAW/BAW resonators," 第 37 回超音波エレクトロニクスの基礎と応用に関するシンポジウム (2016) 1E4-2.

(2) B. Zhang, T. Tan, Q. Zhang, **G. Tang**, T. Omori, and K. Hashimoto, "Influence of coupling with SH SAW on lateral propagation of Rayleigh SAW on 128°YX-LiNbO$_3$," 第 37 回超音波エレクトロニクスの基礎と応用に関するシンポジウム (2016) 1P3-1.

(3) **G. Tang,** T. Han, K. Yamazaki, Q. Zhang, T. Omori, and K. Hashimoto, "Validity evaluation of Sc$_x$Al$_{1-x}$N material constants based on SAW characteristics," 日本学術振興会弾性波素子技術第 150 委員会第 144 回研究会 (2016) pp. 19-23.

(4) **G. Tang,** T. Han, J. Chen, B. Zhang, T. Omori, and K. Hashimoto, "Thin Plate Model for Transverse Mode Analysis of Surface Acoustic Wave Devices," 圧電材料・デバイスシンポジウム 2016 (2016) pp. 99-104.

(5) **G. Tang**, T. Han, J. Chen, B. Zhang, T. Omori, and K. Hashimoto, "Model Parameter Extraction for Obliquely Propagating Surface Acoustic Waves in Infinitely Long Grating Structures," 第 36 回超音波エレクトロニクスの基礎と応用に関するシンポジウム (2015) 1P3-5.

(6) **G. Tang**, T. Han, J. Chen, B. Zhang, T. Omori, and K. Hashimoto, "Thin Plate Model for Transverse Mode Analysis of Surface Acoustic Wave Devices," 第 36 回超音波エレクトロニクスの基礎と応用に関するシンポジウム (2015) 1P3-6.

(7) **G. Tang**, T. Han, A. Teshigahara, T. Iwaki, T. Omori, and K. Hashimoto, "Enhancement of Effective Electromechanical Coupling Factor by Mass Loading

in Layered SAW Device Structures," 第 36 回超音波エレクトロニクスの基礎 と応用に関するシンポジウム (2015) 2E3-3.

(8) **G. Tang**, T. Han, A. Teshigahara, T. Iwaki, T. Omori, and K. Hashimoto, "Enhancement of Effective Electromechanical Coupling Factor by Mass Loading in Layered SAW Device Structures," 日本学術振興会弾性波素子技術第 150 委 員会第 140 回研究会 (2015) pp. 9-13.

(9) **G. Tang,** T. Han, A. Teshigahara, T. Iwaki, T. Omori, and K. Hashimoto, "Enhancement of Effective Electromechanical Coupling Factor by Mass Loading in Layered SAW Device Structures," 圧電材料・デバイスシンポジウム 2015 (2015) pp. 75-79.